ABSTRACT

OBRINGER, NATHAN DONALD. Flexible Structure Impact Modeling With a Particle Method. (Under the direction of Jeffrey W. Eischen).

The purpose of this research was to develop the capability to handle flexible structure impact problems using the particle method. A MATLAB computer code that implemented the particle-based formulation capable of handling stretch and bend forces, external forces, and contact was created and thoroughly tested. The computer code was validated where possible using classical beam and plate theories. After developing a MATLAB computer code particle model, the particle model is to be embedded in the computational fluid dynamic code produced at North Carolina State University termed, the Room Simulator. In order to do so, the particle model had to be capable of reading and writing STL (stereo-lithography) files to use as input and output. The particle model is three-dimensional and can handle internal and external forces. Internal forces include in-plane membrane forces, out-of-plane bending forces, and absolute damping forces. External forces include all external applied loads, gravitational forces, and effective forces due to pressure. The MATLAB computer code was equipped with a contact detection and update algorithm with a point-to-plane collision detection and a velocity update scheme. In order to produce simulations involving actual materials, the procedure to measure actual material properties has been documented. Also, the procedure to convert from experimentally determined fabric mechanical properties to effective stiffness values useful in the MATLAB computer code is described. Seven simulations were used to demonstrate the utility of the MATLAB computer code.

Flexible Structure Impact Modeling With a Particle Method

by
Nathan Donald Obringer

A thesis submitted to the Graduate Faculty of
North Carolina State University
in partial fulfillment of the
requirements for the degree of
Master of Science

Mechanical Engineering

Raleigh, North Carolina

2010

APPROVED BY:

_____	_____
Dr. Jack R. Edwards	Dr. Arkady Kheyfets

_____
Dr. Jeffrey W. Eischen
Committee Chair

DEDICATION

To my parents, Tim and Patty Obringer.

You have loved and cared for me,

And you have been there from day one.

I hope you cherish all the memories

And are proud of the man I have become!

To my brother, Adam Obringer.

As you have begun to mature into a fine young man,

The bond we share has grown tighter than ever before!

Thank you for the support!

To the one and only, Lauren Boris.

I am glad you found me on that summer day.

While times have been tough being apart from you,

I hope this brings a smile to your face

And signifies a new chapter in the book we write together!

You deserve more credit than I can offer,

But let me just say thank you for being there when times were rough

And I needed you more than you knew!

BIOGRAPHY

Nathan Obringer was born in September 1985 in Pittsburgh, Pennsylvania to Tim and Patty Obringer. Five years later, in August 1990, his brother Adam became a part of his life! Nathan attended school in the Baldwin-Whitehall School District before graduating from Baldwin High School in 2003. Nathan went on to pursue his Bachelor's Degree in Mechanical Engineering at Penn State University. After obtaining his degree from Penn State University in May 2008, he enrolled at North Carolina State University where he pursued his Master's Degree in Mechanical Engineering. His time in North Carolina concluded with the successful defense of his thesis on June 4, 2010. Nathan is returning to Pittsburgh to continue to explore life's many challenges while using his skills and knowledge to contribute to a world which has given him so much!

ACKNOWLEDGMENTS

This thesis would not have been possible had it not been for the guidance and support of a few very important people. I express my sincere gratitude to:

- Dr. Jeffrey W. Eischen, who stuck with me when times were tough, and through your help and support, we were able to make huge strides, culminating with the completion of my part of this project. I appreciate all of your help and the knowledge I have gained under your guidance.
- Dr. Jung-Il Choi, you were the one I turned to when I had programming questions. Thank you for your help, suggestions, and for the contributions you made to this project.
- I would like to thank Dr. Jack Edwards and Dr. Arkady Kheyfets for serving on my research committee.
- I would like to thank the Naval Surface Warfare Center for providing the grant which made this research possible.
- To my family, you were there for me and offered me encouragement when I was down; you reminded me that this would be an accomplishment I would cherish for the rest of my life!
- Laur, you were my rock when I needed support and you always knew what to do or what to say to brighten my day; I appreciate you putting up with me and listening to me describe my project to you day-in and day-out; you are the best!

TABLE OF CONTENTS

LIST OF TABLES

LIST OF FIGURES

1 Introduction

1.1 Background and Objective of Research

The long term goal of this research project was to produce computational simulations of human ingress/egress events into flexible structures located in chemically contaminated areas, while tracking the concentration of toxic species during such events. In a chemically contaminated environment, it is known that certain gas species may be transported from one location to another via human motion. This transportation can cause the infiltration of a previously safe environment with harmful pollutants. In an attempt to understand how this transportation occurs, the immediate goal of this research project was to create a structural particle-based computer code capable of producing realistic results aimed at studying the deformation of flexible structures accounting for contact with models of moving humans. Through recent work, Dr. Jack Edwards's research group at North Carolina State University has developed a Room Simulator computational fluid dynamics (CFD) code. The Room Simulator solves the time-dependent, incompressible Navier-Stokes equations, expanded to include gas-phase heat conduction and gas-phase agent transport. The Room Simulator combines large-eddy simulation techniques for turbulent wake resolution with immersed-boundary methods to account for the effects of moving features. This approach embeds a surface mesh consisting of structured or unstructured elements within a flow. The surface meshes may be closed or of zero-thickness and can consist of multiple parts which can be separately animated. The framework of the Room Simulator is highly suited for a detailed examination of ingress/egress events into flexible structures. A long-term goal is for Room

Simulator to be updated to incorporate pre-programmed, mission-specific human activity and to link with existing urban airflow models that will provide external environmental conditions. Also, there is a need to add a particle model for fabric structural response to enable realistic simulations of flexible or semi-rigid entryways. The contribution of this research project stems from this need to add a particle model.

The response of a flexible structure is crucial when studying ingress/egress events. Depending on the type of door, entry/exit into these structures can cause deformation of a flexible or semi-rigid fabric structure. The door opening/closing event itself can cause separation and reconstitution of fabric panels and fabric deformation can occur due to impact loads. The effects of gravity and pressure can also cause fabric deformation, ultimately affecting the structural response. This motion of the fabric may affect the local hydrodynamics and thus can influence agent transport. While shell-based finite-element methods can be used to account for these effects, the matrix algebra necessary to solve the time-dependent deformation problem can be substantial, and very difficult to embed in a CFD code. Particle method coding is a far simpler alternative. External forces and impact/collision events act on the particle model to produce internal strains (out-of-plane bending, in-plane extension and shear). Implementing a contact algorithm allows the particle model to handle fabric/surface collisions, such as human entry into a tent. The benefit to using a particle model is that the surface meshes are directly analogous to the zero-thickness immersed bodies used by the Room Simulator to simulate door motions. As a result, the particle model could be incorporated into the Room Simulator to influence the local flow

field near the door. Two-way coupling of the Room Simulator and particle code has not yet been completed but the capability to do so is available.

1.2 Literature Review

The interest in physically-based models for cloth animation goes back over two decades. A physical model is one which provides physically realistic simulations based on the laws of physics. Research on these topics is very closely related to the textile and computer graphics industries. Early models were kinematic until Terzopoulos et al. (1987) began creating a physical model based on the theory of elasticity. The development of a physically-based model continued with Terzopoulos and Fleischer (1988), who saw the importance in using inelastically deformable models.

Particle models use particles arranged in triangular or quadrilateral elements to model a given fabric. Membrane stiffness can be modeled using interaction between a given particle and its nearest neighbors while bending stiffness can be modeled employing common edges between two elements. When dealing with large deformation drape response of fabrics, buckling is another important behavior which must be accounted for through bending stiffness. In addition to buckling behavior, collision detection is critical for accurate particle models and has been handled many different ways. This discussed in more detail below.

In the textile and apparel industries, the drape of a fabric is very important. Breen et al. (1994) explicitly represents the microstructure of woven cloth with interacting particles. Using a Kawabata fabric testing device, they are able to tune their model to represent the

original material. Eischen et al. (1996) used finite-element modeling to simulate 3D motions related to the real fabric manufacturing process used in the textile and apparel industries. The issues they discussed are nonlinear material response, fabric contact with rigid surfaces, and adaptive arc-length control. Furthermore, Fontana et al. (2004) present a physical model which simulates multi-layered fabric for virtual prototyping applications. Their research follows from the woven material fabric and the use of a Kawabata bending test as described by Breen et al. (1994). Fontana et al. use a computer-aided design (CAD)-oriented system to make their contribution to the apparel manufacturing industry more useful.

Collision detection is one of the most difficult problems to deal with when modeling clothing or fabric drape. The most significant limitation with incorporating collision detection is the computation time and cost. There are generally two steps to the collision process, collision detection and collision correction. After a collision is detected, a method to correct the detected collision must be implemented. Along with the two steps in the collision process, there are generally two types of collision, cloth/solid and cloth/cloth self-collisions. The latter presents additional problems beyond basic cloth/solid collisions. Key research efforts guided toward improvements in computation time and realism focus on the methods of solving particle model differential equations and more efficient collision detection. Namely, explicit or implicit integration methods can be used to solve the differential equations necessary when using a particle method. With explicit integration such as a fourth-order Runge-Kutta method, the time-step must be less than the critical time-step for a stable solution whereas, an implicit method is unconditionally stable. As a result, with an implicit method, a larger time-step can be used which results in faster computing times. Baraff and

Witkin (1998) were one of the first to successfully implement large time-steps in cloth simulation. Their contribution was to couple a new technique for constraining individual cloth particles with a modified conjugate gradient method to solve the linear system generated by the implicit integrator. Their simulation stably handles large time-steps.

Another way to speed up the computational time for collision detection is to incorporate a more efficient searching and detection scheme. Zhang and Yuen (2000) use a voxel-based collision detection method for clothed human animation. An assumption they use is cloth and human models are represented by triangular meshes. Then, they only treat edge-to-triangle collisions: an edge of a triangle intersects another triangle. A voxel is a uniform spatial subdivision of the object space. Collision triangles are limited to the voxels associated with that edge of the triangle. As a result, the number of potential collision regions is limited and potential collision regions can be located quickly.

Bigliani and Eischen (2000) presented a method for collision detection and handling for cloth modeling. They present a node-to-triangle collision detection algorithm in which all possible node-triangle pairs are checked. If collision is detected, the position and velocity of the collision node are updated according to the momentum conservation law and integrated in the subsequent step. In order to make the collision detection more efficient, a spatial enumeration method is used. The 3D space is broken up into volume elements or boxes. Collision detection is checked only for nodes of the network which fall in the same box.

Volino and Thalman (2000) adopted use of the modified conjugate gradient method used by Baraff and Witkin (1998) with added improvements to realism and simplicity. In order to increase the collision detection searching efficiency, the hierarchical method described in

Volino and Thalman (1994) was used. After collision is detected, they implement a correction on the particle acceleration rather than directly correcting the state of the system.

In order to improve collision resolution in cloth simulations, Huh et al. (2001) introduce a collision detection scheme using swept-volumes which are volumes made up of two sets of positional entities at a face; one at time t and one at time $t + \Delta t$. Detected collisions are saved in a data structure known as, "zones of impact". Then, to resolve collisions they use a cloth collision resolution method to simultaneously solve collisions while ensuring the conservation of momentum.

Choi and Ko (2002) introduce a semi-implicit cloth simulation which produces stable and responsive cloth. With their technique, they can stably use a large time-step while producing realistic results. Significant improvements to the stability and realism of the simulations were made possible by their ability to introduce a way to overcome the post-buckling instability resulting in a major contribution to the field of study. Choi and Ko implement a voxel-based collision detection method similar to that proposed by Zhang and Yuen (2000).

Cloth/cloth collision response is very important in simulations involving production character animation used by companies such as Pixar Animation Studios. Previous attempts to handle these collisions involve history-based methods to decide whether cloth regions have interpenetrated. History-based methods present a problem with production character animation because their bodies often times intersect and cloth becomes pinched in these areas. The cloth self-intersects and becomes tangled when the body parts separate. To handle this problem, Baraff et al. (2003) present a history-free method capable of untangling

cloth after pinching based on a global intersection analysis of the cloth. They also present a method called flypapering, to handle pinches caused by cloth/solid collisions.

To improve drape simulation speed, Sul and Kang (2004) use a height and radial constraint to detect collisions. This includes cloth/cloth and cloth/human collisions. The fabric patterns were made into finite elements and given a local area number; only elements within a certain area can contact. The result is faster collision detection resulting in improved drape simulation speed.

More recently, Zink and Hardy (2007) have proposed a method of using geometry images in cloth simulation. Geometry images allow for the representation of a triangulated mesh as a regular 2D image file. Geometry images were introduced by Gu et al. (2002) to store surface geometry in a completely regular structure. Improvements to existing methods were achieved through the use of an implicit/explicit integration scheme by utilizing the regular structure of geometry images to improve performance. The demand for simulating real-time cloth motion is increasing and this method can provide this real-time simulation.

After detecting collisions, it is necessary to correct the collisions. A few ways to handle the collision resolution were described earlier, including updating positions and velocities or updating accelerations. Another very popular collision resolution technique is the penalty method described in the LS-DYNA Theory Manual (2006). Each slave node is checked for penetration through the surface of the master surface. If there is no penetration, nothing is done. If penetration does occur, an interface force is applied between the slave node and the contact point on the master surface. The magnitude is proportional to the amount of

penetration. This method is very common and works well although violations of the penalty method are possible.

There has been an extensive amount of research done involving particle models, finite element analysis and collision detection/resolution for the textile and computer graphics industries. Free-falling cloth, the draping of cloth over solid objects (i.e. tables, chairs, blocks, balls, etc.) and modeling clothing on the human body are some of the most common examples. Other examples include flags waving and drapes blowing in the wind. One interesting case done by Huh et al. (2001) involves cloth draped over a solid ring; a ball is dropped on the cloth so both the ball and the cloth fall through the ring. Also, research done by O'Brien et al. (1997) introduces the combination of active and passive simulations for secondary motion. Some interesting examples examined through their simulations are: a gymnast on a trampoline, a bungee jumper, a gymnast vaulting on a mat, a girl swinging while wearing a skirt, and kites in the air. The primary contribution of the work is to examine three types of coupling: full, partial and one-way which they describe through the example of a basketball going through the net.

Although there has been a lot of research done in the area of clothing and cloth drape, human/cloth interaction has been limited to clothing resting on the human body. While our research takes many of the same ideas discussed with stretching and bending stiffness and collision detection/resolution, we apply these principles for a much different application. Using a human to produce a contact scenario with a flexible structure is something, which to the best of our knowledge, has not been documented.

2 Particle Method Formulation

This chapter contains the development of the stretch and bend forces used in the particle method. In order to do so, these forces were first formulated in one-dimension and validated using beam theory. Then, these forces were formulated in three-dimensions and validated using plate theory. Additional forces which were assembled in the equations of motion include: gravitational forces, damping forces, external forces, and the effective force due to pressure.

2.1 One-Dimensional Formulation

As a logical first step, a simple one-dimensional treatment of the particle method accounting for stretch, bend, damping, and external forces is introduced. Then, to validate the MATLAB computer code, results comparing the code to beam theory are presented.

2.1.1 One-Dimensional Stretch Formulation

An arrangement of particles along a line (x-direction) interconnected with simple linear springs can be termed one-dimensional. Forces acting on the particles were assumed to be in the x-y plane and result in deformations in the x-y plane. Stretching was accounted for in the model through the use of simple linear springs between neighboring particles.

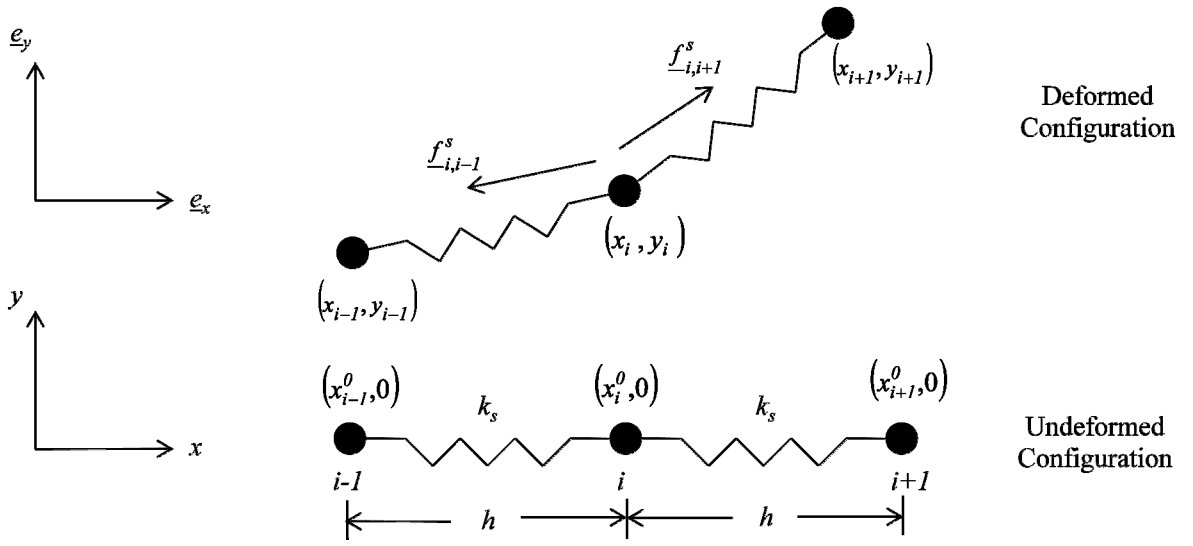

Figure 2.1. Stretching Elements

Figure 2.1 shows the undeformed and deformed configurations of particle *i* and its nearest neighbors. Unit vectors directed along the *x* and *y* coordinate directions are denoted $\underline{e}_x$ and $\underline{e}_y$. The position vectors of the three particles under consideration are $\underline{x}_i$, $\underline{x}_{i-1}$, and $\underline{x}_{i+1}$.

$$\underline{x}_i = x_i \underline{e}_x + y_i \underline{e}_y \tag{2.1}$$

$$\underline{x}_{i-1} = x_{i-1} \underline{e}_x + y_{i-1} \underline{e}_y \tag{2.2}$$

$$\underline{x}_{i+1} = x_{i+1} \underline{e}_x + y_{i+1} \underline{e}_y \tag{2.3}$$

The stretching forces shown acting on particle *i* due to particles *i-1* and *i+1* are the forces, $\underline{f}_{i,i-1}$ and $\underline{f}_{i,i+1}$, respectively. The force on particle *i* due to particle *j* (*j* is either *i-1* or *i+1* in Figure 2.1) was taken from Choi and Ko (2002) and given as

$$\underline{f}^s_i = k_s \left(\left| \underline{x}_{ij} \right| - h \right) \frac{\underline{x}_{ij}}{\left| \underline{x}_{ij} \right|} \tag{2.4}$$

where k_s is the spring constant and

$$\underline{x}_{ij} = \underline{x}_j - \underline{x}_i \tag{2.5}$$

where $|\underline{x}_{ij}|$ is the magnitude of $\underline{x}_{ij}$ and h is the distance or natural length between particles i and j in the undeformed configuration, defined as

$$h = \left| \underline{x}_{ij}^{0} \right| \tag{2.6}$$

In equation 2.6, the superscript 0 refers to the particle coordinates in the undeformed configuration. Then, k_s in equation 2.4 is replaced by k_0/h and written as

$$\underline{f}_i^s = \frac{k_0}{h}\left(\left|\underline{x}_{ij}\right| - h\right)\frac{\underline{x}_{ij}}{\left|\underline{x}_{ij}\right|} \tag{2.7}$$

The stretching stiffness coefficient (which is mesh size dependent) value k_0/h was determined by the following procedure:

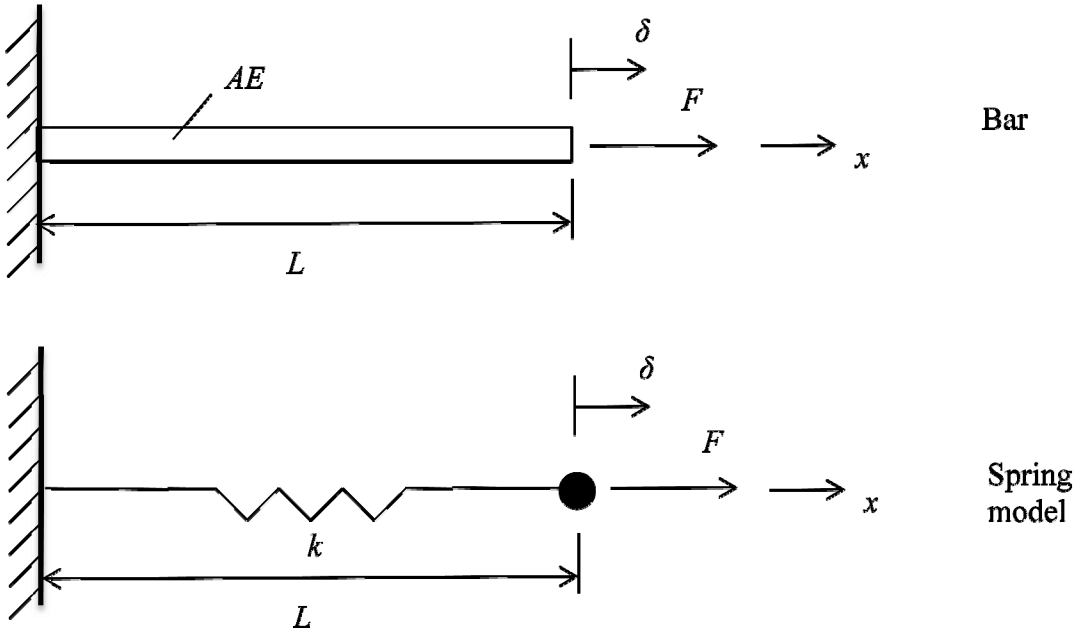

Figure 2.2. Single Spring Model of a Bar

Figure 2.2 shows a single spring particle model of a classical bar element. The spring constant $k = AE/L$, where A is the cross-sectional area, E is the modulus of elasticity, and L is the length of the bar. The force-deflection response of the spring model (or the bar) is

$$F = k\delta = \frac{AE}{L}\delta \tag{2.8}$$

Figure 2.3 shows the case where multiple springs have been used to model the same bar. The spring constant for each of the springs is k_s.

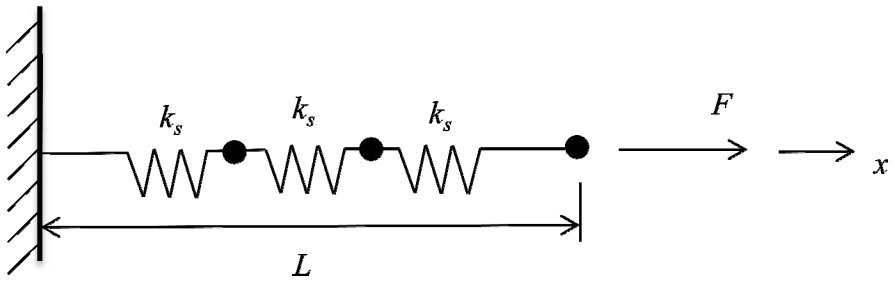

Figure 2.3. Multiple Spring Model of a Bar

Figure 2.3 shows the spring model with three springs (as an example) where k_s is the effective spring constant (equivalent to the particle spring). It is then desired to have equal deflection δ for the single and multiple spring models. For a particle model with n number of springs, the force-deflection response is

$$F = \frac{k_s}{n}\delta \tag{2.9}$$

Then, to match deflections, solving for the effective spring constant k_s,

$$\frac{k_s}{n} = k \tag{2.10}$$

or

$$k_s = nk = nk\frac{L}{L} = \frac{kL}{L/n} = \frac{k_0}{h} \tag{2.11}$$

Note again that *h* is the particle spacing.

Then, boundary conditions require special considerations.

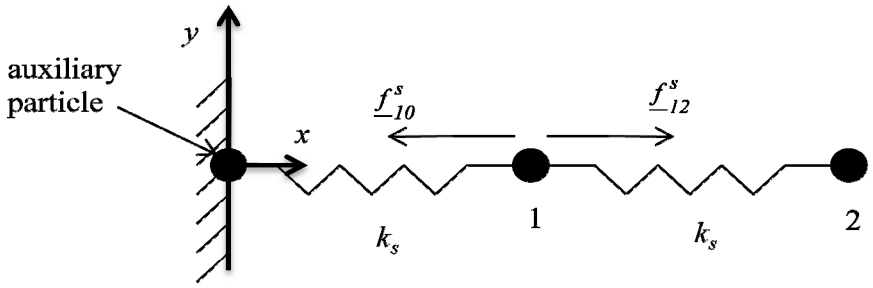

Figure 2.4. Fixed Displacement Boundary Condition for Particle 1

Figure 2.4 shows a fixed displacement boundary condition when the particle being examined is particle 1. When particle 1 is in question, there is a force on particle 1 due to particle 2, $\underline{f}^s_{12}$. An auxiliary particle (fixed position, no position update during simulation) must be placed at position $x = y = 0$ during calculation of the force ($\underline{f}^s_{10}$) on particle 1 due to the fixed displacement boundary condition.

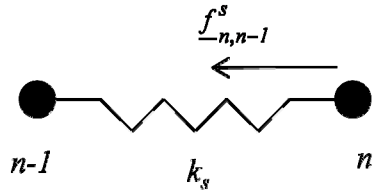

Figure 2.5. Free Edge Boundary Condition for Particle *n*

Figure 2.5 shows a free edge boundary condition when the particle being examined is particle *n*, the last particle. In this case, since there are no particles following particle *n*, the only force accumulated on particle *n* is from particle *n-1*, $\underline{f}^{s}_{n,n-1}$.

2.1.2 One-Dimensional Bend Formulation

In order for a particle mesh to resist bending deformation, the curvature of the particle mesh must be considered. Curvature can be related to the incremental angle change between neighboring particles, as shown in Figure 2.6. The one-dimensional model was developed to include bend forces that resist bending deformation. The bending model has the ability to handle large deflections, as well as small deflections, with small relative rotation. When talking about small relative rotation, this refers to the angle $\Delta\varphi$ in Figure 2.6. In order to calculate $\Delta\varphi$, the unit vectors $\underline{t}_{i-1,i}$, $\underline{t}_{i,i+1}$ and $\underline{t}_{i-1,i+1}$ must be calculated in terms of the particle coordinates. In order to say that the natural length between particles in the deformed configuration was equal to that in the undeformed configuration, the assumption was made that there is small stretching deformation. The bending model to be presented next assumes a uniform particle spacing *h*.

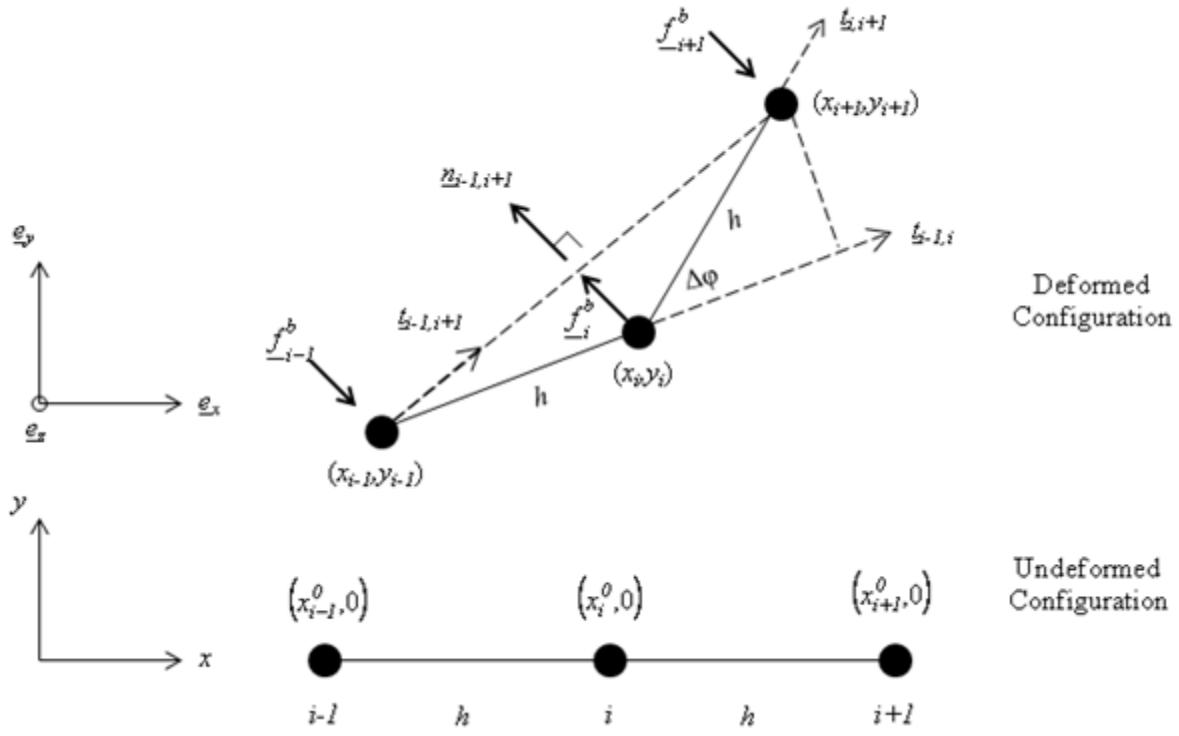

Figure 2.6. Bending Stiffness Element

Figure 2.6 shows a schematic of the bend forces applied to particles *i-1*, *i*, and *i+1* that resist the bending deformation. In order to find the forces, $\underline{f}^b_{i-1}, \underline{f}^b_i$, and $\underline{f}^b_{i+1}$, the following unit vectors $\underline{t}_{i-1,i}$, $\underline{t}_{i,i+1}$ and $\underline{t}_{i-1,\,i+1}$ are defined as:

$$\underline{t}_{i-1,i} = t_{i-1,ix}\,\underline{e}_x + t_{i-1,iy}\,\underline{e}_y = \frac{(x_i - x_{i-1})\underline{e}_x + (y_i - y_{i-1})\underline{e}_y}{\left|\underline{t}_{i-1,i}\right|} \tag{2.12}$$

$$\underline{t}_{i,i+1} = t_{i,i+1x}\,\underline{e}_x + t_{i,i+1y}\,\underline{e}_y = \frac{(x_{i+1} - x_i)\underline{e}_x + (y_{i+1} - y_i)\underline{e}_y}{\left|\underline{t}_{i,i+1}\right|} \tag{2.13}$$

$$\underline{t}_{i-1,i+1} = t_{i-1,i+1x}\,\underline{e}_x + t_{i-1,i+1y}\,\underline{e}_y = \frac{(x_{i+1} - x_{i-1})\underline{e}_x + (y_{i+1} - y_{i-1})\underline{e}_y}{\left|\underline{t}_{i-1,i+1}\right|} \tag{2.14}$$

where

$$\left|\underline{t}_{i-1,i}\right| = \sqrt{(x_i - x_{i-1})^2 + (y_i - y_{i-1})^2} \tag{2.15}$$

$$\left|\underline{t}_{i,i+1}\right| = \sqrt{(x_{i+1} - x_i)^2 + (y_{i+1} - y_i)^2} \tag{2.16}$$

$$\left|\underline{t}_{i-1,i+1}\right| = \sqrt{(x_{i+1} - x_{i-1})^2 + (y_{i+1} - y_{i-1})^2} \tag{2.17}$$

The vector $\underline{n}_{i-1,i+1}$ is normal to the $\underline{t}_{i-1,i+1}$ vector and is computed using a cross product

$$\underline{n}_{i-1,i+1} = \underline{e}_z \times \underline{t}_{i-1,i+1} = -t_{i-1,i+1y}\underline{e}_x + t_{i-1,i+1x}\underline{e}_y \tag{2.18}$$

where $\underline{e}_z = \underline{e}_x \times \underline{e}_y$.

Referring to Figure 2.6, $\Delta\varphi$ is the angle between the vectors $\underline{t}_{i,i+1}$ and $\underline{t}_{i-1,i}$ and is referred to as the bend angle.

$$\Delta\varphi = \arcsin\left(t_{i,i+1y}\right) - \arcsin\left(t_{i-1,iy}\right) \tag{2.19}$$

The curvature at particle i is then approximated using

$$\kappa_i = \frac{\Delta\varphi}{h} \tag{2.20}$$

Then, the bend forces are taken from Bigliani and Eischen (2000) given by

$$\underline{f}^b_{i-1} = -2k_b \frac{\kappa_i}{h}\underline{n}_{i-1,i+1} \tag{2.21}$$

$$\underline{f}^b_{i} = 4k_b \frac{\kappa_i}{h}\underline{n}_{i-1,i+1} \tag{2.22}$$

$$\underline{f}^b_{i+1} = -2k_b \frac{\kappa_i}{h}\underline{n}_{i-1,i+1} \tag{2.23}$$

where $\underline{f}^b_{i-1}, \underline{f}^b_i$, and $\underline{f}^b_{i+1}$ are the forces on the corresponding particles and k_b is termed the bending stiffness coefficient.

Similar to handling stretching, bending also requires special consideration at boundaries.

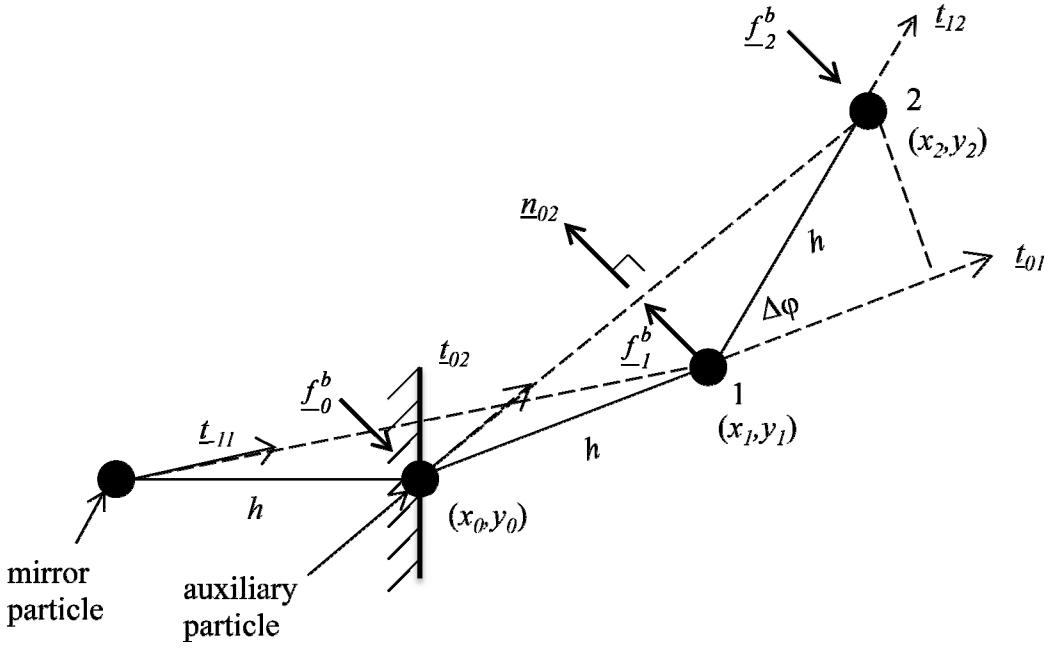

Figure 2.7. Fixed Displacement Boundary Condition for Particle 1

Figure 2.7 shows how a mirror particle and an auxiliary particle must be added to the model when the particle being examined is particle 1, and a fixed edge is present (zero deflection and slope). The reason for this is the bend forces assembled for particle 1 depend on κ_0, κ_1 and κ_2. In order to find κ_0, the equations given above must be used with the mirror particle, auxiliary particle, and particle 1. When examining particle 2, this case differs from the general case because it depends on κ_1. Therefore, the auxiliary particle needs to be used when examining particle 2 as well.

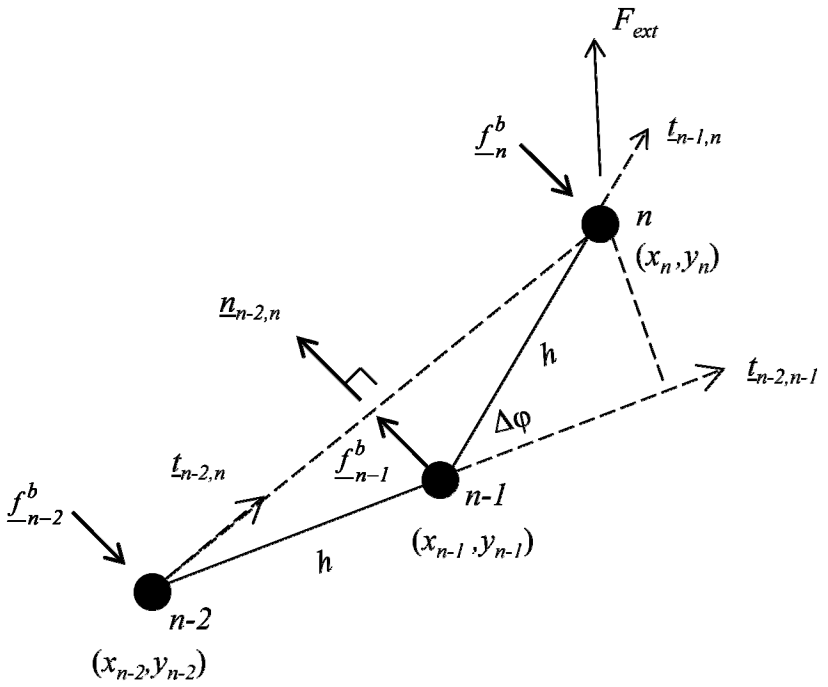

Figure 2.8. Free Edge Boundary Condition for Particle *n*

Figure 2.8 shows a particle at a free end with an applied external force. The curvature, κ_n at the free end is set to zero. As a result, the only force assembled on particle *n* is due to the curvature at particle *n-1*, κ_{n-1}. Particle *n-1* also does not accumulate the three forces $\underline{f}^b_{i-1}, \underline{f}^b_i$, and $\underline{f}^b_{i+1}$ but simply $\underline{f}^b_{i-1}$ and $\underline{f}^b_i$ since $\kappa_n = 0$, $\underline{f}^b_{i+1} = \underline{f}^b_n = 0$.

2.1.3 Damping Force

A velocity dependent force was included in the formulation to enable damping of structural motions, if desired. An absolute damping approach was used and the damping force is calculated according to

$$\underline{f}_i^d = -c\underline{v}_i \tag{2.24}$$

where c is the damping coefficient and $\underline{v}_i$ is the velocity vector at particle i.

2.1.4 One-Dimensional Equation of Motion

Once the stretch, bend, and damping forces have been accumulated for all particles, an equation of motion for the typical particle i can be written as

$$\underline{f}_i^s + \underline{f}_i^b + \underline{f}_i^d + \underline{f}_i^{ext} = m\underline{a}_i \tag{2.25}$$

where $\underline{f}_i^{ext}$ is the external force applied at particle i, m is the mass of particle i, and $\underline{a}_i$ is the acceleration vector of particle i. A similar equation of motion is written for each particle. In this work it has been assumed that the particle mass m was the same for each particle.

2.1.5 One-Dimensional Validation with Beam Theory

To validate the particle model, the results were compared with several classical deflection solutions based on small and large deflection theory.

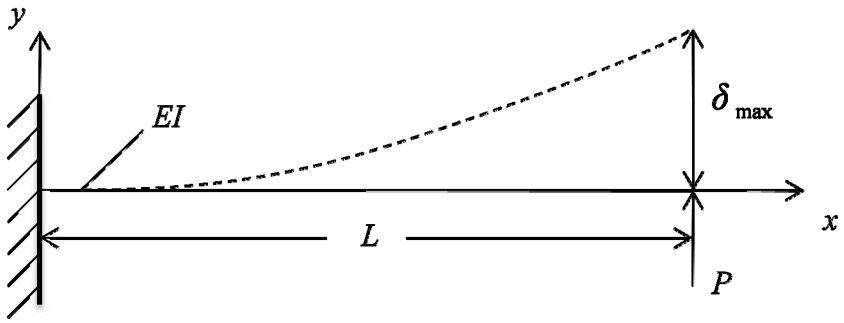

Figure 2.9. Standard Small Deflection Beam Theory Parameters

Figure 2.9 shows the parameters used in standard small deflection beam theory for the deflection of a cantilever beam with a tip load P. The equation for the deflection curve is given as,

$$y = \frac{Px^2}{6EI}(3L - x) \tag{2.26}$$

The tip deflection for beam theory was fixed at $\delta_{\max} = 0.1$ using $P = 1$, $L = 1$, $EI = 3.333$. The deflection curve for beam theory was plotted and used as the baseline for comparison in Figure 2.10. The stiffness coefficient values that were required to match the beam theory tip deflection are shown in Table 2.1.

Table 2.1. Particle Model Stiffness Coefficient Values

# Particles	k_0	k_b
5	4000	2.16
10	4000	1.89
20	4000	1.76
40	4000	1.69

Then, using $m = 1$, $c = 5$, and the stiffness values in Table 2.1 the particle model deflections using 5, 10, 20 and 40 particles were computed and compared with small deflection beam theory in Figure 2.10.

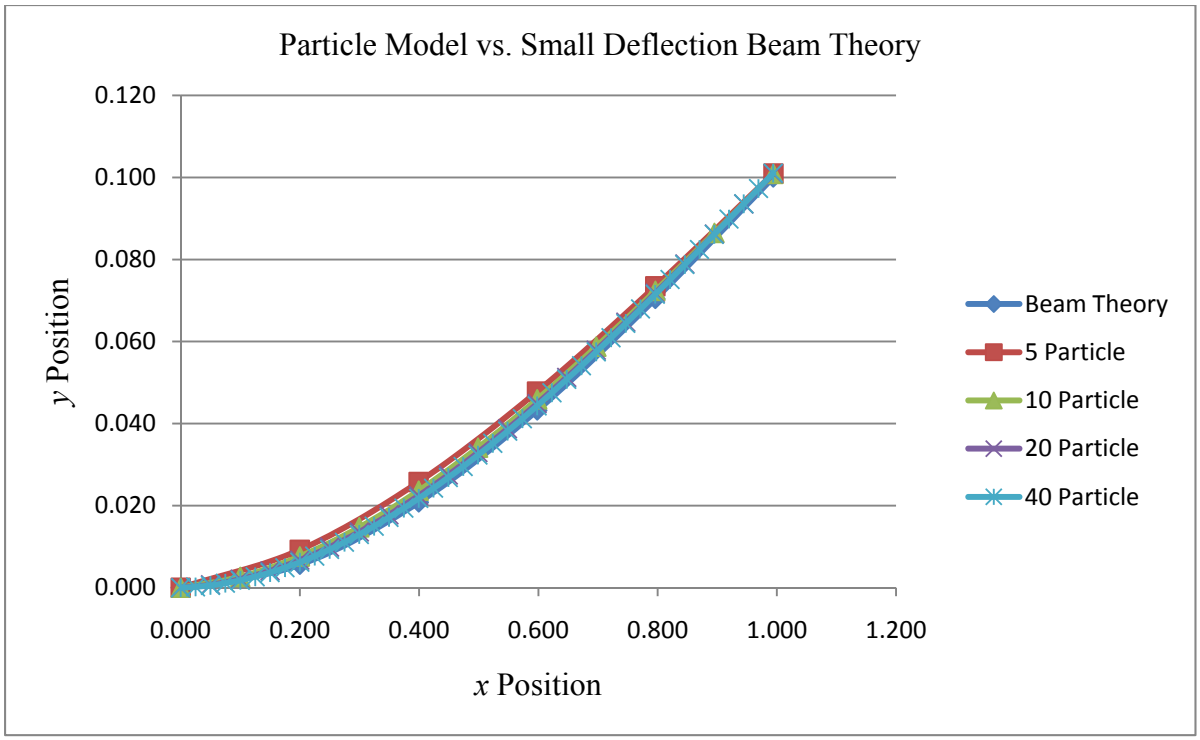

Figure 2.10. Bending Model vs. Small Deflection Beam Theory

Figure 2.10 shows the entire deflection curve for beam theory and the particle method for four different particle meshes. The deflection curve predicted by the particle model converged to the small deflection theory between the ends of the beam.

After finding the model agreed with standard small deflection beam theory, it was validated by large deflection beam theory as well.

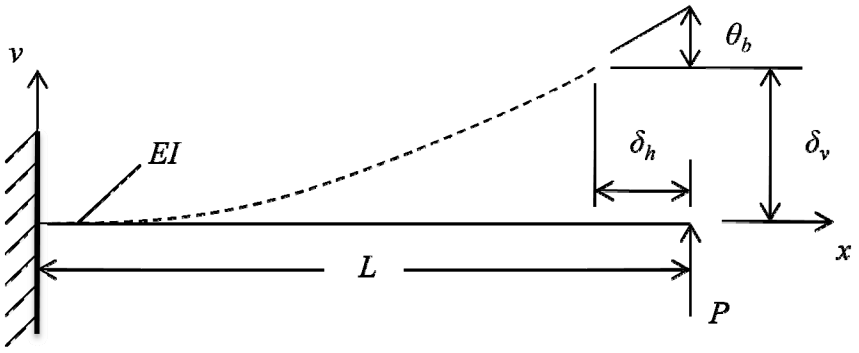

Figure 2.11. Large Deflection Beam Theory Parameters

Figure 2.11 shows the parameters used in large deflection beam theory where δ_h is the longitudinal tip deflection, δ_v is the transverse tip deflection, θ_b is the tip rotation, P is the applied load, and L is the length of the beam. This is based on the formulation presented in Mechanics of Materials by Gere and Timoshenko (1997). For large deflection beam theory,

$$\sqrt{\frac{PL^2}{EI}} = F(k) - F(k,\varphi) \tag{2.27}$$

where

$$k = \sqrt{\frac{1+\sin\theta_b}{2}} \tag{2.28}$$

and

$$\varphi = \sin^{-1}\left(\frac{1}{k\sqrt{2}}\right) \tag{2.29}$$

The complete elliptic integral of the 1st kind is defined as,

$$F(k) = \int_0^{\frac{\pi}{2}} \frac{dt}{\sqrt{1-k^2\sin^2 t}} \tag{2.30}$$

The incomplete elliptic integral of the 1st kind is defined as,

$$F(k,\varphi)=\int_0^{\varphi}\frac{dt}{\sqrt{1-k^2\sin^2 t}} \tag{2.31}$$

The dimensionless transverse tip deflection δ_v/L is

$$\frac{\delta_v}{L}=1-\sqrt{\frac{4EI}{PL^2}}\left[E(k)-E(k,\varphi)\right] \tag{2.32}$$

where *E(k)* is the complete elliptic integral of the 2nd kind

$$E(k)=\int_0^{\frac{\pi}{2}}\sqrt{1-k^2\sin^2 t}dt \tag{2.33}$$

and *E(k,φ)* is the incomplete elliptic integral of the 2nd kind

$$E(k,\varphi)=\int_0^{\varphi}\sqrt{1-k^2\sin^2 t}dt \tag{2.34}$$

The dimensionless longitudinal tip deflection δ_h/L is

$$\frac{\delta_h}{L}=1-\sqrt{\frac{2EI\sin\theta_b}{PL^2}} \tag{2.35}$$

As a result, given the values θ_b and PL^2/EI, the deflections δ_v/L and δ_h/L can be obtained from large deflection beam theory. If PL^2/EI is known, the corresponding load which must be applied to the particle model can be determined since L and EI are also known. Then, after calculating the load which must be applied, it was possible to obtain deflection values, δ_v/L and δ_h/L from the particle model. The stiffness values used for the particle model with large deflection beam theory are the same values shown in Table 2.1 for small deflection theory.

The comparison results for δ_v/L and δ_h/L between large deflection beam theory and the 40 particle model are shown in Table 2.2. The data used for the comparison was the same data used for small deflection theory validation.

Table 2.2. Comparison Results: Large Deflection Theory vs. 40 Particle Model

Large Deflection Theory			40 Particle Model			
θ_b	δ_h	δ_v	δ_x	% Error	δ_v	% Error
0.785	0.16213	0.49551	0.166	2.6%	0.505	1.9%
1.12	0.32912	0.67011	0.336	2.1%	0.682	1.8%
1.41	0.53935	0.80286	0.548	1.7%	0.818	1.9%

The results in Table 2.2 show the percent error values between the deflection values for large deflection theory and the 40 particle model are all less than 2.6 %. This shows that using the k_0 and k_b values tuned for small deflection theory worked for large deflection theory as well.

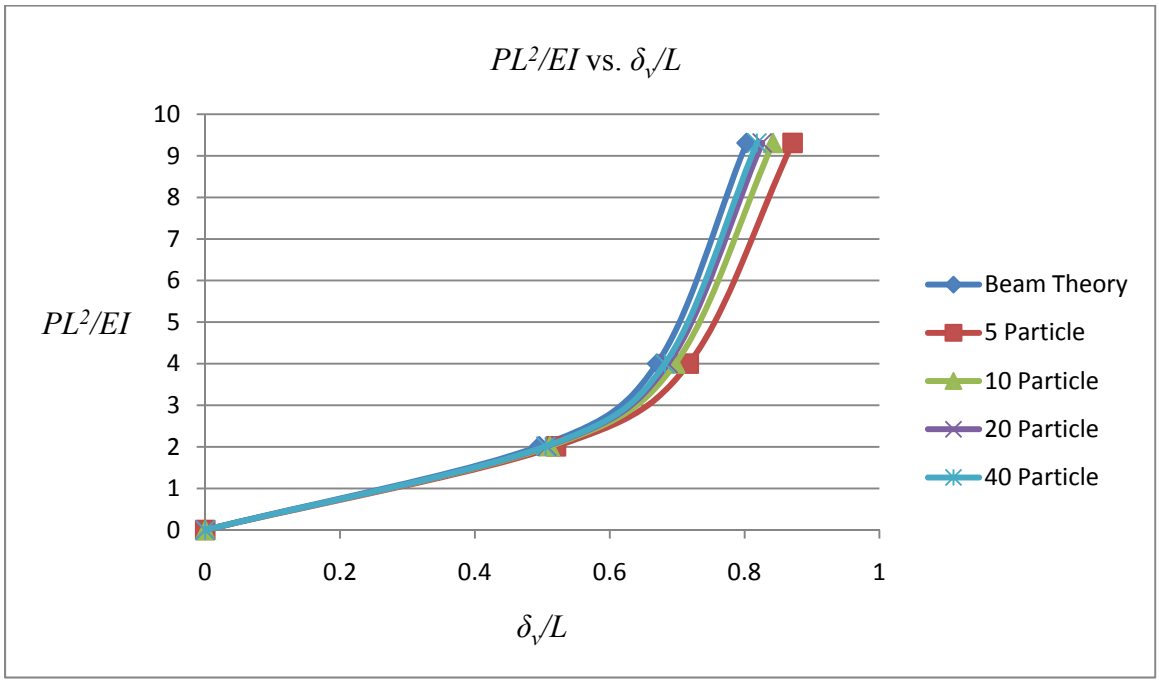

Figure 2.12. PL^2/EI vs. δ_v/L

Figure 2.12 displays PL^2/EI versus δ_v/L for the large deflection beam theory and the four particle model meshes. As the number of particles increased, the particle model converged to the beam theory curve. This is representative of the deflection values presented in Table 2.2.

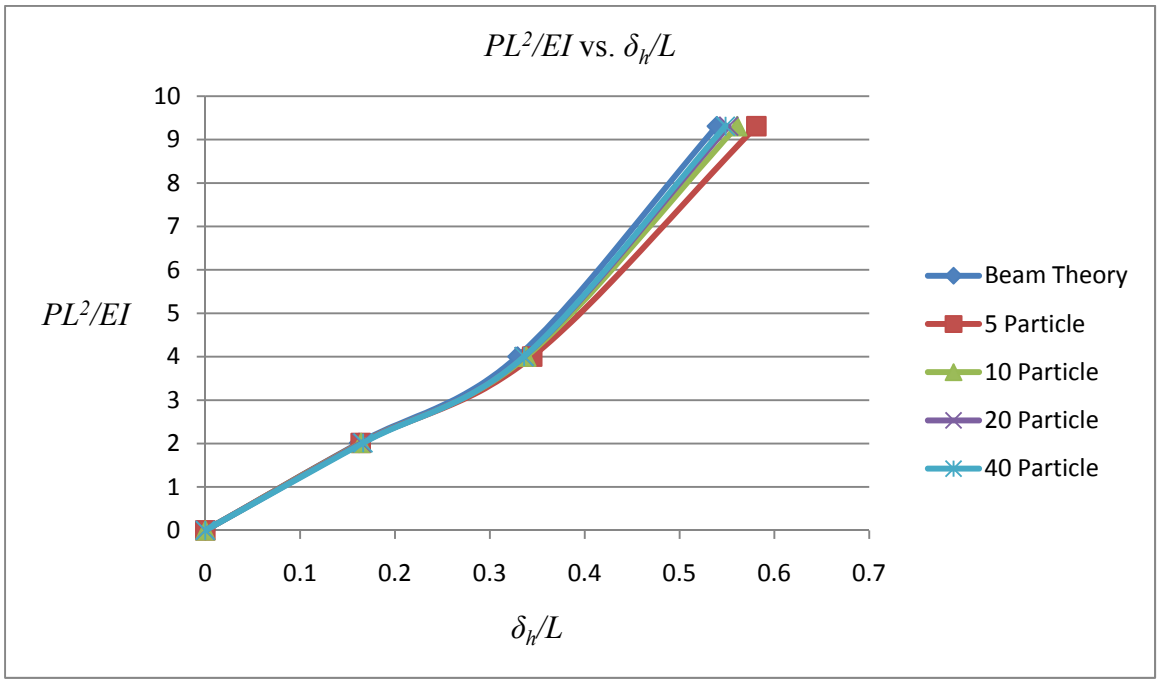

Figure 2.13. PL^2/EI vs. δ_h/L

Figure 2.13 shows the results of PL^2/EI versus δ_h/L for large deflection beam theory and the four particle model meshes. Again, as the number of particles increased, the particle model results converged to the beam theory results. From the results in Figure 2.10, Table 2.2 and Figures 2.12 and 2.13, the particle model has been shown to agree with small deflection theory as well as large deflection theory.

2.2 Three-Dimensional Formulation

In this section, the forces used in the three-dimensional MATLAB computer code are formulated. Additional forces added to the model which were not included in the one-dimensional formulation are: gravitational forces and the effective force due to pressure. In the three-dimensional formulation, a triangular mesh data structure was used by the particle model. The motivation for this mesh structure was the desire to read STL files as input and write STL files as output. STL files use a triangular data structure where the normal to the element and the coordinates of each triangular element vertex are provided. Each vertex for a given triangular element represents a particle on the flexible structure mesh. Using a triangular mesh data structure lends itself well to working with STL files.

2.2.1 Three-Dimensional Stretch Formulation

An arrangement of particles in a general three dimensional arrangement will be treated next. It was assumed that the particle mesh was contained in a plane in the initial undeformed configuration. The formulation of the stretching forces is the same in three dimensions as it is in one dimension, with the difference being the number of particles which contribute forces on particle i. In the one-dimensional case, the stretching forces assembled for particle i were due only to neighboring particles i+1 and i-1. In the three-dimensional case, particle i has an arbitrary number (n) of neighbor particles, all of which contribute forces to particle i.

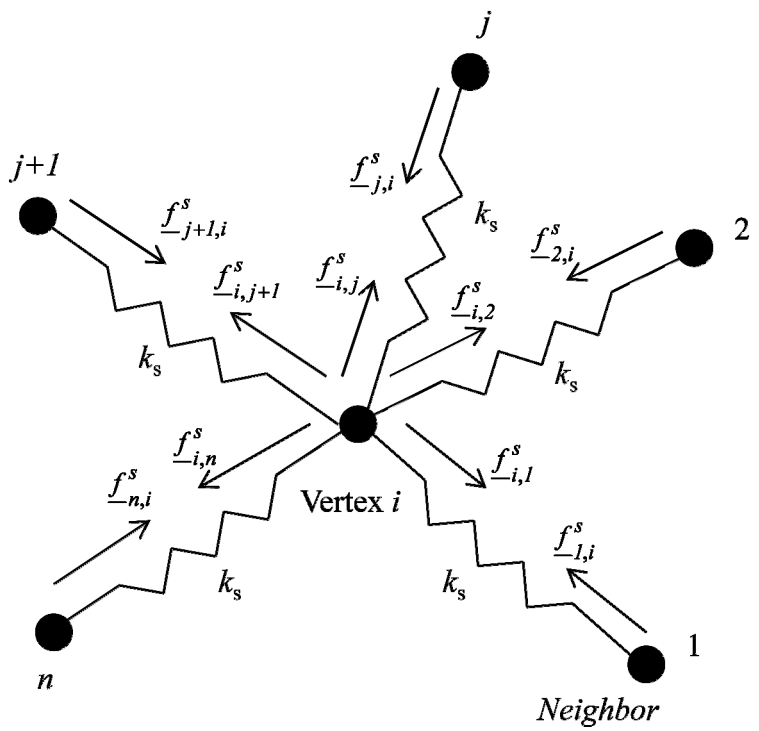

Figure 2.14. 3D Stretching Elements

Figure 2.14 shows the forces on particle i from a general number (n) of neighbor particles. The force $\underline{f}^s_i$ is then the force on particle i due to particle j and is given by

$$\underline{f}^s_i = \sum_{j=1}^{n} \frac{k_0}{h}\left(\left|\underline{x}_{ij}\right| - h\right)\frac{\underline{x}_{ij}}{\left|\underline{x}_{ij}\right|} \tag{2.36}$$

where $k_0 = k_s h$ is the mesh size dependent stretch stiffness coefficient and

$$\underline{x}_i = x_i \underline{e}_x + y_i \underline{e}_y + z_i \underline{e}_z \tag{2.37}$$

$$\underline{x}_j = x_j \underline{e}_x + y_j \underline{e}_y + z_j \underline{e}_z \tag{2.38}$$

whereas before

$$\underline{x}_{ij} = \underline{x}_j - \underline{x}_i \tag{2.39}$$

And again $|\underline{x}_{ij}|$ is the magnitude of $\underline{x}_{ij}$ and h is the spacing between particles i and j in the initial undeformed configuration.

$$h = \left|\underline{x}_{ij}^{0}\right| \tag{2.40}$$

2.2.2 Three-Dimensional Bend Formulation

The three-dimensional bend formulation is a direct extension of the one-dimensional case. Figure 2.15 shows an arbitrary triangular mesh with a zoomed-in view on two typical elements which share a common edge.

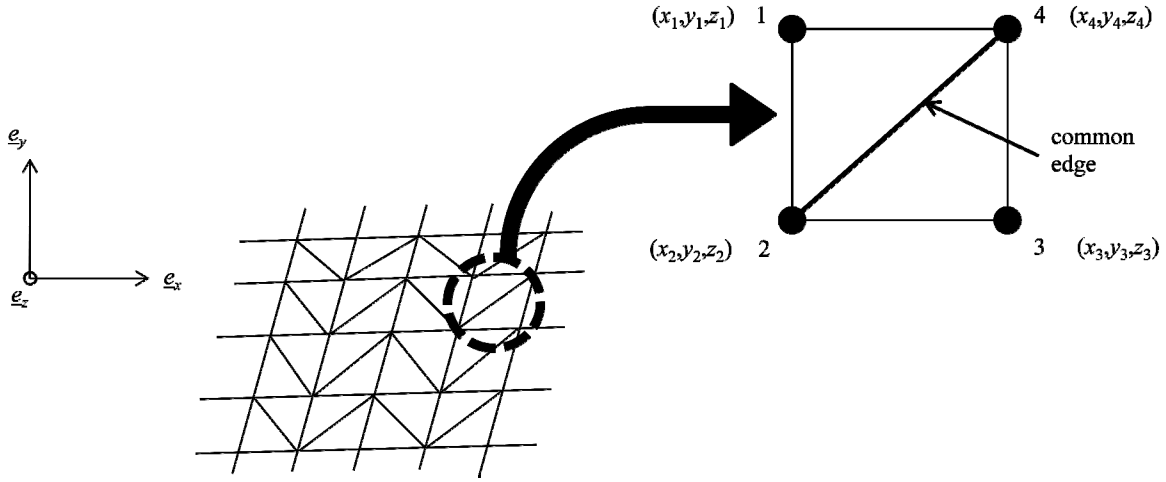

Figure 2.15. Triangular Mesh with Emphasis on Two Elements Sharing Common Edge

By definition, when using a triangular mesh, neighboring elements share one common edge (edge 2-4 in Figure 2.15). Bending deformation is present when the two adjoining planar elements rotate relative to one another around this common edge (axis). The objective is then

to compare the angle change between element 1-2-4 and element 2-3-4. The notation 1-2-4 and 2-3-4 indicates the vertex node numbers of the two elements under consideration. This angle change is termed the bend angle, $\Delta\varphi$. Figure 2.16 shows element 1-2-4 and element 2-3-4 in the undeformed and deformed configurations in which bending occurs along the common edge 2-4. The vectors and unit normal vectors needed to find $\Delta\varphi$ are also shown in Figure 2.16.

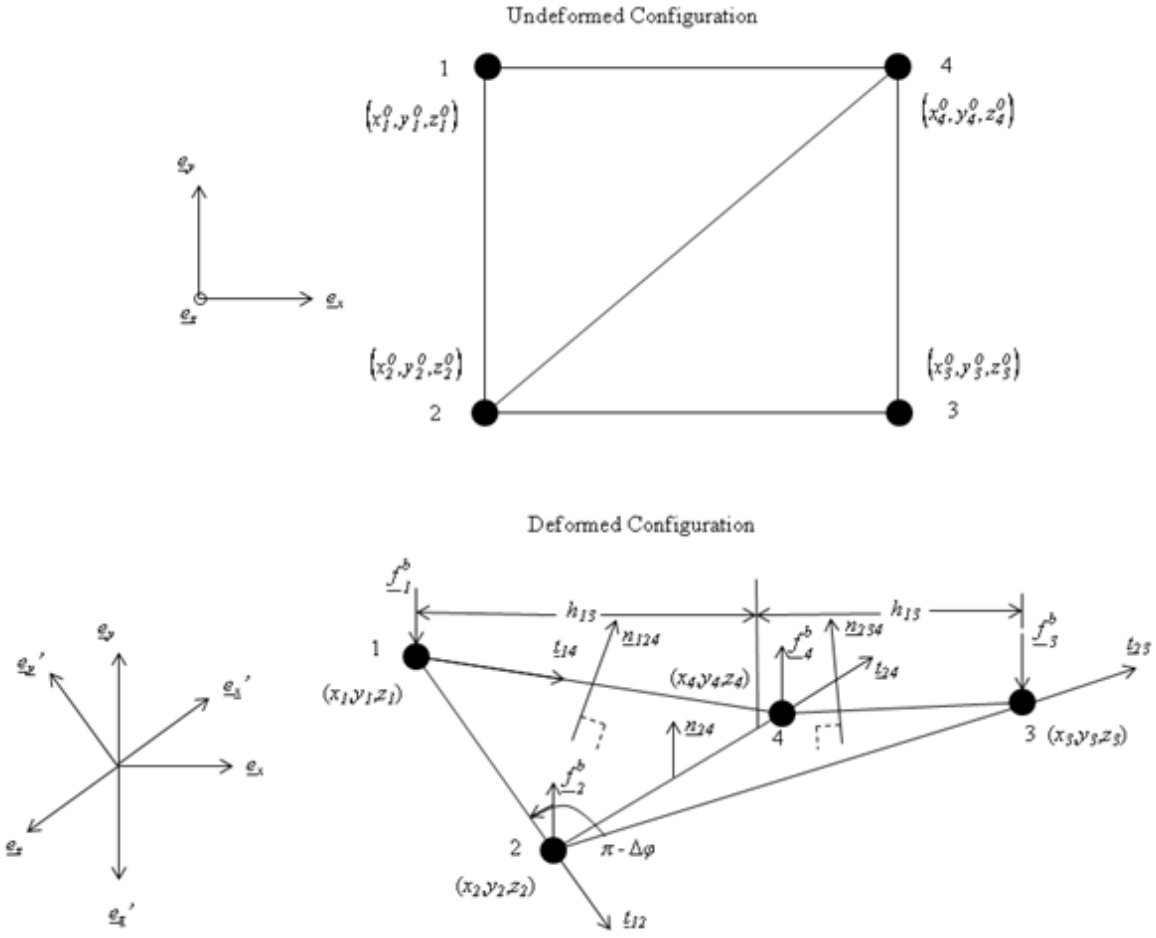

Figure 2.16. 3D Triangular Mesh- Undeformed and Deformed Elements

In order to compute the required normal vectors, several auxiliary vectors are needed. The unit vector directed along the edge between vertices 1 and 2 is

$$\underline{t}_{12} = t_{12x}\underline{e}_x + t_{12y}\underline{e}_y + t_{12z}\underline{e}_z \tag{2.41}$$

where the components of $\underline{t}_{12}$ are

$$t_{12x} = \frac{(x_2 - x_1)}{|\underline{t}_{12}|} \tag{2.42}$$

$$t_{12y} = \frac{(y_2 - y_1)}{|\underline{t}_{12}|} \tag{2.43}$$

$$t_{12z} = \frac{(z_2 - z_1)}{|\underline{t}_{12}|} \tag{2.44}$$

and

$$|\underline{t}_{12}| = \left[(x_2 - x_1)^2 + (y_2 - y_1)^2 + (z_2 - z_1)^2\right]^{\frac{1}{2}} \tag{2.45}$$

The unit vector directed along the edge between vertices 1 and 4 is

$$\underline{t}_{14} = t_{14x}\underline{e}_x + t_{14y}\underline{e}_y + t_{14z}\underline{e}_z \tag{2.46}$$

where the components of $\underline{t}_{14}$ are

$$t_{14x} = \frac{(x_4 - x_1)}{|\underline{t}_{14}|} \tag{2.47}$$

$$t_{14y} = \frac{(y_4 - y_1)}{|\underline{t}_{14}|} \tag{2.48}$$

$$t_{14z} = \frac{(z_4 - z_1)}{|\underline{t}_{14}|} \tag{2.49}$$

and

$$\left|\underline{t}_{14}\right| = \left[(x_4 - x_1)^2 + (y_4 - y_1)^2 + (z_4 - z_1)^2\right]^{\frac{1}{2}} \tag{2.50}$$

Then, the unit normal vector to element 1-2-4 is computed using a cross product according to

$$\underline{n}_{124} = \frac{\underline{t}_{12} \times \underline{t}_{14}}{\left|\underline{t}_{12} \times \underline{t}_{14}\right|} = n_{124x}\underline{e}_x + n_{124y}\underline{e}_y + n_{124z}\underline{e}_z \tag{2.51}$$

where

$$\underline{t}_{12} \times \underline{t}_{14} = \left(t_{12y}t_{14z} - t_{12z}t_{14y}\right)\underline{e}_x + \left(t_{12z}t_{14x} - t_{12x}t_{14z}\right)\underline{e}_y + \left(t_{12x}t_{14y} - t_{12y}t_{14x}\right)\underline{e}_z \tag{2.52}$$

and

$$\left|\underline{t}_{12} \times \underline{t}_{14}\right| = \left[\left(t_{12y}t_{14z} - t_{12z}t_{14y}\right)^2 + \left(t_{12z}t_{14x} - t_{12x}t_{14z}\right)^2 + \left(t_{12x}t_{14y} - t_{12y}t_{14x}\right)^2\right]^{\frac{1}{2}} \tag{2.53}$$

Finally, the components of $\underline{n}_{124}$ are

$$n_{124x} = \frac{\left(t_{12y}t_{14z} - t_{12z}t_{14y}\right)}{\left|\underline{t}_{12} \times \underline{t}_{14}\right|} \tag{2.54}$$

$$n_{124y} = \frac{\left(t_{12z}t_{14x} - t_{12x}t_{14z}\right)}{\left|\underline{t}_{12} \times \underline{t}_{14}\right|} \tag{2.55}$$

$$n_{124z} = \frac{\left(t_{12x}t_{14y} - t_{12y}t_{14x}\right)}{\left|\underline{t}_{12} \times \underline{t}_{14}\right|} \tag{2.56}$$

A similar calculation is required to construct the unit normal vector for element 2-3-4. The vector directed along the edge between vertices 2 and 3 is

$$\underline{t}_{23} = t_{23x}\underline{e}_x + t_{23y}\underline{e}_y + t_{23z}\underline{e}_z \tag{2.57}$$

where the components of $\underline{t}_{23}$ are

$$t_{23x} = \frac{(x_3 - x_2)}{|\underline{t}_{23}|} \tag{2.58}$$

$$t_{23y} = \frac{(y_3 - y_2)}{|\underline{t}_{23}|} \tag{2.59}$$

$$t_{23z} = \frac{(z_3 - z_2)}{|\underline{t}_{23}|} \tag{2.60}$$

where

$$|\underline{t}_{23}| = \left[(x_3 - x_2)^2 + (y_3 - y_2)^2 + (z_3 - z_2)^2\right]^{\frac{1}{2}} \tag{2.61}$$

The unit vector directed along the edge between vertices 2 and 4 is

$$\underline{t}_{24} = t_{24x}\underline{e}_x + t_{24y}\underline{e}_y + t_{24z}\underline{e}_z \tag{2.62}$$

where the components of $\underline{t}_{24}$ are

$$t_{24x} = \frac{(x_4 - x_2)}{|\underline{t}_{24}|} \tag{2.63}$$

$$t_{24y} = \frac{(y_4 - y_2)}{|\underline{t}_{24}|} \tag{2.64}$$

$$t_{24z} = \frac{(z_4 - z_2)}{|\underline{t}_{24}|} \tag{2.65}$$

where

$$|\underline{t}_{24}| = \left[(x_4 - x_2)^2 + (y_4 - y_2)^2 + (z_4 - z_2)^2\right]^{\frac{1}{2}} \tag{2.66}$$

Then, the unit normal vector to element 2-3-4 is

$$\underline{n}_{234} = \frac{\underline{t}_{23} \times \underline{t}_{24}}{\left|\underline{t}_{23} \times \underline{t}_{24}\right|} = n_{234x}\underline{e}_x + n_{234y}\underline{e}_y + n_{234z}\underline{e}_z \tag{2.67}$$

where

$$\underline{t}_{23} \times \underline{t}_{24} = \left(t_{23y}t_{24z} - t_{23z}t_{24y}\right)\underline{e}_x + \left(t_{23z}t_{24x} - t_{23x}t_{24z}\right)\underline{e}_y + \left(t_{23x}t_{24y} - t_{23y}t_{24x}\right)\underline{e}_z \tag{2.68}$$

and

$$\left|\underline{t}_{23} \times \underline{t}_{24}\right| = \left[\left(t_{23y}t_{24z} - t_{23z}t_{24y}\right)^2 + \left(t_{23z}t_{24x} - t_{23x}t_{24z}\right)^2 + \left(t_{23x}t_{24y} - t_{23y}t_{24x}\right)^2\right]^{\frac{1}{2}} \tag{2.69}$$

Finally, the components of $\underline{n}_{234}$ are

$$n_{234x} = \frac{\left(t_{23y}t_{24z} - t_{23z}t_{24y}\right)}{\left|\underline{t}_{23} \times \underline{t}_{24}\right|} \tag{2.70}$$

$$n_{234y} = \frac{\left(t_{23z}t_{24x} - t_{23x}t_{24z}\right)}{\left|\underline{t}_{23} \times \underline{t}_{24}\right|} \tag{2.71}$$

$$n_{234z} = \frac{\left(t_{23x}t_{24y} - t_{23y}t_{24x}\right)}{\left|\underline{t}_{23} \times \underline{t}_{24}\right|} \tag{2.72}$$

The vector bisecting the angle between $\underline{n}_{124}$ and $\underline{n}_{234}$ is simply the average of $\underline{n}_{124}$ and $\underline{n}_{234}$

$$\underline{n}_{avg} = \frac{n_{124x} + n_{234x}}{2}\underline{e}_x + \frac{n_{124y} + n_{234y}}{2}\underline{e}_y + \frac{n_{124z} + n_{234z}}{2}\underline{e}_z \tag{2.73}$$

where

$$\left|\underline{n}_{avg}\right| = \left[\left(\frac{n_{124x} + n_{234x}}{2}\right)^2 + \left(\frac{n_{124y} + n_{234y}}{2}\right)^2 + \left(\frac{n_{124z} + n_{234z}}{2}\right)^2\right]^{\frac{1}{2}} \tag{2.74}$$

Defining the unit vector along $\underline{n}_{\text{avg}}$ as $\underline{n}_{24}$ gives

$$\underline{n}_{24} = \frac{\underline{n}_{\text{avg}}}{\left|\underline{n}_{\text{avg}}\right|} = n_{24x}\underline{e}_x + n_{24y}\underline{e}_y + n_{24z}\underline{e}_z \tag{2.75}$$

where the components of $\underline{n}_{24}$ are

$$n_{24x} = \frac{\left(\frac{n_{124x} + n_{234x}}{2}\right)}{\left|\underline{n}_{avg}\right|} \tag{2.76}$$

$$n_{24y} = \frac{\left(\frac{n_{124y} + n_{234y}}{2}\right)}{\left|\underline{n}_{avg}\right|} \tag{2.77}$$

$$n_{24z} = \frac{\left(\frac{n_{124z} + n_{234z}}{2}\right)}{\left|\underline{n}_{avg}\right|} \tag{2.78}$$

Referring to Figure 2.16, the angle between the unit normal vectors $\underline{n}_{124}$ and $\underline{n}_{234}$ (bend angle) is

$$\begin{gathered}\Delta\phi = -sign(\underline{t}_{12} \bullet \underline{n}_{234}) \cos^{-1}\left(\underline{n}_{124} \bullet \underline{n}_{234}\right) \\ \Delta\phi = -sign\,(\underline{t}_{12} \bullet \underline{n}_{234})\cos^{-1}(n_{124x}n_{234x} + n_{124y}n_{234y} + n_{124z}n_{234z})\end{gathered} \tag{2.79}$$

The *sign* term accounts for the relative rotation of element 2-3-4 with respect to element 1-2-4, i.e. a positive angle change is counter-clockwise rotation while negative angle change is clockwise rotation. The characteristic arc-length h_{13}^0 used to approximate the curvature is half the distance between vertices 1 and 3 in the undeformed configuration (see Figure 2.16).

$$h_{13}^0 = \frac{1}{2}\sqrt{\left(x_1^0 - x_3^0\right)^2 + \left(y_1^0 - y_3^0\right)^2 + \left(z_1^0 - z_3^0\right)^2} \tag{2.80}$$

It has been assumed that negligible stretch exists and that the distance between vertices 1 and 3 changes very little during deformation. So, the curvature defined by the relative rotation between the elements is,

$$\kappa = \frac{\Delta\phi}{h_{13}^0} \tag{2.81}$$

Finally, the bend forces are constructed following the one-dimensional treatment, with an adjustment to account for the fact that they are directed along $\underline{n}_{24}$

$$\underline{f}_1^b = -2k_b \frac{\kappa}{h_{13}^0} \underline{n}_{24} \tag{2.82}$$

$$\underline{f}_2^b = 2k_b \frac{\kappa}{h_{13}^0} \underline{n}_{24} \tag{2.83}$$

$$\underline{f}_3^b = -2k_b \frac{\kappa}{h_{13}^0} \underline{n}_{24} \tag{2.84}$$

$$\underline{f}_4^b = 2k_b \frac{\kappa}{h_{13}^0} \underline{n}_{24} \tag{2.85}$$

2.2.3 Boundary Conditions

The three-dimensional bending stiffness formulation was equipped with the capability of enforcing boundary conditions at a given particle where this particle can either be fixed (simply supported) or free. If the particle was simply supported, displacement but not rotation of this particle was prohibited. Therefore, if all the particles on a given edge were simply supported, this edge was essentially hinged since a hinge prevents displacement but not rotation. Fixed (clamped or cantilever) boundary conditions were not treated.

2.2.4 Initially Curved Surfaces

For a flexible structure which begins as a curved surface or its elements meet at a curved junction, an initial curvature was computed. The initial curvature for each bend element was stored. Then, the bend forces depend on the difference between the current and the initial curvature.

2.2.5 Gravitational Forces

In order to produce realistic results, a gravitational force was incorporated in the formulation. The gravitational force is given simply as,

$$\underline{f}_i^g = f_{gx}\underline{e}_x + f_{gy}\underline{e}_y + f_{gz}\underline{e}_z = m_i g_x \underline{e}_x + m_i g_y \underline{e}_y + m_i g_z \underline{e}_z \tag{2.86}$$

where m_i is the particle mass and either g_x, g_y, or g_z is equal to the gravitational acceleration constant g, depending on the direction in which gravity acts.

2.2.6 Effective Force due to Pressure

The ability to handle pressure loading was another important effect that needed to be treated in the particle method formulation. Figure 2.17 shows a typical element (assume vertex numbers 1-2-4) with unit normal vector $\underline{n}_{124}$ and uniform pressure p.

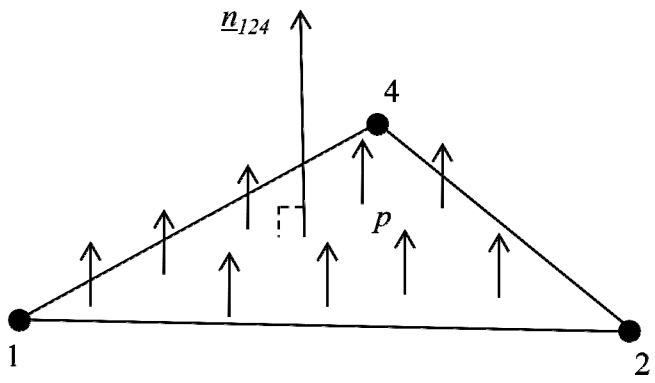

Figure 2.17. Applied Uniform Pressure on Element 1-2-4

As the unit normal vector and the pressure are oriented in Figure 2.17, the effective forces acting on the element vertices are calculated according to

$$\underline{f}_i^p = \frac{pA}{3}\underline{n}_{124} \tag{2.87}$$

where A is the element area. If the pressure and unit normal vectors are oriented in opposite directions, a negative sign would be introduced in equation 2.87.

2.2.7 Damping Force

As with the one-dimensional formulation, a velocity dependent force was included in the three-dimensional formulation to enable damping of structural motions, if desired. An absolute damping approach was used and the damping force was calculated according to

$$\underline{f}_i^d = -c\underline{v}_i \tag{2.88}$$

where c is the damping coefficient and $\underline{v}_i$ is the velocity vector at particle i.

2.2.8 Equations of Motion

The equation of motion for particle i can be written as

$$\underline{f}_i^s + \underline{f}_i^b + \underline{f}_i^g + \underline{f}_i^p + \underline{f}_i^d + \underline{f}_i^{ext} = m_i \underline{a}_i \tag{2.89}$$

where m_i is the mass of particle i and $\underline{a}_i$ is the acceleration vector for particle i.

MATLAB has been used to implement the particle element formulation algorithm. Appendix A contains the MATLAB particle code that accumulates the equations of motion for all of the particles. An explicit fourth-order Runge-Kutta method (Abramowitz & Stegun, 1972) was employed to solve the equations of motion. Refer to Appendix B for the fourth-order Runge-Kutta MATLAB code.

2.2.9 Three-Dimensional Validation with Plate Theory

To validate the particle model, results obtained from the particle model were compared with the results from classical plate theory (Timoshenko & Woinowsky-Krieger, 1959). To obtain results, an initially flat, square flexible structure with dimensions $L_x = L_y = 1$ (arbitrary units) was discretized with an 11 x 11 mesh of particles (121 total particles with 200 triangular elements) shown in Figure 2.18. Refer to Appendix C to view the input file read by the MATLAB computer code to obtain coordinate and connectivity information for the mesh.

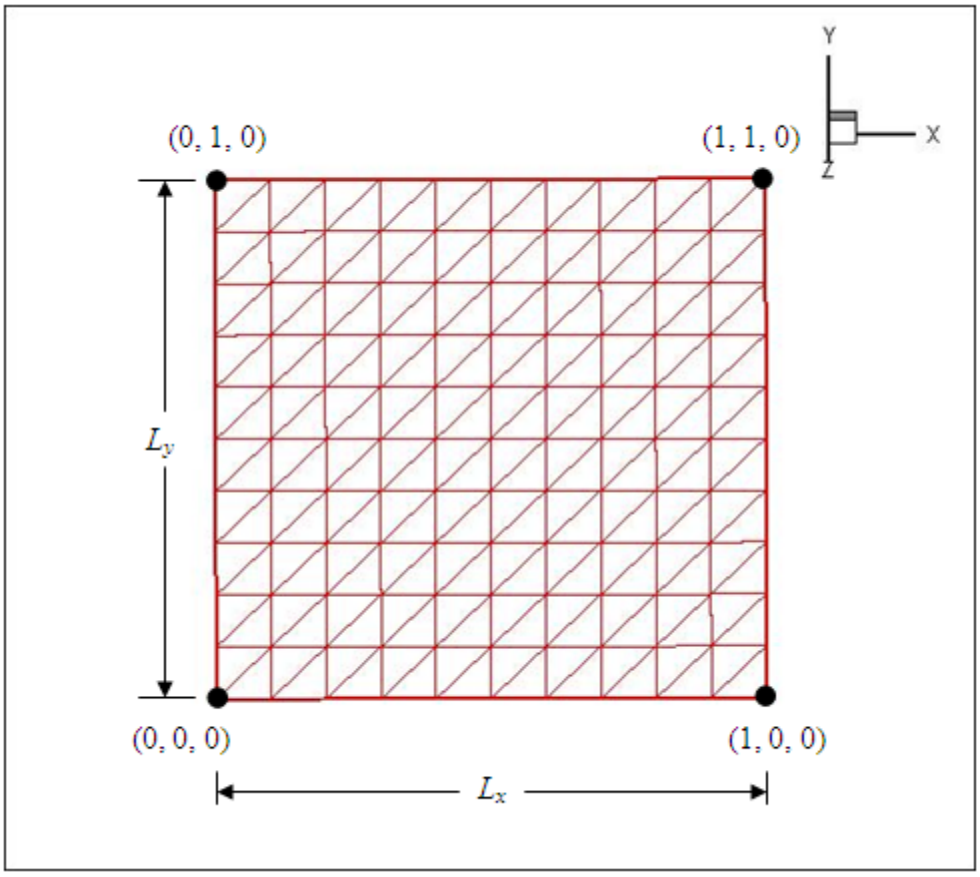

Figure 2.18. Flexible Structure: Triangular Mesh

The flexible structure was simply supported on all four edges. A point load *P* was applied at the center, shown in Figure 2.19.

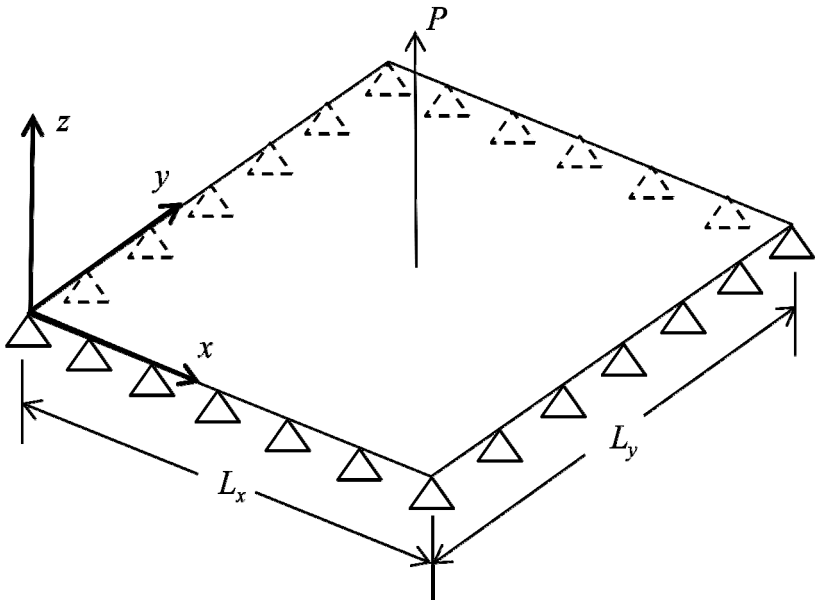

Figure 2.19. Simply Supported on all Four Sides, Center Point Load

The formula for the deflection of such a square plate from the classical theory is

$$\delta_z = \frac{4P}{\pi^4 L_x L_y D} \sum_{m=1}^{\#terms} \sum_{n=1}^{\#terms} \frac{\sin\left(\frac{m\pi\xi}{L_x}\right)\sin\left(\frac{n\pi\eta}{L_y}\right)}{\left(\frac{m^2}{L_x{}^2}+\frac{n^2}{L_y{}^2}\right)^2} \sin\left(\frac{m\pi x}{L_x}\right)\sin\left(\frac{n\pi(L_y-y)}{L_y}\right) \qquad (2.90)$$

where D is the bending/flexural rigidity of the plate, ζ is the x-location of the load point, η is the y-location of the load point, while x and y are the coordinates of the point in question. For the maximum deflection at the center, equation 2.90 reduces to

$$\delta_z = \frac{4PL_x{}^2}{\pi^4 D} \sum_{m=1}^{\#terms} \sum_{n=1}^{\#terms} \frac{1}{\left(m^2+n^2\right)^2} \qquad (2.91)$$

The data used for the particle model was: $P = 1$, $m = 1$, $c = 0.5$, $L_x = L_y = 1$, $k_0 = 1$, $k_b = 0.0345$ (arbitrary units). The value of k_0 was chosen arbitrarily while the k_b value was chosen to limit

the maximum particle model deflection to 0.1 ± 0.001 for the given applied load P. The value of D was adjusted in computation of the theoretical deflection so that the center deflection predicted by plate theory matched the particle model result (both giving δ_z = 0.1004). The required value for D was 0.11509.

Table 2.3 shows the results of the particle model deflection compared with the theoretical results.

Table 2.3: Square Plate, Deflection Results, Comparing Particle Model with Plate Theory

		Particle Model	Plate Theory	
x	y	δ_z	δ_z	% Error
0	0.5	0.0000	0.0000	0.0%
0.1	0.5	0.0232	0.0221	4.8%
0.2	0.5	0.0474	0.0540	12.2%
0.3	0.5	0.0704	0.0796	11.5%
0.4	0.5	0.0902	0.0952	5.3%
0.5	0.5	0.1004	0.1004	0.0%
0.6	0.5	0.0902	0.0952	5.3%
0.7	0.5	0.0704	0.0796	11.5%
0.8	0.5	0.0474	0.0540	12.2%
0.9	0.5	0.0232	0.0221	4.8%
1	0.5	0.0000	0.0000	0.0%

Table 2.3 shows the deflection values for the particles along the line y = 0.5. Since the deflection at the center was forced to be equal for plate theory and the particle model, a 0.0 % error is shown in Table 2.3 at the center of the plate. Also, since all four edges were simply supported, the deflection of the two edge particles located along the line y = 0.5 was also zero. The maximum error occurs at x = 0.2 and x = 0.8 with just over 12 % error. One major

assumption with plate theory is it is based solely on bending stiffness; membrane (stretching) stiffness is neglected. When attempting to use the particle model with $k_0 = 0$, the model did not produce favorable results. Therefore, stretching stiffness was included in the model which may provide an explanation for the discrepancies between plate theory and the particle model. Figure 2.20 shows a graphical representation of the comparison of the deflection curves shown in Table 2.3.

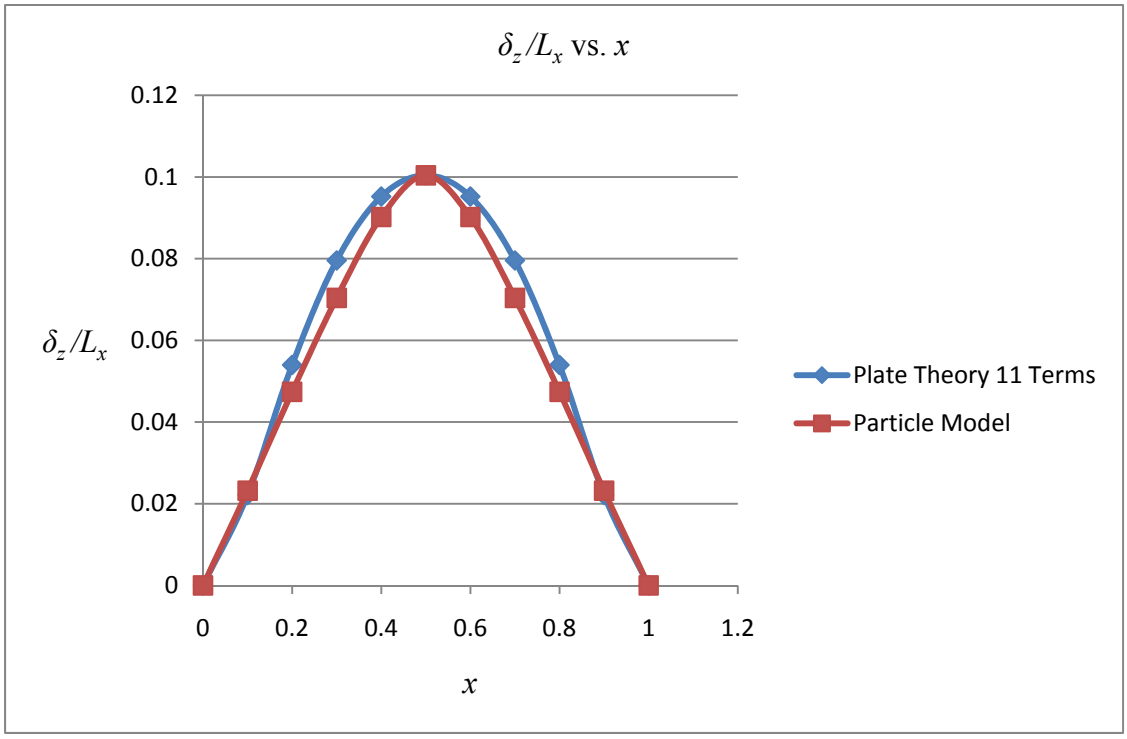

Figure 2.20. δ_z/L_x vs. x: Particle Model Compared with First 11 Terms of Plate Theory (for $y = 0.5$)

Figure 2.20 shows the particle model curve matches the plate theory curve between the edges very closely. The points on the curves which do not match exactly are highlighted by the percent error values reported in Table 2.3.

Next, to investigate the effect of the bending stiffness coefficient on the deformation of the structure, deflection curves generated by the particle model were created as the value of k_b was varied for several values of k_0. The flexible structure shown in Figure 2.18 was used to produce the results for the load case and boundary conditions shown in Figure 2.19. Figure 2.21 shows δ_z/L_x vs. k_b for the k_0 values 1, 5, 10 and 20. The dimensionless deflection δ_z/L_x was computed at the center particle.

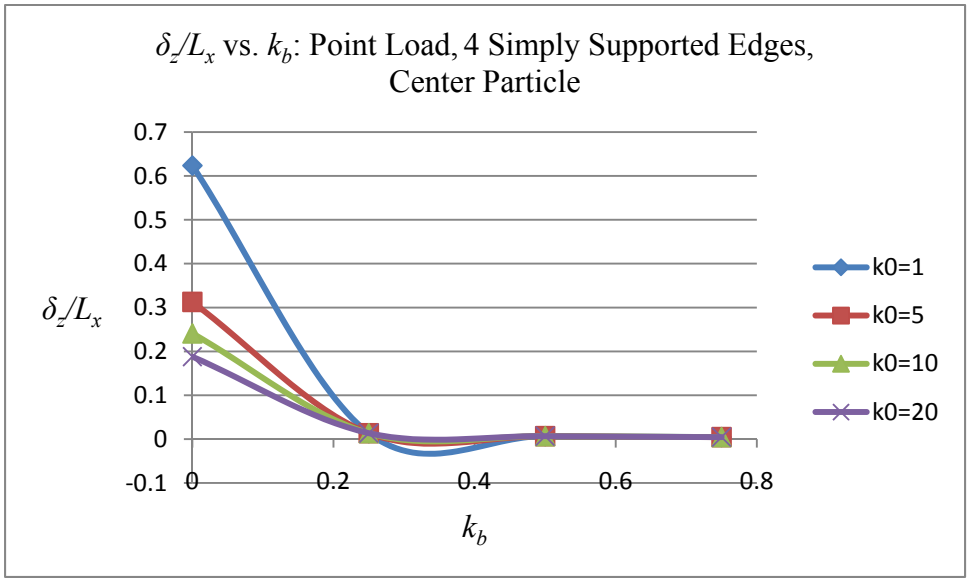

Figure 2.21. δ_z/L_x vs. k_b, Point Load, 4 Simply Supported Edges, Center Particle

Figure 2.21 shows the relationship between changing the k_0 and k_b values. When $k_b = 0$, the deflection decreases as k_0 increases, as expected. Then, for a fixed value of k_0, as k_b increases, the deflection converges to a fixed value ($\delta_z/L_x = 0.0045$). Thus for very high bending stiffness, the deflection was controlled by the stretching springs.

Then, to qualitatively check that the particle model was deforming as expected, contour plots for several load cases were examined. Figure 2.22 shows the loading and boundary

conditions along with the contour plot of the final deformed mesh for the given load-case. The parameters used were: $P = 1$, $L_x = L_y = 1$.

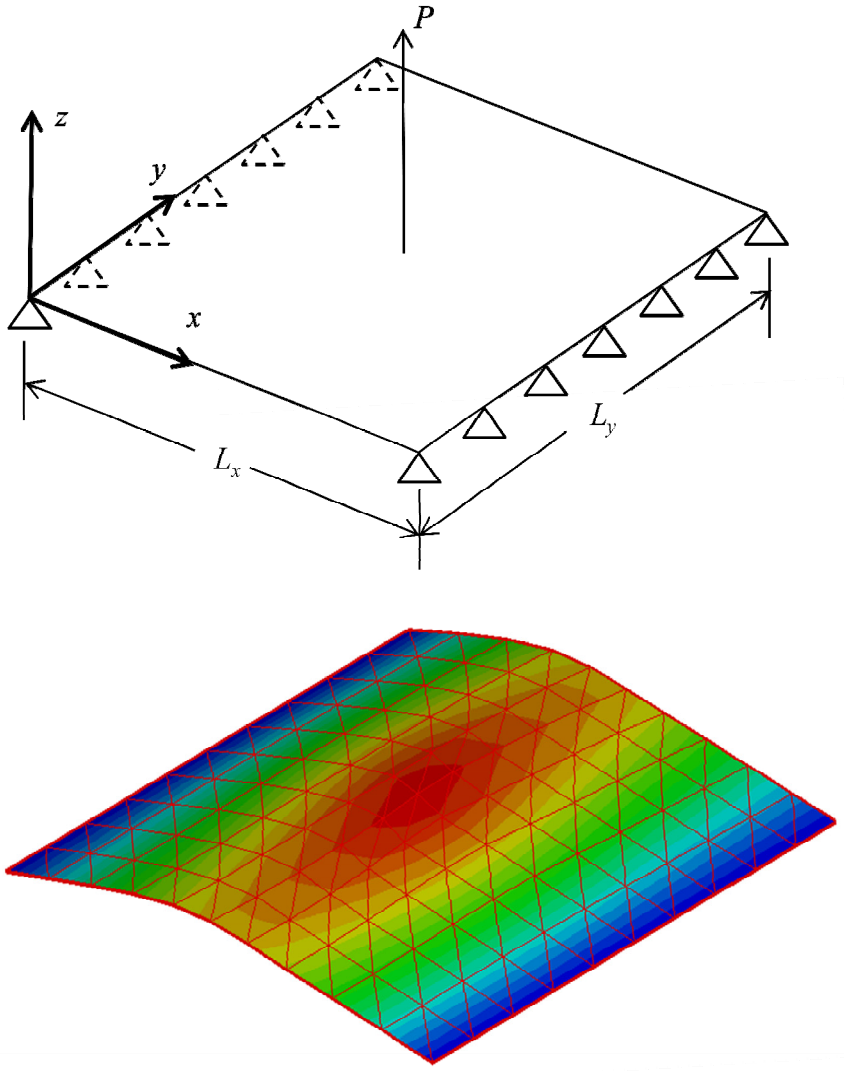

Figure 2.22. Simply Supported on Two Edges with a Center Point Load

Examining the final deformed shape of the particle mesh makes it easier to visualize how the mesh deforms due to an applied point load. For a center point load applied in the positive *z*-

direction with two simply supported edges, Figure 2.22 shows the contour plot of the final deformed shape of the mesh. The largest deflection (shown in red) occurred at the point of the applied load, as expected. The deformation of the mesh was symmetric, with the smallest deflection occurring at the two simply supported edges (shown in blue).

In the next case, the particle mesh was simply supported on two edges with a line load along $x = 0.5$ in the positive z-direction. Figure 2.23 shows the loading and boundary conditions along with the contour plot of the final deformed mesh for this case. The parameters used were: $P = 1$, $L_x = L_y = 1$.

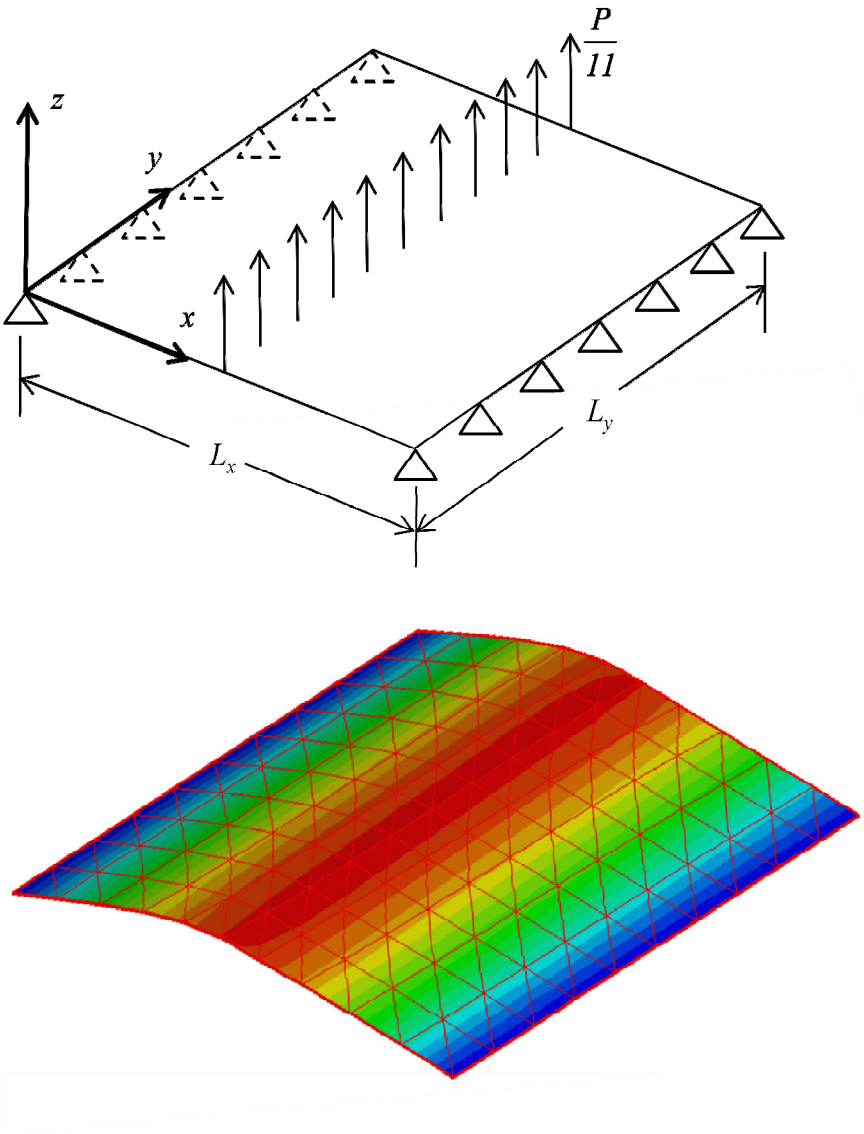

Figure 2.23. Simply Supported on Two Edges with a Line Load

Figure 2.23 shows the maximum deflection occurred along the line of applied load where the deflection was also uniform as expected. Again, the minimum deflection occurs at the two simply supported edges and the deformation of the mesh was symmetric.

Then, the next load-case was used to validate the particle model with plate theory. The mesh was simply supported on all four edges with a center point load applied in the positive *z*-direction. Figure 2.24 shows the loading and boundary conditions along with the final contour plot of the deformed mesh for this case. The parameters used were: $P = 1$, $L_x = L_y = 1$.

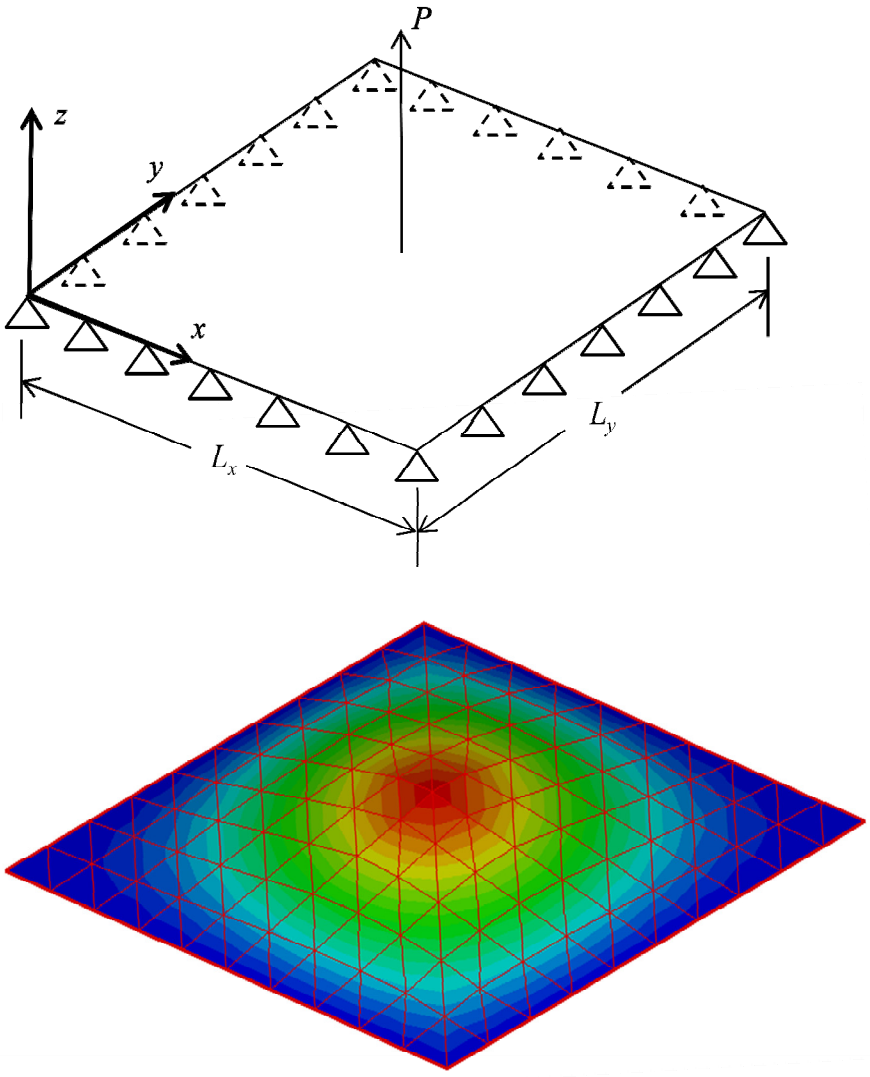

Figure 2.24. Simply Supported on all Four Edges with a Center Point Load

As expected, the largest deflection occurred at the point of the applied load and the deformation of the mesh was symmetric. The smallest deflection occurred at all four simply supported edges.

Finally, the last case was a mesh simply supported on all four edges with a line load applied at $x = 0.5$ in the positive z-direction. Figure 2.25 shows the loading and boundary conditions along with the contour plot of the final deformed mesh for this case. The parameters used were: $P = 1$, $L_x = L_y = 1$.

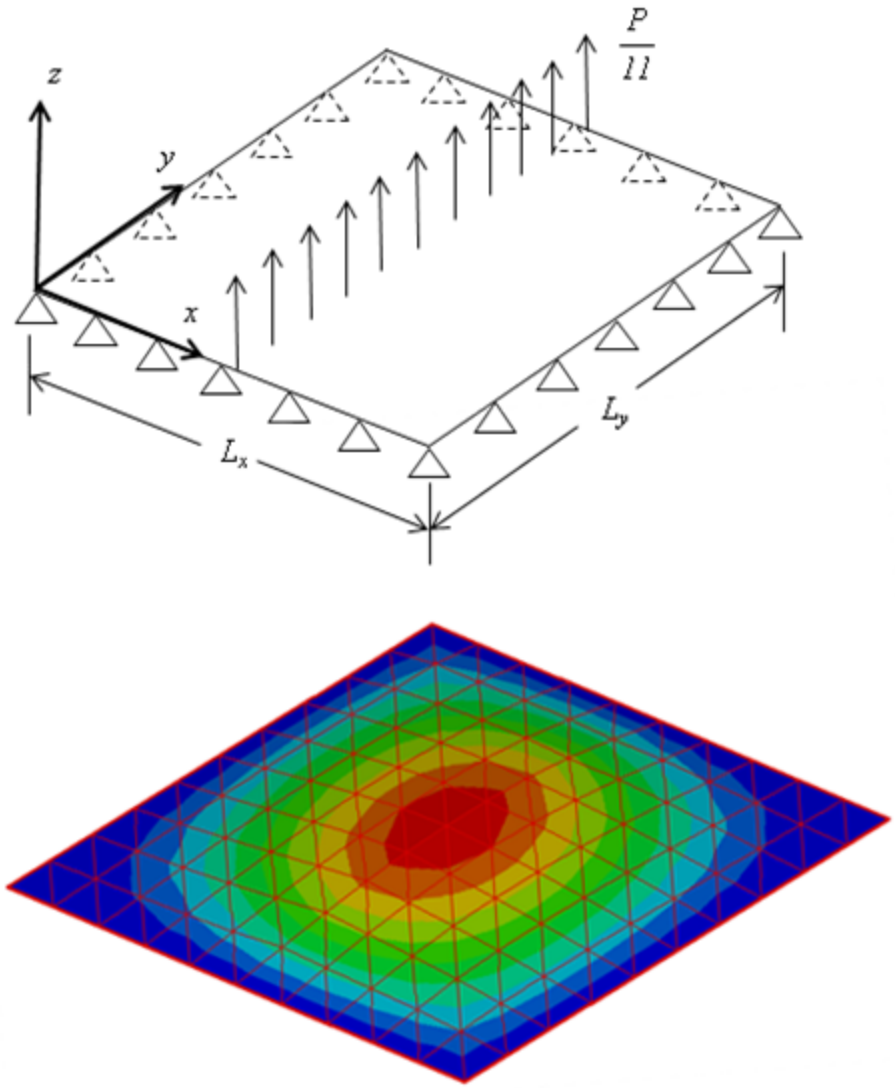

Figure 2.25. Simply Supported on all Four Edges with a Line Load

Figure 2.25 shows the largest deflection occurred for three particles along the line of the applied load but deflection was limited near the edges due to the simply supported condition. The deflection differs in Figure 2.25 from that of Figure 2.24 because the load was distributed along the line $x = 0.5$, rather than applying the full magnitude of the load at the

center particle. This qualitative analysis showed that for a set of load-cases, the particle model deformed as expected.

3 Contact Formulation

One of the project goals was to account for the interaction between a rigid impactor, modeled as a moving surface meshed with triangular elements, with a flexible structure, also modeled with a triangular mesh of particles. The positions of the impactor vertices are tracked to detect whether they have crossed any elements on the flexible structure. The flexible structure was modeled with the particle method formulation discussed in the previous chapter. The basic contact detection scheme must determine whether the impactor vertices have pierced structural elements, and if so, appropriate action must be taken.

Contact is often times a very difficult, yet very important issue. When speaking of contact, there are generally two steps to every contact algorithm, contact detection and contact correction. The algorithm described in this chapter uses a point-to-plane contact detection scheme with an update made to the velocity of the element vertices when contact has been detected.

3.1 Contact Detection

The contact algorithm uses a point (impactor vertices)-to-plane (structural element) detection scheme. In order to detect contact between the impactor vertices and the flexible structure elements, it must first be determined which particle element, if any, an impactor vertex has crossed. In terms of computer programming, the contact algorithm is computationally demanding; requiring a loop over all possible flexible structure contact elements within a loop over all impactor vertices. The nearest projection of an impactor vertex onto a structural

element was based on the point-to-plane method. Figure 3.1 shows the ultimate goal of implementing the contact algorithm: to handle the contact sequence of a human (modeled as a surface mesh of impactor vertices) and a tent door (modeled as a surface mesh of structural elements).

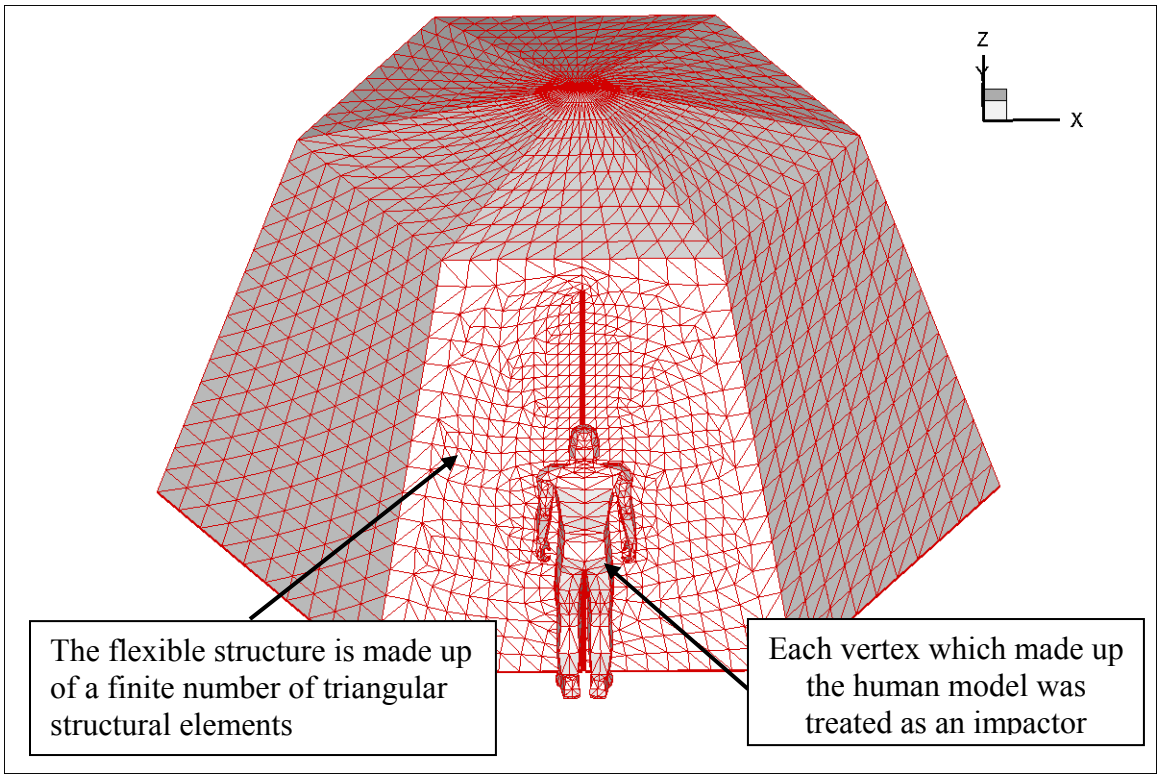

Figure 3.1. Defining the Ultimate Goal of the Contact Algorithm

This complex problem can be simplified by discussing a single impactor vertex, *P* and a single structural element *i-j-k*. Figure 3.2 introduces a schematic of the four possible contact situations for a given impactor vertex where element *i-j-k* is viewed on edge.

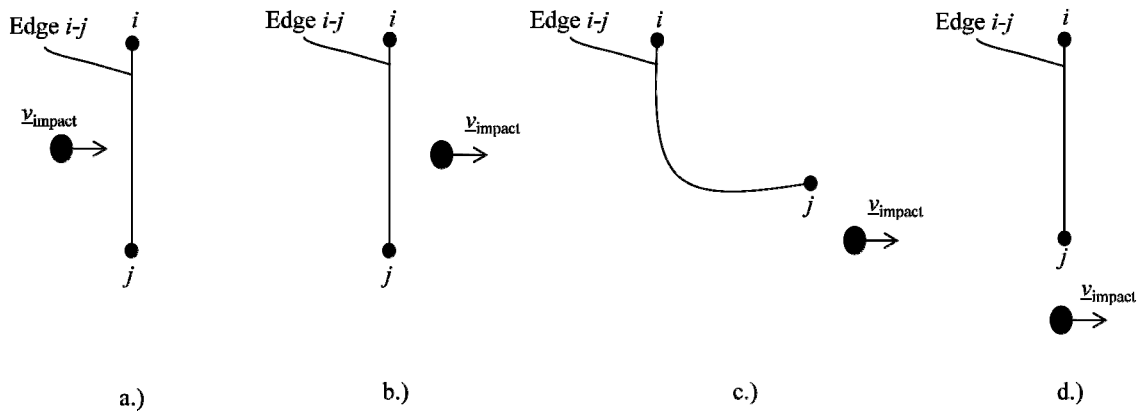

Figure 3.2. Possible Contact Situations

Figure 3.2.a. shows a typical impactor vertex approaching the structural element *i-j-k*. The projection of this vertex would lie within a structural element on the flexible structure mesh. At this point, since the impactor has not yet crossed the element, contact should not be detected. At some later time, after having crossed the element this impactor vertex would be at a position as in Figure 3.2.b. Again, the projection of this vertex would lie within a structural element on the flexible structure mesh and contact should be detected. Determining whether contact has occurred will be described in more detail in Section 3.2. Then, at some time later than that of Figure 3.2.b. the impactor vertex would be at a position as in Figure 3.2.c. At this time, the projection of the impactor vertex would not lie within a structural element on the flexible structure mesh; contact should no longer be detected. Finally, Figure 3.2.d. shows an impactor vertex whose projection does not lie within a structural element on the flexible structure mesh and whose projection will never lie within a structural element. As a result, contact should never be detected. Figure 3.2 illustrates the

possible contact situations which had to be accounted for when developing the contact algorithm.

Figure 3.3 shows vertices *i*, *j*, and *k* of a typical structural element. By definition these three vertices lie in a plane, shown in grey in the figure.

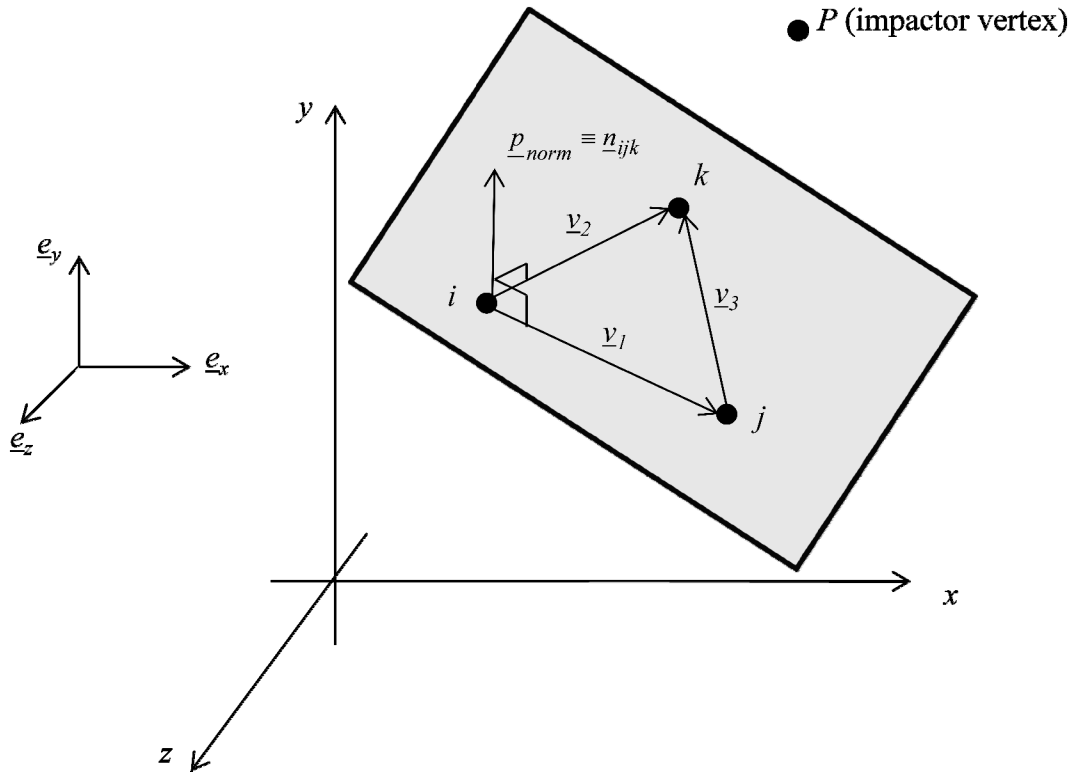

Figure 3.3. Plane *ijk*

Plane *ijk* is the plane defined by element *i*-*j*-*k* in the *xyz*-coordinate system. The position vectors of points *i*, *j*, and *k* are $\underline{x}_i$, $\underline{x}_j$, and $\underline{x}_k$, respectively where

$$\underline{x}_i = x_i \underline{e}_x + y_i \underline{e}_y + z_i \underline{e}_z \tag{3.1}$$

$$\underline{x}_j = x_j \underline{e}_x + y_j \underline{e}_y + z_j \underline{e}_z \tag{3.2}$$

$$\underline{x}_k = x_k \underline{e}_x + y_k \underline{e}_y + z_k \underline{e}_z \tag{3.3}$$

The position vector of impactor vertex P is $\underline{P}$ where

$$\underline{P} = P_x \underline{e}_x + P_y \underline{e}_y + P_z \underline{e}_z \tag{3.4}$$

Then, $\underline{v}_1$ is a vector which points from vertex i to j, $\underline{v}_2$ is a vector which points from vertex i to k, and $\underline{v}_3$ is a vector which points from vertex j to k, i.e.

$$\underline{v}_1 = \underline{x}_j - \underline{x}_i = (x_j - x_i)\underline{e}_x + (y_j - y_i)\underline{e}_y + (z_j - z_i)\underline{e}_z \tag{3.5}$$

$$\underline{v}_2 = \underline{x}_k - \underline{x}_i = (x_k - x_i)\underline{e}_x + (y_k - y_i)\underline{e}_y + (z_k - z_i)\underline{e}_z \tag{3.6}$$

$$\underline{v}_3 = \underline{x}_k - \underline{x}_j = (x_k - x_j)\underline{e}_x + (y_k - y_j)\underline{e}_y + (z_k - z_j)\underline{e}_z \tag{3.7}$$

The unit normal to element i-j-k, $\underline{p}_{\text{norm}}$, is found by taking the cross product of $\underline{v}_1$ and $\underline{v}_2$. Note that the unit normal $\underline{p}_{\text{norm}}$ discussed here in the contact development chapter is equivalent to $\underline{n}_{124}$ or $\underline{n}_{234}$ developed in the three-dimensional bend formulation (Section 2.2.2).

$$\underline{p}_{norm} = \underline{p}_{normx}\underline{e}_x + \underline{p}_{normy}\underline{e}_y + \underline{p}_{normz}\underline{e}_z = \frac{\underline{v}_1 \times \underline{v}_2}{\left|\underline{v}_1 \times \underline{v}_2\right|}$$

$$\underline{p}_{norm} = \frac{(v_{1y}v_{2z} - v_{1z}v_{2y})\underline{e}_x + (v_{1z}v_{2x} - v_{1x}v_{2z})\underline{e}_y + (v_{1x}v_{2y} - v_{1y}v_{2x})\underline{e}_z}{\left|\underline{v}_1 \times \underline{v}_2\right|} \tag{3.8}$$

Figure 3.4 illustrates the closest projection of point P on the plane defined by element i-j-k. This point on the plane is denoted Q.

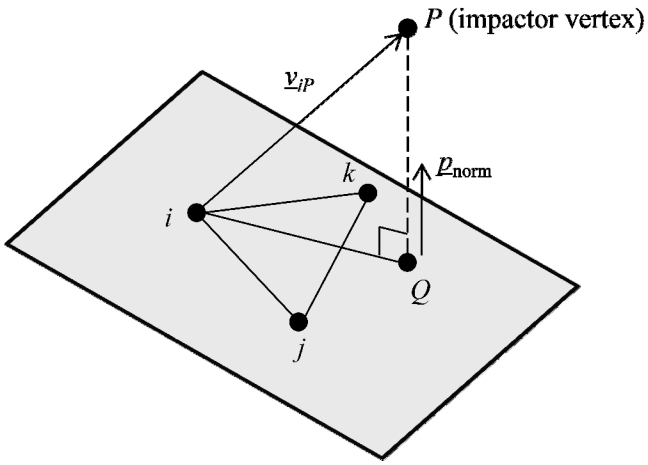

Figure 3.4. Closest Projection of Point *P* onto the Plane

The vector $\underline{v}_{iP}$ which points from vertex *i* to point *P* is calculated according to

$$\underline{v}_{iP} = \underline{P} - \underline{x}_i = (P_x - x_i)\underline{e}_x + (P_y - y_i)\underline{e}_y + (P_z - z_i)\underline{e}_z \tag{3.9}$$

Then, the vector which points from *Q* to *P* along the normal direction $\underline{p}_{\text{norm}}$ is

$$\underline{v}_{QP} = v_{QPx}\underline{e}_x + v_{QPy}\underline{e}_y + v_{QPz}\underline{e}_z = (\underline{p}_{norm} \bullet \underline{v}_{iP})\underline{p}_{norm} \tag{3.10}$$

The position vector of point *Q* can be obtained from

$$\underline{Q} = \underline{P} - \underline{v}_{QP} \tag{3.11}$$

The point *Q* does not necessarily lie within element *i-j-k*, only in the plane defined by element *i-j-k*.

Before continuing with the development of the contact algorithm, it is useful to illustrate the contact detection sequence. Figure 3.5 shows the before and after configurations of the impactor vertex and the structural element during a typical contact detection sequence. Providing a visual representation of the contact algorithm is helpful in improving the understanding of the basic idea which defines contact.

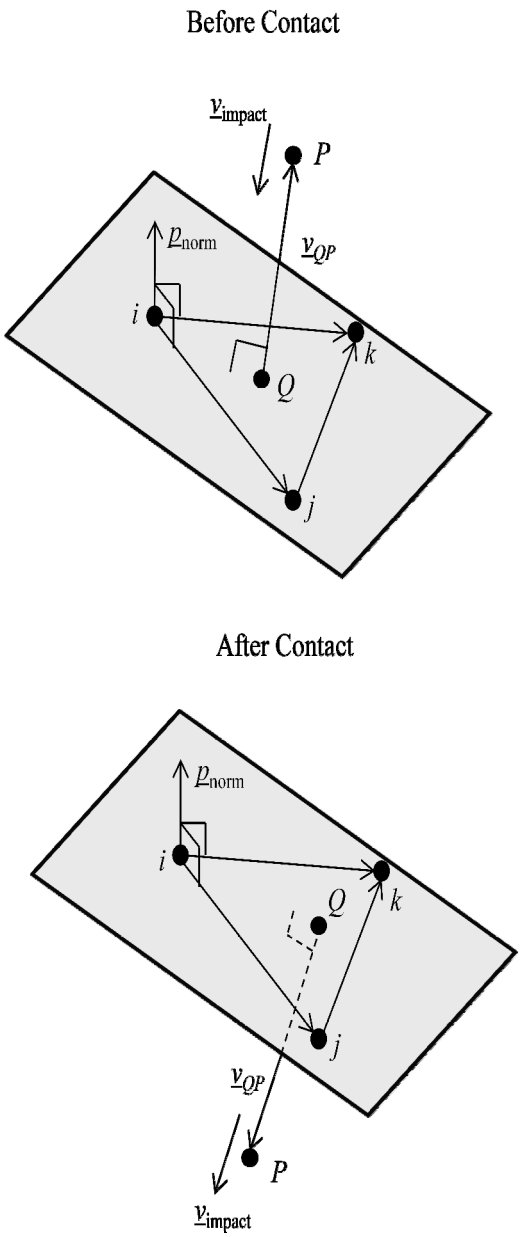

Figure 3.5. Before and After Configurations used to Define Contact

Contact is defined when the relative orientation of the unit normal vector, $\underline{p}_{norm}$ and the vector $\underline{v}_{QP}$ changes. When this occurs, the impactor vertex is said to have "penetrated" the structural element. Up until this point, it has not yet been defined in which structural element

contact occurs. It is necessary to determine which structural element, if any, contains the projection Q of a given impactor vertex. Therefore, determining whether or not point Q lies within element *i-j-k* is the next issue.

In order to do so, the distance from each vertex in element *i-j-k* to point Q is calculated.

$$\underline{iQ} = \underline{Q} - \underline{x}_i = (Q_x - x_i)\underline{e}_x + (Q_y - y_i)\underline{e}_y + (Q_z - z_i)\underline{e}_z \tag{3.12}$$

and

$$\underline{jQ} = \underline{Q} - \underline{x}_j = (Q_x - x_j)\underline{e}_x + (Q_y - y_j)\underline{e}_y + (Q_z - z_j)\underline{e}_z \tag{3.13}$$

and

$$\underline{kQ} = \underline{Q} - \underline{x}_k = (Q_x - x_k)\underline{e}_x + (Q_y - y_k)\underline{e}_y + (Q_z - z_k)\underline{e}_z \tag{3.14}$$

Figure 3.6 shows the case when point Q is contained inside element *i-j-k* with vectors $\underline{iQ}$, $\underline{jQ}$, and $\underline{kQ}$ defined along with the subdivided areas A_1, A_2, and A_3.

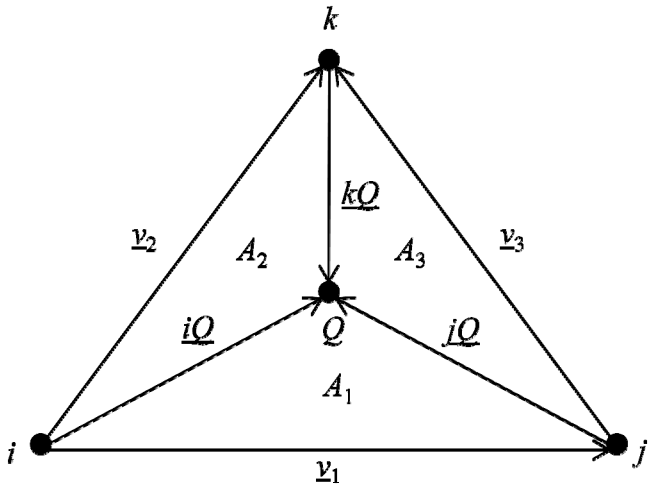

Figure 3.6. Point Q Projected Inside Element *i-j-k*

The total area A for element *i-j-k* can be conveniently calculated with a cross product

$$A = \frac{1}{2}\left|\underline{v}_1 \times \underline{v}_2\right| = \frac{1}{2}\left|(v_{1y}v_{2z} - v_{1z}v_{2y})\underline{e}_x + (v_{1z}v_{2x} - v_{1x}v_{2z})\underline{e}_y + (v_{1x}v_{2y} - v_{1y}v_{2x})\underline{e}_z\right| \tag{3.15}$$

The three sub-areas defined by point Q and vertices i, j, k are

$$A_1 = \frac{1}{2}\left|\underline{v}_1 \times \underline{iQ}\right| = \frac{1}{2}\left|(v_{1y}iQ_z - v_{1z}iQ_y)\underline{e}_x + (v_{1z}iQ_x - v_{1x}iQ_z)\underline{e}_y + (v_{1x}iQ_y - v_{1y}iQ_x)\underline{e}_z\right| \tag{3.16}$$

and

$$A_2 = \frac{1}{2}\left|\underline{iQ} \times \underline{v}_2\right| = \frac{1}{2}\left|(iQ_y v_{2z} - iQ_z v_{2y})\underline{e}_x + (iQ_z v_{2x} - iQ_x v_{2z})\underline{e}_y + (iQ_x v_{2y} - iQ_y v_{2x})\underline{e}_z\right| \tag{3.17}$$

and

$$A_3 = \frac{1}{2}\left|\underline{v}_3 \times \underline{jQ}\right| = \frac{1}{2}\left|(v_{3y}jQ_z - v_{3z}jQ_y)\underline{e}_x + (v_{3z}jQ_x - v_{3x}jQ_z)\underline{e}_y + (v_{3x}jQ_y - v_{3y}jQ_x)\underline{e}_z\right| \tag{3.18}$$

When point Q lies within element *i-j-k*, the total area A must be the same as the sum of the sub-areas, i.e.

$$A = A_1 + A_2 + A_3 \tag{3.19}$$

Figure 3.7 shows the case when point Q does not lie inside element *i-j-k*.

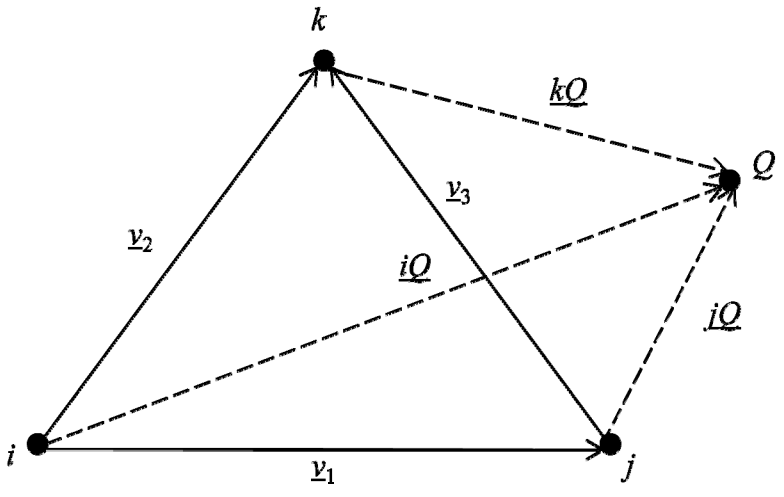

Figure 3.7. Point Q Lying Outside Triangle *ijk*

Now, area A_1 is defined by triangle *ijQ*, A_2 by triangle *ikQ*, and A_3 by triangle *jkQ*. Then, when point *Q* lies outside element *i-j-k*, the sum of the sub-areas is generally greater than *A*, i.e.

$$A_1 + A_2 + A_3 > A \tag{3.20}$$

Before moving forward, it is necessary to determine which impactor vertices may be in contact with which structural elements. In order to do so, the sub-areas defined by equations 3.16, 3.17, and 3.18 are compared with the total area given by equation 3.15. For a given impactor vertex *P*, a search over the number of structural elements on the flexible structure mesh is executed. The conditions which must be checked are:

1. If for impactor vertex *P*, $A_1+A_2+A_3 > A$ for all the structural elements, this impactor vertex will not be in contact with any structural elements; the algorithm stops checking the given impactor vertex for contact.
2. If for impactor vertex *P*, $A_1+A_2+A_3 > A$, but all structural elements have not been checked, the next structural element was checked.
3. If for impactor vertex *P*, $A_1+A_2+A_3 < A$ for a given structural element, then this structural element was determined to be a potential contact element for the given impactor vertex. If this was the case, the algorithm must continue checking for contact.

Next, Table 3.1 describes several important variables used in the contact algorithm which was coded using MATLAB. Provided are the variable name, the initial value, the index range (for array variables), the possible range of values the variable can have, and a short

description. The variable *nimpact* refers to the total number of impactor vertices and the variable *nelem* refers to the total number of structural elements.

Table 3.1. Contact Algorithm Variables

Variable	Initial Value	Index Range	Value Range	Description
contactelem	0	1 : *nimpact*	1 : *nelem*	stores the element where possible contact could occur for a given impactor vertex
trialsign	NA	NA	0,1,-1	a variable which stores the sign of the dot product between the unit normal and the vector $\underline{v}_{QP}$; The values are +1 if the dot product is greater than zero, 0 if it is equal to zero, and -1 if it is less than zero
preimpactdotsign	0	1:*nimpact*	0,1,-1	a variable which stores the sign of the dot product between the unit normal and the vector $\underline{v}_{QP}$ prior to contact; the values are determined just as they are for *trialsign*
maxdist	0	1:*nelem*	NA	a variable used to determine the largest penetration for all contact elements at any given time-step
maxdistnode	0	1:*nelem*	1:*nimpact*	a variable used to store the impactor vertex which has penetrated a given structural element the furthest

The variable *contactelem* was used to store the structural element where contact may possibly occur for each impactor vertex. The process for locating the structural element where contact may possibly occur for a given impactor vertex was just described above. The next four variables are used to determine if contact has been detected. The variable *trialsign*

was assigned the value of the sign (+1, -1, 0) of the dot product between the unit normal vector, p_{norm} and the vector $\underline{v}_{QP}$. Then, *preimpactdotsign* (stores the sign of the dot product between the unit normal vector, p_{norm} and the vector $\underline{v}_{QP}$ prior to contact; shown in the before contact configuration of Figure 3.5) was compared to *trialsign* to determine whether an impactor vertex has penetrated a structural element in any given time-step. If this was the case, contact has been detected. Once contact had been detected, it was important to locate the impactor vertex which had penetrated a given structural element the furthest. This was done using the variable, *maxdist*, which was assigned the value of the distance from point *Q* to point *P*, $|\ \underline{v}_{QP}\ |$ for the impactor vertex which has penetrated the structural element the furthest. The final variable, *maxdistnode*, was assigned the index value of the impactor vertex which has penetrated the structural element the furthest. These variables are used to determine which impactor vertices are in contact with which structural elements.

After determining the projection *Q* of impactor vertex *P* lies within element *i-j-k*, $\underline{p}_{\text{norm}} \bullet \underline{v}_{QP}$ was calculated and stored at each time-step.

$$\underline{p}_{norm} \bullet \underline{v}_{QP} = (p_{normx} \cdot v_{QPx}) + (p_{normy} \cdot v_{QPy}) + (p_{normz} \cdot v_{QPz}) \tag{3.21}$$

The variable *trialsign* is simply the sign of the above dot product

$$trialsign = sign\left(\underline{p}_{norm} \bullet \underline{v}_{QP}\right) \tag{3.22}$$

Then, the following conditions are checked to determine if contact has been detected:

Condition 1. If *preimpactdotsign* for impactor vertex *P* is equal to zero, the value of *trialsign* is assigned to *preimpactdotsign*. There is no contact detected so the algorithm continues checking the next impactor vertex.

Condition 2. If *preimpactdotsign* equals *trialsign* for impactor vertex *P*, there is no contact detected so the algorithm continues checking the next impactor vertex.

Condition 3. If *preimpactdotsign* does not equal *trialsign* for impactor vertex *P*, contact has been detected.

Note that multiple impactor vertices can make contact with a given element *i-j-k*. Figure 3.8 shows a schematic of this contact situation where element *i-j-k* is viewed on edge.

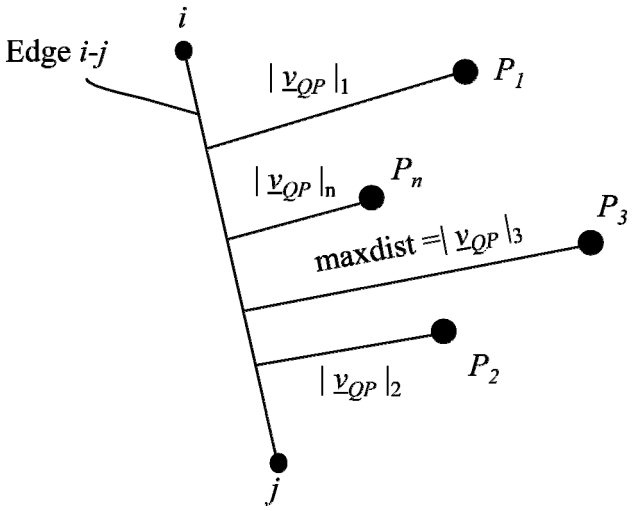

Figure 3.8. Multiple Contact Detections for Element *i-j-k*

As a result of the situation described by Figure 3.8, a sequence of checks was required to determine which impactor vertex had penetrated element *i-j-k* the furthest. The checks proceed in the following order,

a. If *maxdistnode* for element *i-j-k* is equal to zero (i.e. *maxdistnode* has not been overwritten yet), *maxdistnode* for element *i-j-k* is set equal to impactor vertex *P* and *maxdist* for element *i-j-k* is set equal to $|\underline{v}_{QP}|$. At this time, impactor

vertex *P* is the only impactor vertex to make contact with element *i-j-k* (since *maxdistnode* was still equal to zero). The algorithm continues checking the next impactor vertex, unless *P* is the final impactor vertex.

b. If $|\underline{v}_{QP}|$ is less than *maxdist* for element *i-j-k*, another impactor vertex has penetrated further than impactor vertex *P*. As a result, contact from impactor vertex *P* will not be treated by the contact algorithm. The algorithm continues checking the next impactor vertex, unless impactor vertex *P* is the final impactor vertex.

c. If $|\underline{v}_{QP}|$ is greater than *maxdist* for element *i-j-k*, *maxdistnode* for element *i-j-k* is set equal to impactor vertex *P* and *maxdist* for element *i-j-k* is set equal to $|\underline{v}_{QP}|$. At this time, impactor vertex *P* has penetrated element *i-j-k* the furthest. The algorithm continues checking the next impactor vertex, unless impactor vertex *P* is the final impactor vertex.

The algorithm described above identifies which impactor vertices are in contact with which structural elements. Also, the impactor vertex which penetrates a given structural element the furthest has been identified.

3.2 Contact Update

After determining which impactor vertices were in contact with which structural elements, it was necessary to incorporate a contact update scheme. The correction scheme used by the contact algorithm was one which updates the velocity components of the vertices *i*, *j*, *k* depending on the impactor velocity. The basic idea of the contact update scheme used by the contact algorithm was that collisions were inelastic and frictionless. As a result, only the normal component of the impactor vertex velocity, termed $\underline{v}_{\text{norm}}$, was used for updating structural element velocities. Only structural elements which were found to have a penetrating impactor vertex were updated. If a structural element had multiple penetrating impactor vertices, only the impactor vertex which penetrated the structural element the furthest was used to update velocities. The component of the impactor velocity vector along the contacted element normal direction is

$$\underline{v}_{norm} = v_{normx}\underline{e}_x + v_{normy}\underline{e}_y + v_{normz}\underline{e}_z = (\underline{v}_{impact} \bullet \underline{p}_{norm}) \cdot \underline{p}_{norm} \tag{3.23}$$

where $\underline{v}_{\text{impact}}$ is the velocity vector of the relevant impactor vertex.

The next step was to update the vertex velocities of contacted element *i*-*j*-*k* to account for the interaction with the impactor vertex. Since the collisions were inelastic and frictionless, contact with a structural element did not affect the motion of the impactor vertices. Also, contact was only detected after an impactor vertex had penetrated a structural element, so the position of the structural element would always lag behind that of the impactor vertex. Therefore, an adjustable parameter *b* was used to enforce the compatibility of positions of the impactor and structural element vertices at $t = t + \Delta t$. Figure 3.9 shows $x_{n,i}^{t+\Delta t}$, the predicted

position of the impactor vertex, $x_{n,s}^{t+\Delta t}$ the predicted position of the structural element vertex, $x_{n,i}^{t}$ the current position of the impactor vertex, $x_{n,s}^{t}$ the current position of a structural element vertex, and p_{norm} is the unit normal vector to structural element *i-j-k*. The time-step is denoted Δt. A coordinate along the normal direction is denoted x_{n}. The structural element shown in Figure 3.9 is viewed on edge.

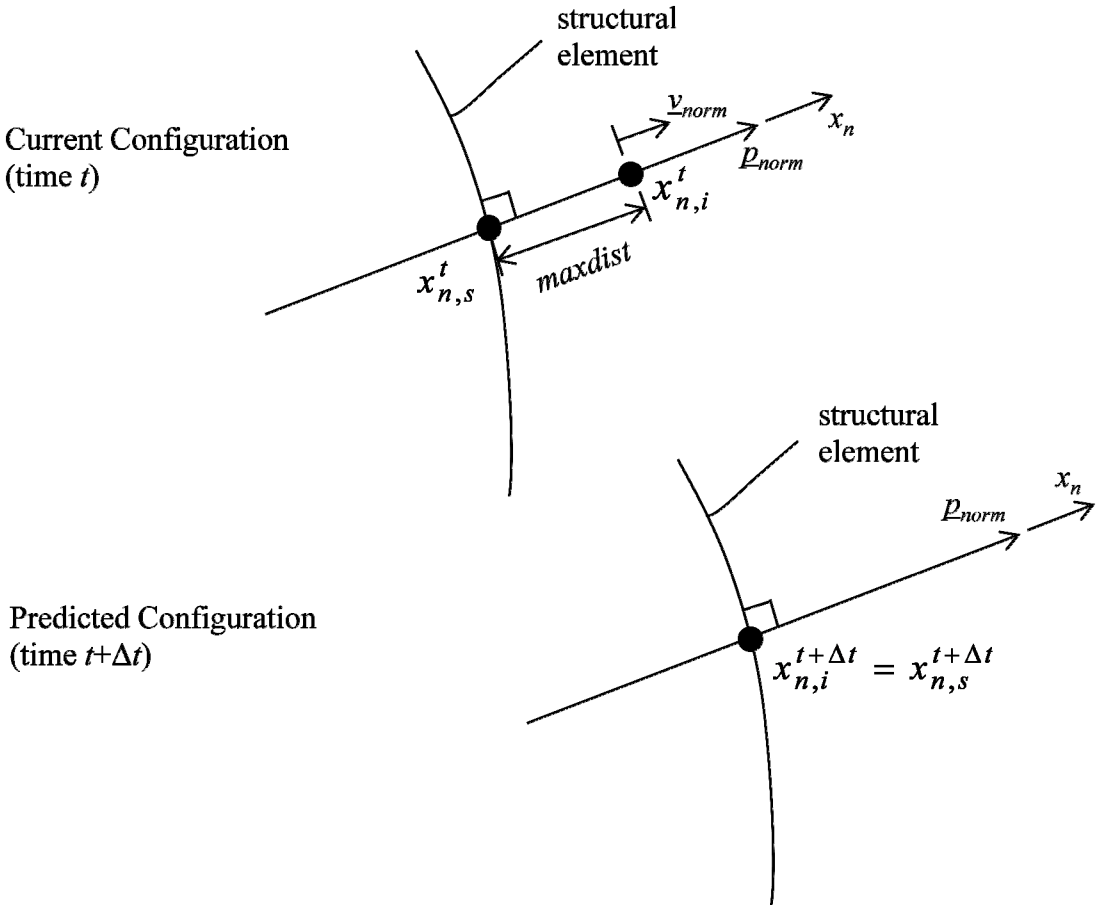

Figure 3.9. Current and Predicted Impactor and Structural Element Vertex Positions

The predicted positions of the impactor and structural element vertex are given by

$$x_{n,i}^{t+\Delta t} = x_{n,i}^{t} + \left|\underline{v}_{norm}\right|\Delta t \tag{3.24}$$

and

$$x_{n,s}^{t+\Delta t} = x_{n,s}^{t} + b\left|\underline{v}_{norm}\right|\Delta t \tag{3.25}$$

Since the impactor vertex moves at constant velocity its updated position can be predicted exactly, while the calculation of the updated position of the structural vertex is influenced by the mass and stiffness of surrounding elements and is hence only an approximation.

Equating the positions of the impactor vertex and the structural element vertex using equations 3.24 and 3.25 gives

$$x_{n,i}^{t} + \left|\underline{v}_{norm}\right|\Delta t = x_{n,s}^{t} + b\left|\underline{v}_{norm}\right|\Delta t \tag{3.26}$$

And it follows that

$$x_{n,i}^{t} - x_{n,s}^{t} = \Delta t\left|\underline{v}_{norm}\right|(b-1) \tag{3.27}$$

Finally

$$b = \left(\frac{x_{n,i}^{t} - x_{n,s}^{t}}{\left|\underline{v}_{norm}\right|\Delta t}\right) + 1 \tag{3.28}$$

or,

$$b = \left(\frac{maxdist}{\left|\underline{v}_{norm}\right|\Delta t}\right) + 1 \tag{3.29}$$

Given the situation when there was almost solely sliding contact (i.e. the unit normal was almost perpendicular to the impactor velocity); *b* can get very large and cause stability issues.

As a result, an upper limit, *blimit*, needed to be placed on *b*. Adding an upper limit improved the stability issues caused by extremely large *b* values.

The final step in the contact algorithm was to update the velocities of vertices *i*, *j*, *k*. Previous attempts were made to determine which element vertex the projection point *Q* was closest to and update only that vertex's velocity. But, the contact algorithm has produced much better results when updating the velocities of all vertices in the contact element. So, the three components of velocity were updated equally for each vertex *i*, *j*, *k* of contact element *i-j-k* as shown in Figure 3.10.

$$\underline{v}_{update} = b \cdot \underline{v}_{norm} \tag{3.30}$$

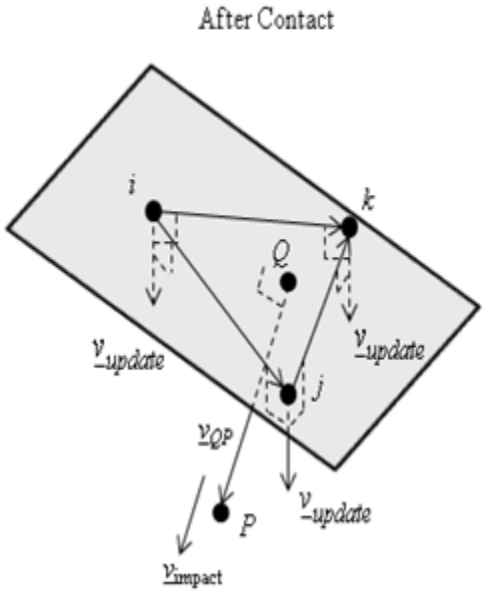

Figure 3.10. Velocity Update Applied at Contact Vertices

After updating the velocities for vertices *i*, *j*, *k* of all contact elements, the time was incremented and the contact algorithm was repeated for each time-step for the total duration of the simulation.

3.3 Contact Algorithm: Efficiency Improvement Methods

Computation times were greatly affected by the contact detection algorithm. The more structural elements the algorithm had to check on a flexible structure, the more time it took to complete. With that idea in mind, it is useful to refer back to Figure 3.1 which shows the overall goal of the contact algorithm: to handle a contact sequence between a human and a tent door. From Figure 3.1, as the human traverses the tent door, the impactor vertices will not make contact with structural elements not located on the tent door. Although the contact detection algorithm described above can handle checking all structural elements on the flexible structure mesh, it is highly inefficient to do so. As a result, two methods are described which limit the possible contact elements the contact algorithm must check. The first method, referred to as "distance check method", involves checking the distance from the impactor vertex P to the centroid c of element *i-j-k*. The position vector $\underline{c}$ of the centroid of a typical structural element *i-j-k* is

$$\underline{c} = \frac{\underline{x}_i + \underline{x}_j + \underline{x}_k}{3} = c_x \underline{e}_x + c_y \underline{e}_y + c_z \underline{e}_z$$
$$\underline{c} = \frac{\left(x_i + x_j + x_k\right)\underline{e}_x + \left(y_i + y_j + y_k\right)\underline{e}_y + \left(z_i + z_j + z_k\right)\underline{e}_z}{3} \tag{3.31}$$

Then, the distance P_{cent} from the impactor vertex P to c is

$$Pcent = \sqrt{\left(P_x - c_x\right)^2 + \left(P_y - c_y\right)^2 + \left(P_z - c_z\right)^2} \tag{3.32}$$

If this distance was greater than a specified distance referred to as *distcheck*, element *i-j-k* was not a candidate for contact. To help simplify the explanation of this distance check method, only the tent door from Figure 3.1 has been used to show the contact radius r (where

r = *distcheck*) in Figure 3.11. This method is not limited to the geometry shown in Figure 3.11 but this door is merely used to help clarify the method. Also, for simplification, a circle rather than a sphere is used to describe the distance check method.

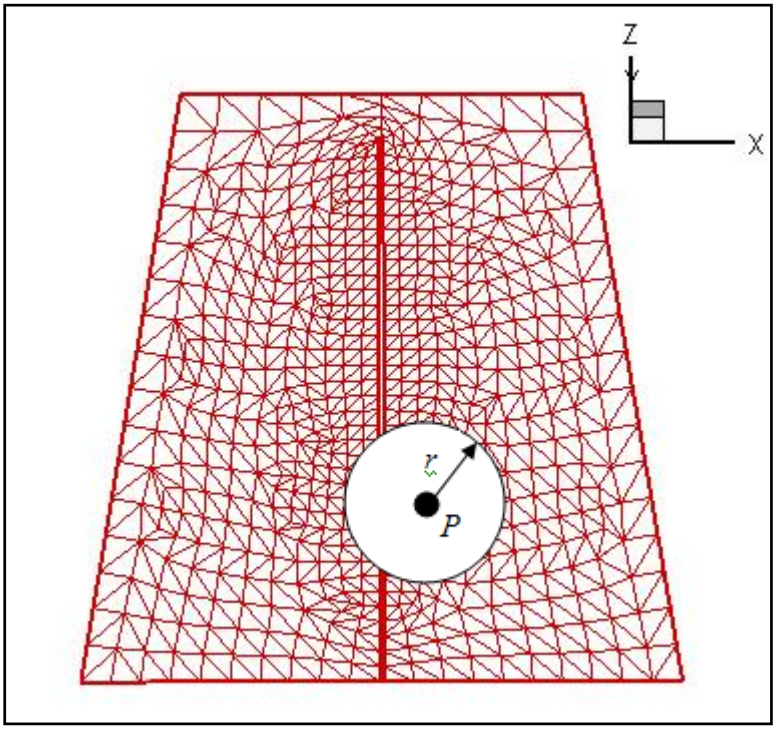

Figure 3.11. Front View of the Distance Check Method

If a structural element is not located within this circle, it is not a potential contact element. Therefore, this method actually serves two purposes. It limits the number of potential contact elements for a given impactor vertex while also forcing an impactor vertex to be located within this radius before the algorithm begins to consider it for contact.

The second method, referred to as "the box method", involves placing a three-dimensional box around a contact location. If all three vertices *i*, *j*, *k* of element *i*-*j*-*k* were not located

within this box, element *i-j-k* was not considered as a potential contact element. If a set of coordinate limits were not specified, it was assumed the box was infinite in that coordinate direction. Figure 3.12 shows a front view used to describe the box method.

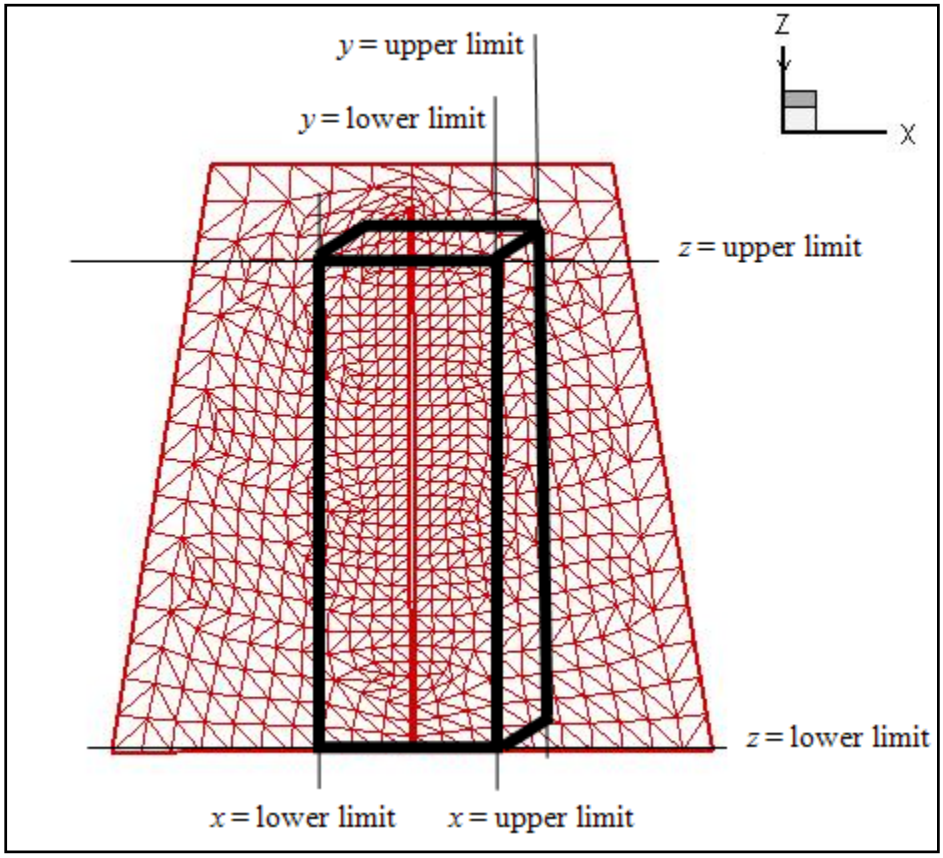

Figure 3.12. Front-View of the Box Method

Figure 3.12 shows how the box method limits possible contact elements by putting an upper and lower limit on the three coordinate directions, *x*, *y*, and *z*.

Adding these two efficiency improvement methods to the contact algorithm has significantly cut down on computation time while not compromising the simulation results.

4 Fabric Material Properties

This chapter outlines the procedure to convert experimentally determined fabric mechanical properties to effective stiffness values useful to the particle model. It was desirable to model actual fabric materials in the MATLAB computer code simulations. The benefits to doing so were the units were no longer arbitrary and the simulations could model actual fabric materials. The necessary properties which must be input to the MATLAB computer code are the mass per unit area ρ^*, the mesh size dependent stretching stiffness coefficient k_0, and the bending stiffness coefficient k_b. In order to measure the mechanical properties of the fabric, a cantilever bending test was used. While it was possible to directly obtain ρ^* from the test, the procedure to convert the mechanical property obtained from the cantilever bending test to the useful k_0 stiffness coefficient is described. Then, as an example, the procedure was carried out for a military grade canvas material and the results are provided. It was not possible to obtain the k_b value directly from performing the cantilever bending test. As a result, the procedure to set the value of the bending stiffness is also described.

4.1 Cantilever Bending Test

For the validation cases discussed in Chapter 2, arbitrary mass, stiffness, damping, and external force values were used to validate the MATLAB computer code. In doing so, the time, length, and force units were also arbitrary. Although a consistent set of units was implied, it was desirable to incorporate the capability to model actual fabric materials with actual values for mechanical properties. A sample of military grade canvas material was

obtained from The College of Textiles at NC State University. In order to obtain the material properties of the canvas to be used for simulations, a cantilever bending test was conducted at the Physical Testing Laboratory. This bending test, which follows ASTM Standard D-1388 (2008), leads to a value of fabric flexural rigidity, termed *G*, after direct measurement of quantities called the overhang length *o* and the mass *m*. The setup of the cantilever bending test apparatus is shown in Figure 4.1. Refer to Appendix D to view a copy of the spreadsheet results for the cantilever bending test.

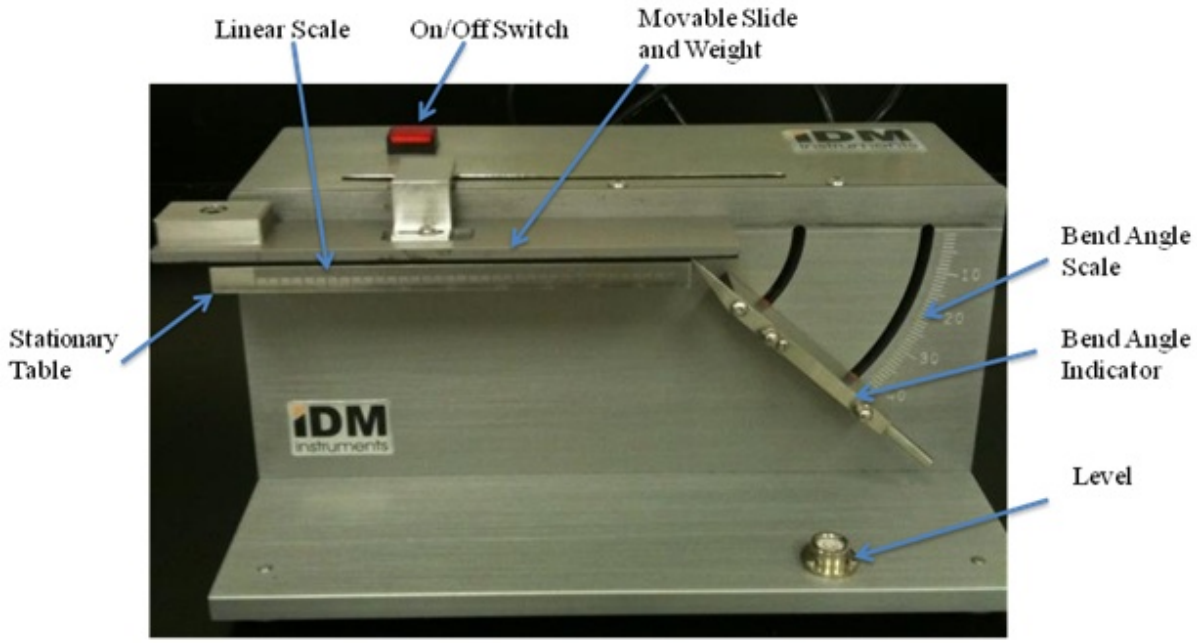

Figure 4.1. Cantilever Bending Test Apparatus

In order to conduct the test, eight fabric specimens were prepared, four oriented in the machine direction and four oriented in the cross direction. Each specimen was loaded on the stationary table with the movable slide and weight zeroed and placed on top. To start the test, the on/off switch was pressed and the movable slide began moving to the right at a speed

of 120 mm/min. The machine was stopped by pressing the on/off switch when the fabric touched the bend angle indicator as shown in Figure 4.2.

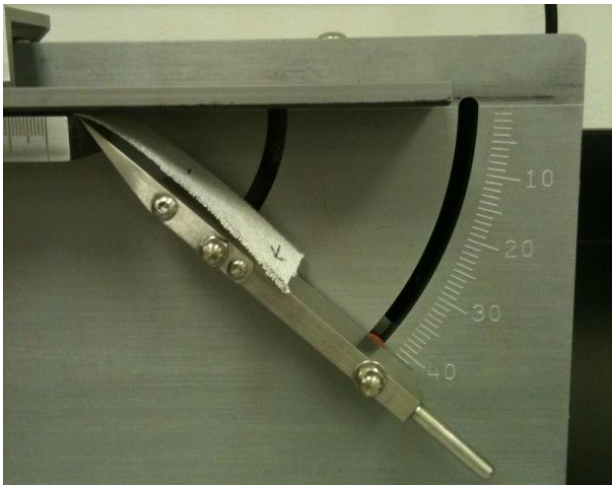

Figure 4.2. Overhang Length of the Fabric

The value measured for each specimen was the overhang length, *o* (units millimeters). Four overhang lengths were recorded for each specimen, specifically both ends, top, and bottom. The overhang length was obtained by directly reading the value on the linear scale shown in Figure 4.1 after the specimen first made contact with the bend angle indicator. Note that as required by the ASTM standard, the bend angle indicator was set to an angle of 41.5°. These four overhang lengths were averaged for each specimen to obtain the measured overhang length.

After finding the overhang lengths, the eight specimens were placed on a scale and weighed to the nearest thousandth of a gram. The total area of the specimens was 64 in^2. In order to calculate *G*, a mass per unit area value *W* was needed to be expressed in mg/cm^2 units. Therefore, the mass of the fabric divided by the area expressed in g/in^2 was converted to mg/cm^2. The resulting value was $W = 37.79\ mg/cm^2$.

The bending length, c, is defined by

$$c \equiv \frac{o}{2} \tag{4.1}$$

After obtaining the mass per unit area and the bending length, the flexural rigidity G was computed according to the ASTM standard by means of

$$G = W \times c^3 \tag{4.2}$$

A flexural rigidity value was computed for each specimen in both fabric directions. These four values were then averaged to yield a final flexural rigidity value of the fabric for each machine direction.

After calculating the flexural rigidity, the interest was in converting to the more useful parameter E, the elastic modulus (or Young's modulus). Young's modulus was used to tune the stiffness values used in the MATLAB computer code.

Using the large deflection theory for a cantilever beam based on Rohde's (1953) article, the bend angle θ during the ASTM test corresponds to

$$\tan\theta = \frac{y_L}{x_L} \tag{4.3}$$

where y_L and x_L are the vertical and horizontal positions of the deflected beam, respectively. Using the chart on page 338 of the Rohde paper, the ratio of y_L/x_L is equal to tan (41.5°) when

$$\frac{wL^3}{EI} = 8 \tag{4.4}$$

where w is the weight per unit length, L is the beam length, and EI is the bending stiffness.

For the cantilever bending test, $L = o$ and $o = 2c$. Plugging $2c$ into equation 4.4 yields

$$\frac{wc^3}{EI} = 1 \tag{4.5}$$

where wc^3 is the flexural rigidity, since $w = W$ when the sample width is 1 inch. Therefore,

$$EI = wc^3 \tag{4.6}$$

where I is the moment of inertia of the test strips (rectangular cross-section $b \times t$). Therefore,

$$I = \frac{bt^3}{12} \tag{4.7}$$

where b is the specimen width and t is the thickness. Finally,

$$E = \frac{wc^3}{I} \tag{4.8}$$

Thus, it is possible to convert from a measured flexural rigidity value G to Young's modulus E.

4.2 Obtaining the k_0 Stiffness Coefficient

The particle stretch and bend stiffness coefficients, k_0 and k_b, cannot be obtained directly from the test specimen or from the cantilever bending test. Instead, an indirect calculation approach was employed.

After using the cantilever bending test to obtain Young's modulus, the equation

$$\delta = \frac{FL}{AE} \tag{4.9}$$

was used to determine the axial deflection of the test specimen. F is the applied axial load, L is the length of the specimen, A is the cross sectional area, and E is Young's modulus. After

determining the deflection for a given load, this same load and deflection were used to solve for the stretching stiffness,

$$k = \frac{F}{\delta} = \frac{AE}{L} \tag{4.10}$$

The stretching stiffness coefficient used in the MATLAB computer code, k_0 was calculated according to

$$k_0 = kh \tag{4.11}$$

Thus a procedure has been developed to convert an experimentally measured mechanical fabric property to the useful stretch stiffness coefficient used in the MATLAB computer code.

4.3 Example: Canvas Tent Material

For the canvas material provided, the measured values obtained from the cantilever bending test are shown in Table 4.1.

Table 4.1. Measured Properties

Property	**Value**
Force (chosen arbitrarily)	F = 1 lb
Length	L = 8 in
Width	b = 1 in
Thickness	t = 0.038 in
Mass	m = 15.6 g
Area	A = 0.038 in^2
Mass per unit area	ρ^* = 0.0024 slug/ft^2
Flexural rigidity (result of material test)	$G = wc^3$ = 0.002627 lb•in

Then, the values calculated through the procedure described in Section 4.2 are provided in Table 4.2.

Table 4.2. Calculated Properties

Property	Equation	Value
Moment of Inertia	(4.7)	I = 4.57267E-6 in^4
Young's modulus	(4.8)	E = 574.5 lb/in^2
Deflection	(4.9)	δ = 0.3665 in
Stretch Coeff. (Actual)	(4.10)	k = 2.7285 lb/in
Stretch Coeff. (Code)	(4.12)	k_0 = 21.83 lb

The mass per unit area and the stretching stiffness coefficient are two of the properties required to model fabric material using the particle method. These values were used in the MATLAB computer code. The procedure to set the value of the bending stiffness, k_b, required to fully model the canvas material is outlined in Section 4.4.

4.4 Obtaining the Bending Stiffness Coefficient k_b

After calculating k_0 to be used in the MATLAB computer code, the final property needed to model the canvas material is the bending stiffness, k_b. In order to obtain this value, the bending deflection was forced to match classical plate theory using a "tuning" approach. The simply supported plate configuration used for the tuning approach is shown in Figure 4.3.

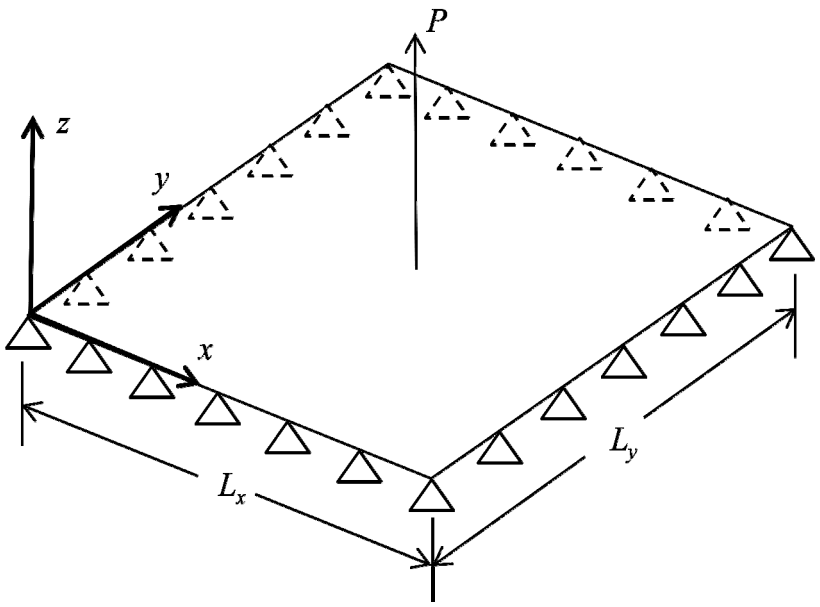

Figure 4.3. Simply Supported Rectangular Plate Used for the Tuning Approach

The deflection equation for plate theory (Timoshenko & Woinowsky-Krieger, 1959) is based on rectangular plates. Figure 4.4 shows the particle mesh used to model a flat, flexible fabric structure with dimensions L_x = 5.833 ft and L_y = 6.75 ft. The plate was discretized with a 23 x 23 mesh of particles, 529 total particles with 968 triangular elements.

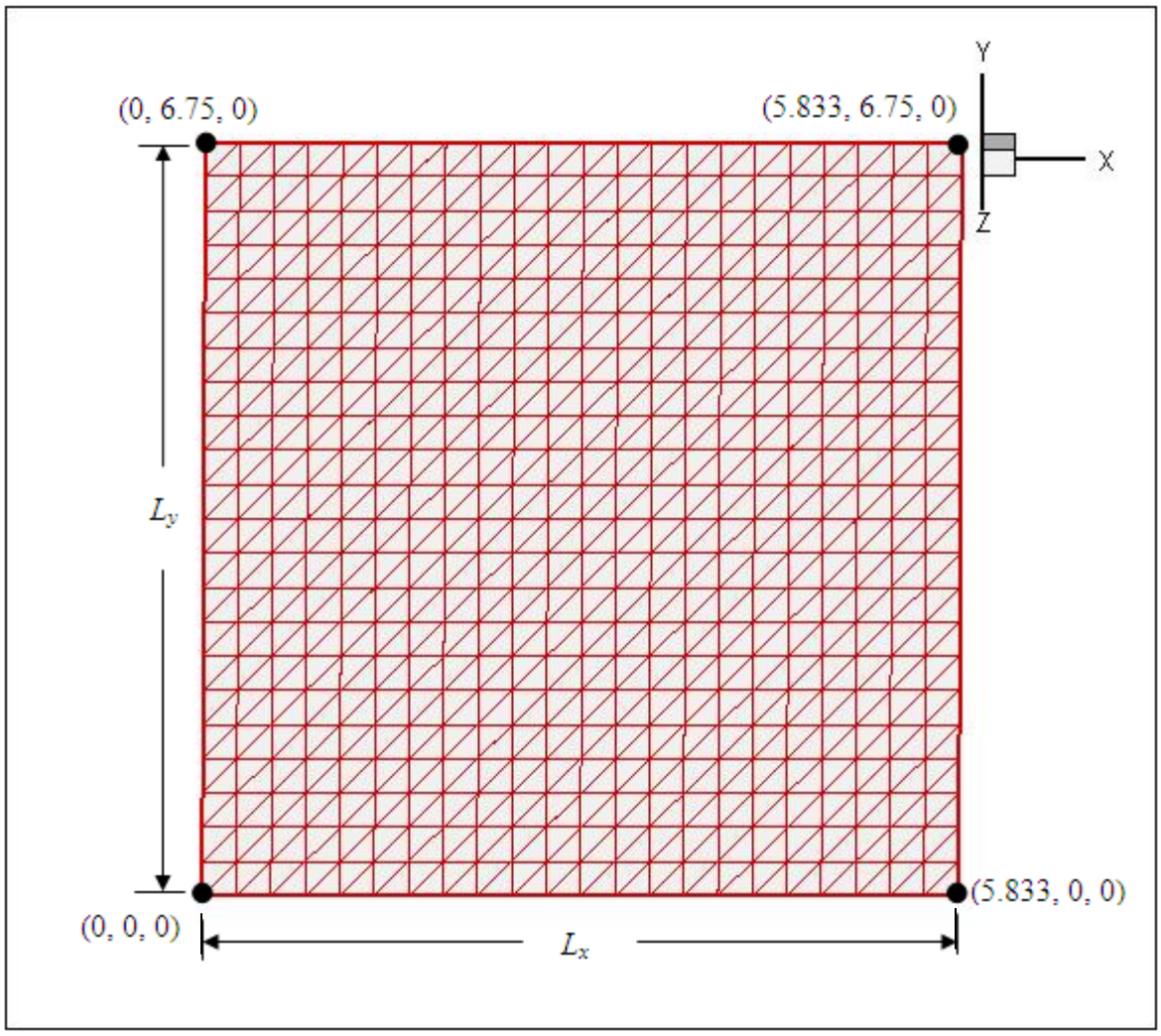

Figure 4.4. Particle Mesh Used for Bending Stiffness Tuning

Plate theory provides an equation for transverse deflection of the plate.

$$\delta_z = \frac{4P}{\pi^4 L_x L_y D} \sum_{m=1}^{\#terms} \sum_{n=1}^{\#terms} \frac{\sin\left(\frac{m\pi\xi}{L_x}\right)\sin\left(\frac{n\pi\eta}{L_y}\right)}{\left(\frac{m^2}{{L_x}^2}+\frac{n^2}{{L_y}^2}\right)^2} \sin\left(\frac{m\pi x}{L_x}\right)\sin\left(\frac{n\pi(L_y-y)}{L_y}\right) \tag{4.12}$$

Using the first four terms of the series with the plate dimensions, equation 4.12 reduces to

$$\omega_{\max} = \frac{0.4336P}{D} \tag{4.13}$$

where P is the applied load and D is the bending/flexural rigidity of the plate defined as

$$D = \frac{Et^3}{12(1-\nu^2)} \tag{4.14}$$

where E is Young's modulus and t is the plate thickness, both obtained from the cantilever bending test. Poisson's ratio ν was assumed to be 0.3.

The only remaining unknown variable in equation 4.13 was the applied load P. For a number of applied loads, the maximum deflection at the center of the mesh was calculated. A convergence analysis was conducted to tune the k_b value so the deflection of the MATLAB computer code matched that of plate theory. Table 4.3 shows the data used to create Figure 4.5 which shows a plot of k_b versus P for the six different cases.

Table 4.3. Data for k_b vs. P

P (lb)	k_b (lb•ft^2)	w_{code} (ft)	w_{plate} (ft)
0.00000075	0.0000046	0.001434	0.001352
0.0000005	0.000005	0.000897	0.000901
0.00000025	0.0000053	0.000447	0.00045
0.0000001	0.0000054	0.00018	0.00018
0.000000075	0.0000054	0.000135	0.000135
0.00000005	0.0000054	0.00009	0.00009

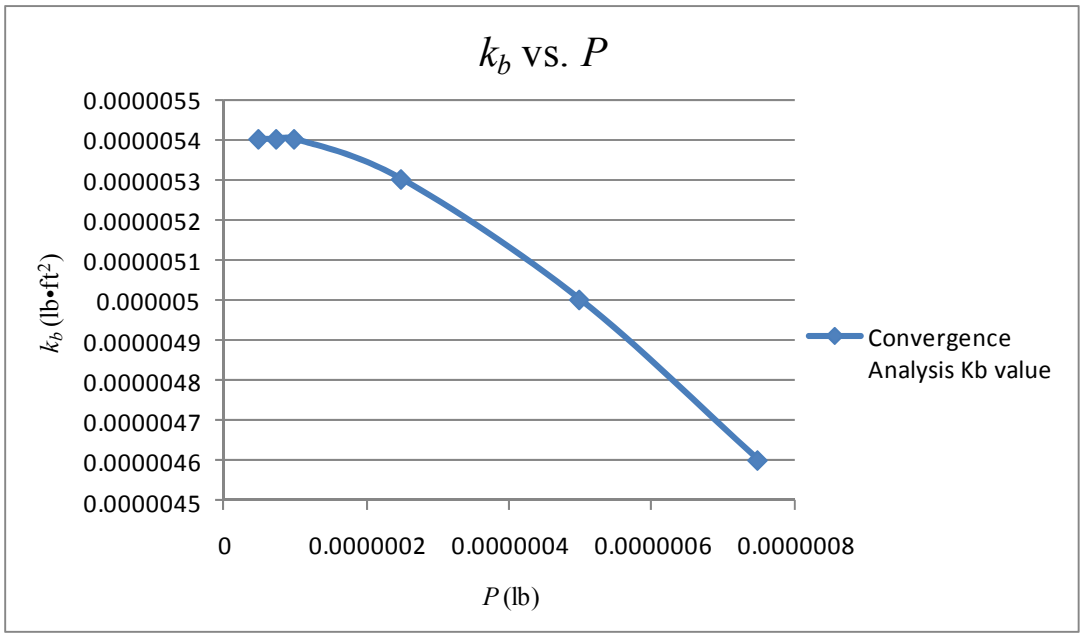

Figure 4.5. k_b vs. P

Figure 4.5 shows that as P decreases, the k_b value approaches a constant value. From the convergence study, k_b = 0.0000054 lb•ft^2. One explanation for the very small applied loads required to force the k_b value to converge is the major assumption with plate theory which is that it is based solely on bending stiffness; membrane (stretching) stiffness is neglected. Therefore, in order to make the effect of the membrane stiffness negligible during a simulation, a very small force must be applied. It is assumed then that the converged value is the appropriate value to use in the particle model simulations to correctly model the bending stiffness of the actual fabric material.

5 Results

This chapter presents the results obtained from seven simulations used to demonstrate the utility of the MATLAB particle method code. Each of the seven cases was used to study a different function of the code. A description of these seven cases follows:

Case 1: contact from a single impactor triangle with a hinged plate

Case 2: contact from multiple impactor triangles with a hinged plate

Case 3: a glancing blow contact event with a hinged plate

Case 4: contact of a sphere with a plate containing a slit

Case 5: a single soldier entering a full tent model without pressure

Case 6: a single soldier entering a full tent model with pressure

Case 7: three soldiers entering a full tent model without pressure

These cases range from the simplest contact event to a very complex contact interaction including large structural deformations. All of the trial cases used the parameters reported in Chapter 4 to model the actual canvas material. Since there are no clear cut forms of validation, the results are presented qualitatively through snapshots of the animation sequences and for the first and last cases, quantitatively as well in the form of plots and figures.

5.1 Case 1: Single Impactor Triangle

The first case was the simplest case used to demonstrate the utility of the MATLAB computer code. With the computer code having been configured to read and write STL files, a triangle is the simplest possible impactor since STL files are presented in terms of triangles. A single impactor triangle (dimensions l_x = 0.3 ft, l_y = 0.3 ft) made contact with a flexible structure (L_x = 5.833 ft, L_y = 6.75 ft) discretized with a 23 x 23 mesh of particles, 529 total particles with 968 triangular elements and hinged along the top edge. Refer to Appendix E for the MATLAB code for this case. The x and y coordinates of the four corners of the flexible structure and the vertices of the impactor triangle in the initial undeformed configuration are shown in Figure 5.1. The initial configuration of the flexible structure was located in the xy-plane. The impactor was moving in the negative z-direction with a constant velocity v_{impact}.

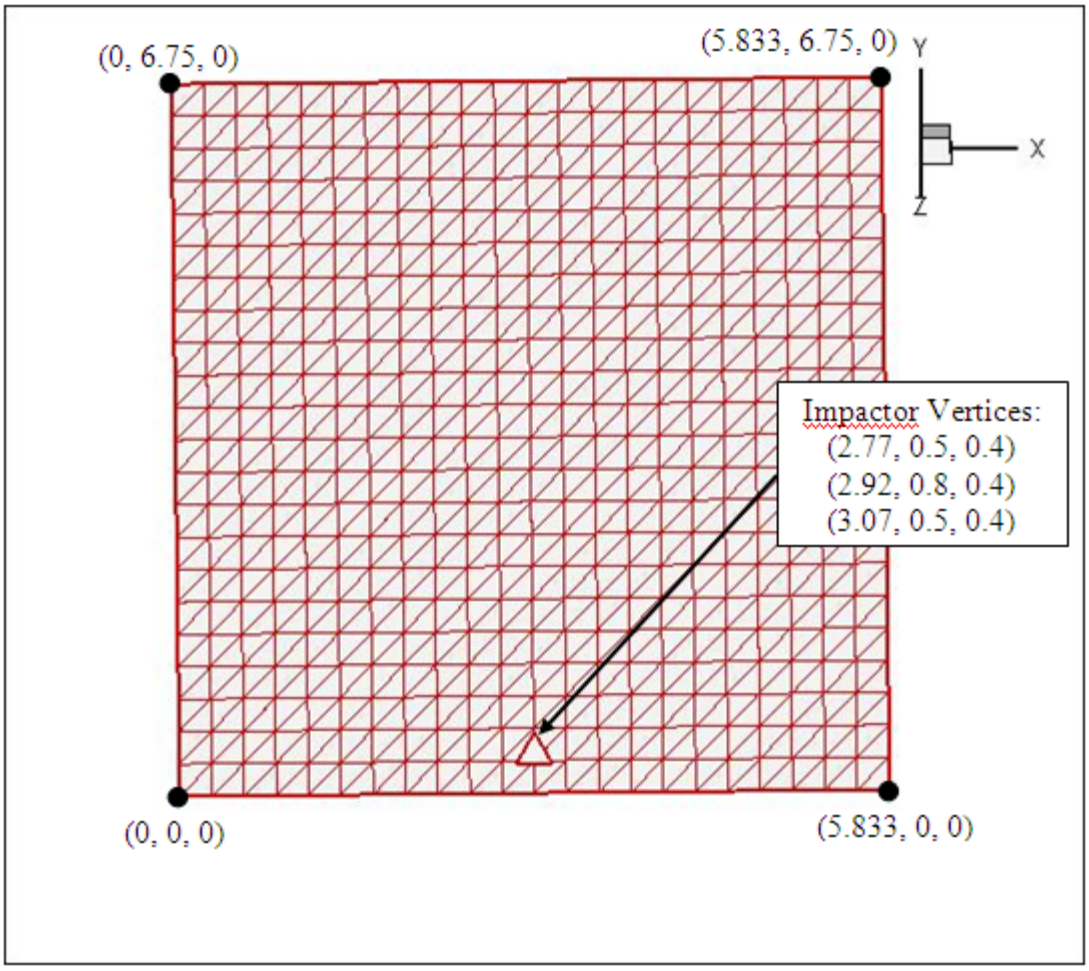

Figure 5.1. Case 1 Initial Flexible Structure and Impactor Configuration

Figure 5.2 shows the input gravitational force (f_{gy}), effective force due to pressure ($\underline{f}_i^p$), and velocity (v_{impact}) versus time for a given animation sequence. The gravitational force was applied as a step function at time $t = 0$. The effective force due to pressure was applied as a ramp function starting at time $t = t_{\text{p,start}}$ and ending at time $t = t_{\text{p,end}}$, then held constant thereafter. The impactor started to move stepwise at time $t = t_{\text{lag}}$.

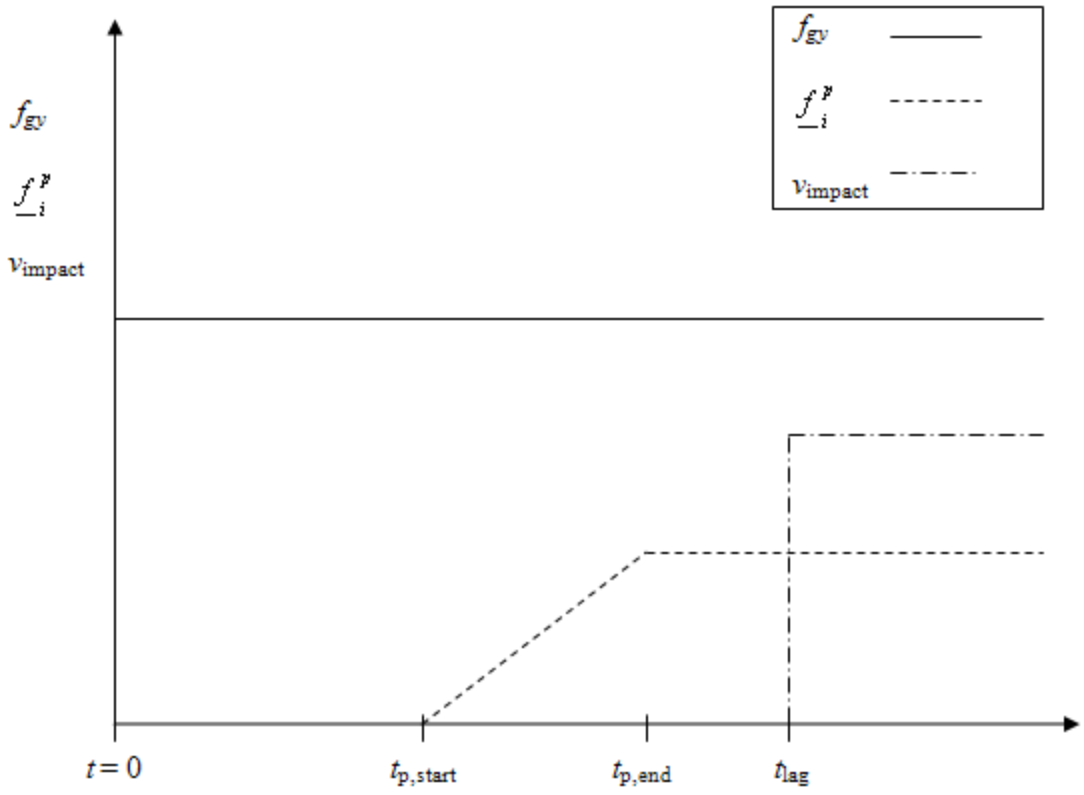

Figure 5.2. Forces and Velocity versus Time Plot

The numerical values of the parameters in the MATLAB particle code were: ρ^* = 0.0024 slug/ft^2, k_0 = 21.828 lb, k_b = 0.0000054 lb•ft^2, c = 0.0005 lb•s/ft, v_{impact} = -0.4 ft/s, g_y = -32.174 ft/s^2. There was no effective force due to pressure applied for this simulation, p = 0 lb/ft^2. The simulation had a total duration of 10 seconds with a time-step of Δt = 0.0004 s. The time lag on the impactor was t_{lag} = 0.1 s. STL files were output every 250 time-steps or at a time interval of 0.1 s. Contact checking on the flexible mesh was only done in the range -0.5 ft < y < 3 ft, for all x and z values (i.e. a horizontal strip). The distance check limit for this simulation was *distcheck* = 1.5 ft. The final parameter was the limit on the adjustable parameter, *blimit* = 40.

The simulation produced the time-lapse results shown in Figure 5.3. At $t = 0$ s, the initial configuration of the impactor and flexible structure is shown. Gravity was activated during the first time-step and the effects of this force are observed to damp to a steady-state value at approximately $t = 0.5$ s. Then, at $t = 1.2$ s, the impactor first contacts the flexible structure. In the images $3.6 \text{ s} < t < 7.3$ s contact is present. At some time after $t = 7.3$ s, contact is lost and the impactor slides off the fabric. Finally, at $t = 10$ s the structure has returned to the steady-state position under the influence of gravity only.

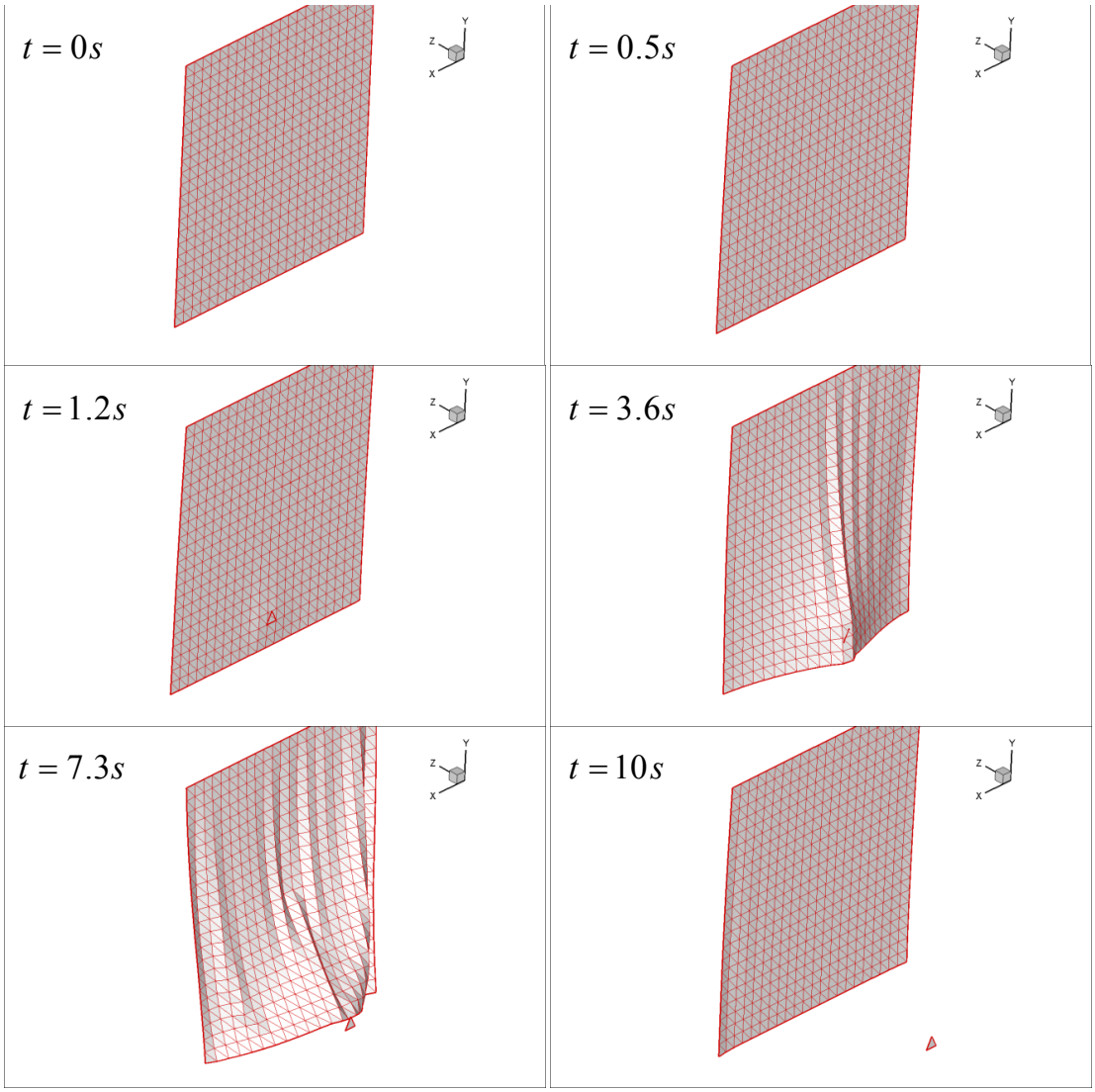

Figure 5.3. Single Impactor Triangle Animation Sequence

Then, Figure 5.4 shows the time-history plot for the x, y, z positions and velocities of the mid-side of the bottom edge (vertex 276 with coordinates x = 2.9165, y = 0, z = 0). This figure was included to provide a quantitative result for the animation sequence shown in Figure 5.3. The results in Figure 5.4 coincide with Figure 5.3.

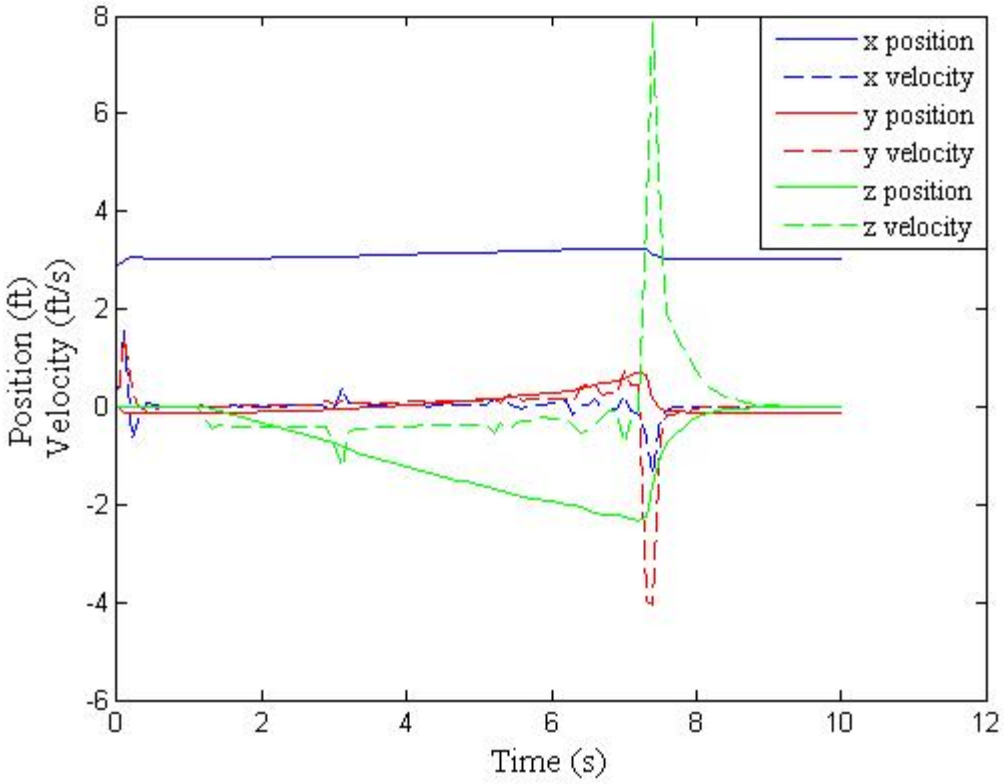

Figure 5.4. Time-History Plot for Structural Element Vertex 276

Also of interest was the maximum penetration value over the total duration of the simulation. The results are shown in Figure 5.5.

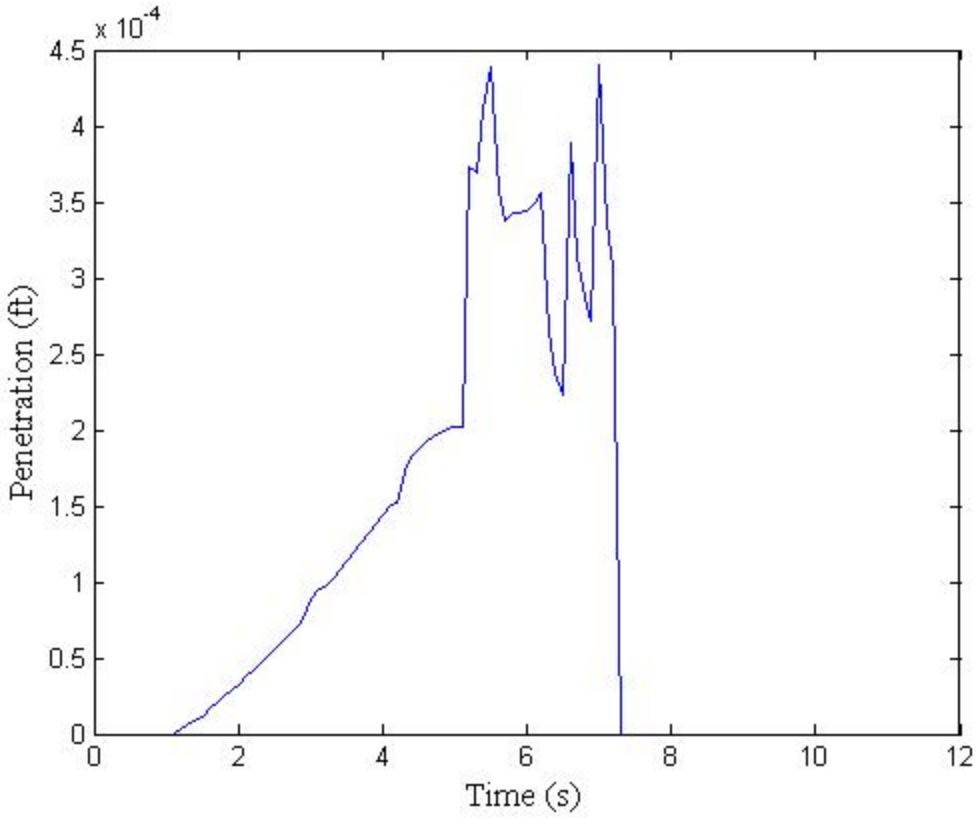

Figure 5.5. Time-History Maximum Penetration

Note that the scale on the penetration axis is very small. Using as a characteristic length for a triangular element, the max edge length, l = 0.4 ft. Figure 5.5 shows the maximum penetration for the simulation was 4.38×10^{-4} ft. This value is 0.1% of the element size which amounts to a very small penetration. The goal was to limit violations of the contact algorithm and this case was able to achieve that goal. This case, involving a single impactor triangle was used to initially demonstrate the utility of the MATLAB particle code. The results provided valuable information about the code's ability to handle a contact event.

5.2 Case 2: Multiple Impacts

Following a single impact event, this case looked at the ability of the MATLAB particle code to handle multiple impacts from multiple impactors. This case used the same flexible structure and material properties as Case 1. The use of impactor triangles was still present in this case where five impactors moved with five different constant velocities in the negative *z*-direction: v_{impact1}, v_{impact2}, v_{impact3}, v_{impact4}, and v_{impact5}. The x and y coordinates of the four corners of the flexible structure and the vertices of the five impactor triangles in the initial undeformed configuration are shown in Figure 5.6. Refer to Appendix F for the inputs to the MATLAB computer code for this case and Appendix G for the impactor input file read by the MATLAB computer code.

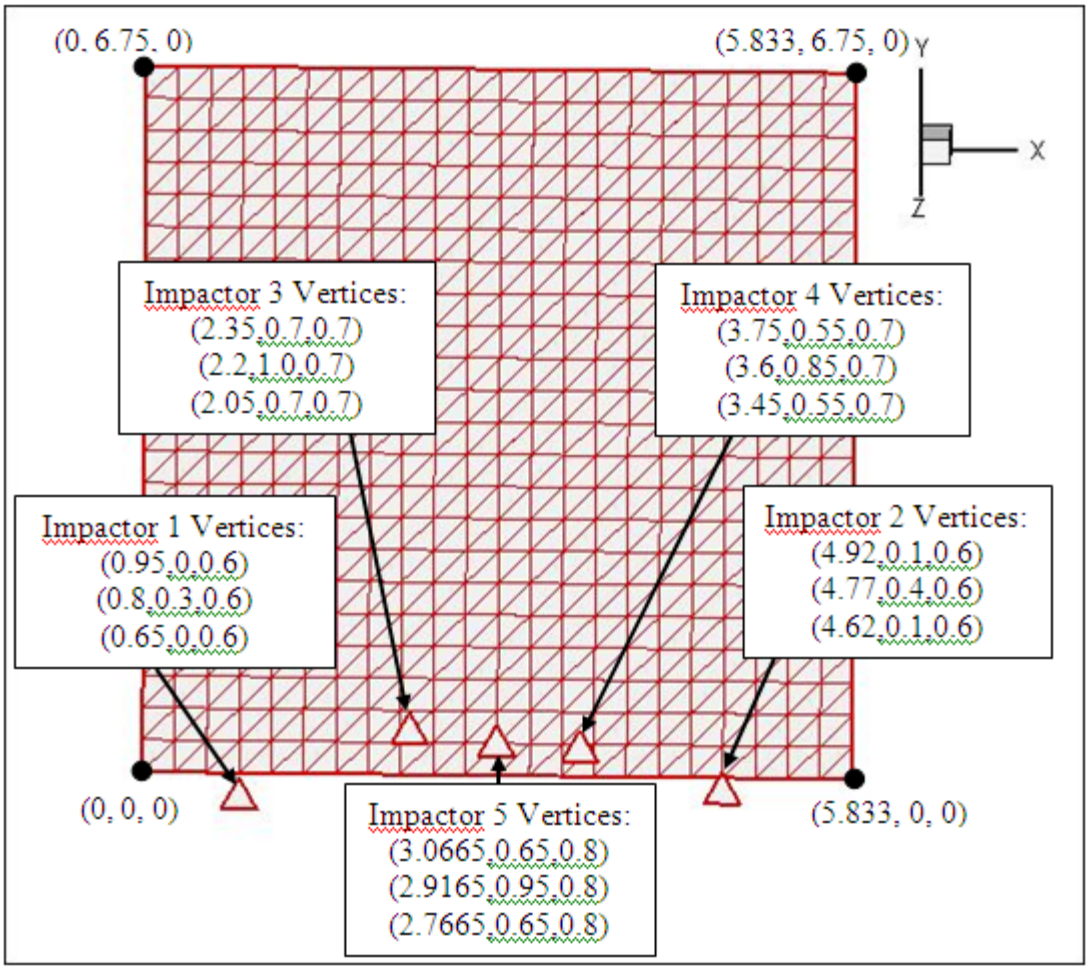

Figure 5.6. Case 2 Initial Flexible Structure and Impactor Configuration

Referencing Figure 5.2 provides a better understanding of how the listed forces and velocities were applied during the simulation.

The numerical values of the parameters in the MATLAB particle code were: ρ^* = 0.0024 slug/ft^2, k_0 = 21.828 lb, k_b = 0.0000054 lb•ft^2, c = 0.0005 lb•s/ft, $v_{impact1}$ = 0.55 ft/s, $v_{impact2}$ = 0.5 ft/s, $v_{impact3}$ = 0.4 ft/s, $v_{impact4}$ = 0.3 ft/s, $v_{impact5}$ = 0.1 ft/s, g_y = -32.174 ft/s^2. There was no effective force due to pressure applied for this simulation, p = 0 lb/ft^2. The simulation had a total duration of 12 s with a time-step of Δt = 0.0004. The time lag on the impactors was t_{lag}

= 0.1 s. STL files were output every 300 time-steps or at a time interval of 0.12 s. Contact checking on the flexible mesh was only done in the range -0.5 ft < y < 1.8 ft, for all x and z values (i.e. a horizontal strip). The distance check limit for this simulation was *distcheck* = 1.5 ft. The final parameter was the limit on the adjustable parameter, *blimit* = 40.

The simulation produced the time-lapse results shown in Figure 5.5. At t = 0 s, the initial configuration of the impactors and flexible structure is shown. Gravity was activated during the first time-step and the effects of this force are observed to damp to a steady-state value at approximately t = 0.5 s. At some time just prior to t = 1.32 s, impactors 1 and 2 make contact with the flexible structure. Then, at t = 2.28 s, contact continues with all five impactors making contact with the flexible structure. At approximately t = 4.56 s, impactor 1 slides off the fabric but contact continues with the other four impactors. Then, at approximately t = 6.6 s, impactor 2 slides off the fabric and contact continues with the remaining three impactors. Then, at some time before t = 7.08 s, the remaining impactors have slid off the fabric and contact is lost. Finally, at t = 12 s the structure has returned to the steady-state position under the influence of gravity only.

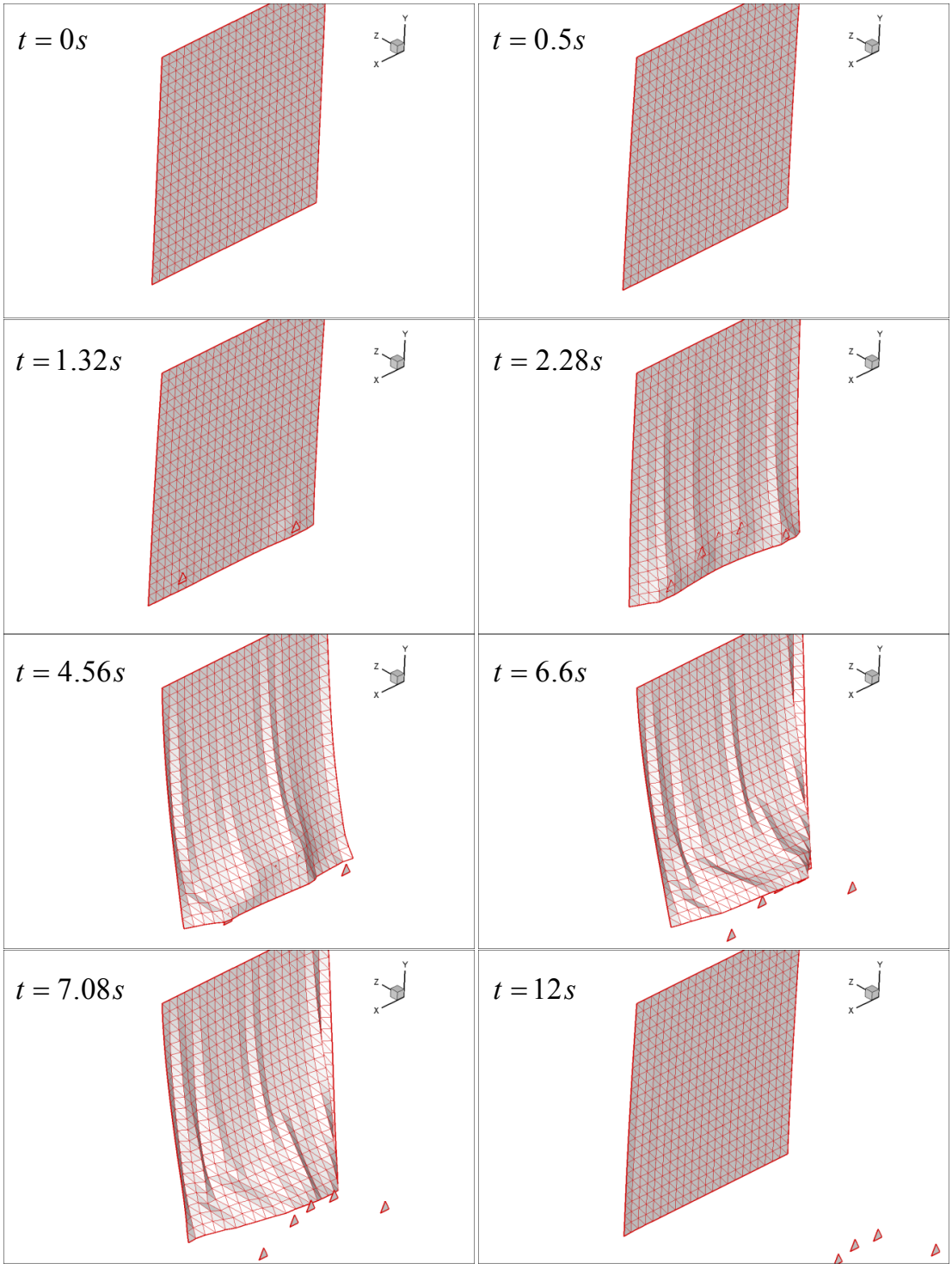

Figure 5.7. Multiple Impacts with Flexible Structure Animation Sequence

5.3 Case 3: Glancing Blow

After completing simulations involving single and multiple contacts, the next case looked at a glancing blow provided by a single impactor triangle (same dimensions as Cases 1 and 2). This case was important in determining whether the MATLAB particle code could handle sliding contact. Again, this case used the same flexible structure and material properties as Cases 1 and 2. The x and y coordinates of the four corners of the flexible structure and the vertices of the impactor triangle in the initial undeformed configuration are shown in Figure 5.8. Refer to Appendix H for the inputs to the MATLAB computer code for this case.

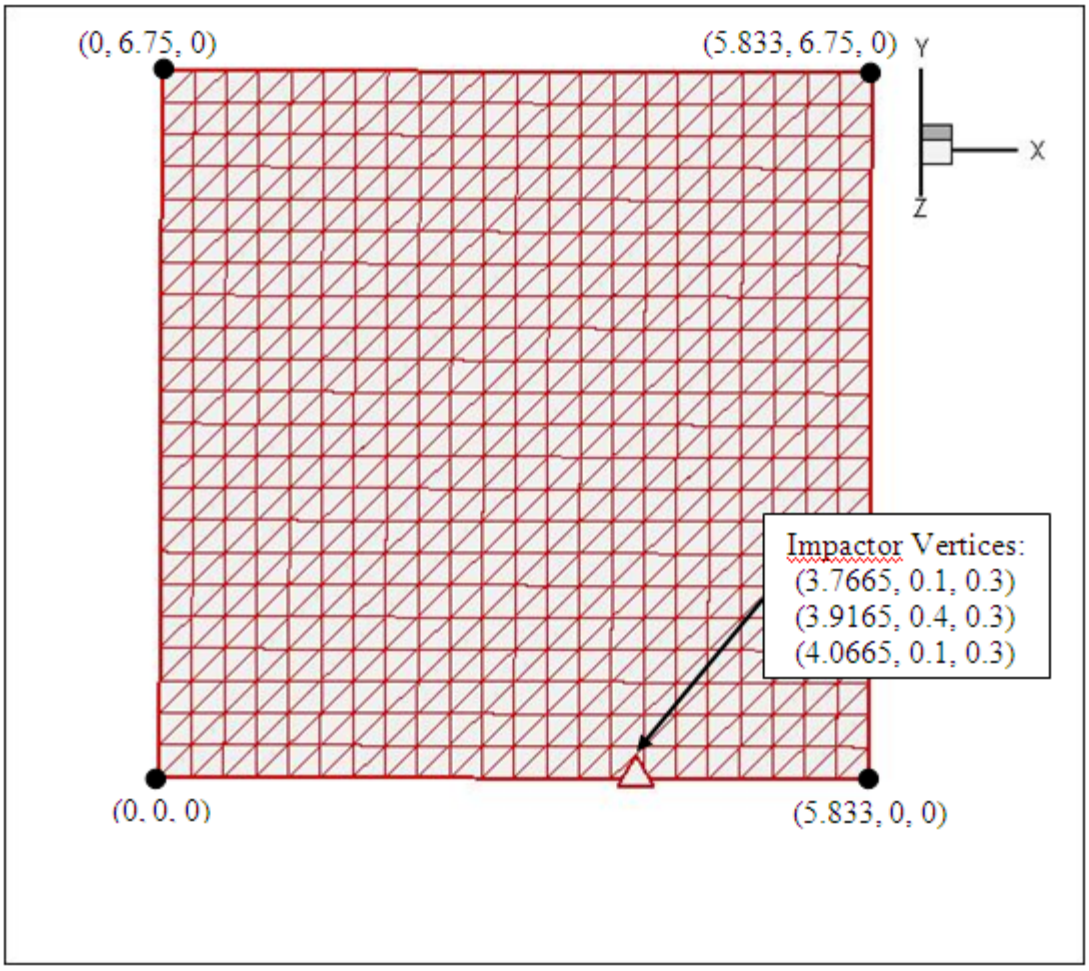

Figure 5.8. Case 3 Initial Flexible Structure and Impactor Configuration

The desired impact location for this case was 1 ft away from the initial impactor configuration in the negative x-direction and 0.3 ft away in the negative z-direction. With the respective distances to the impact location, the impactor was given constant velocities, v_{impact1} in the negative x-direction and v_{impact2} in the negative z-direction, forcing contact to occur at this desired location to produce a glancing blow effect.

The numerical values of the parameters in the MATLAB particle code were: $\rho^* = 0.0024$ slug/ft^2, $k_0 = 21.828$ lb, $k_b = 0.0000054$ lb•ft^2, $c = 0.0005$ lb•s/ft, $v_{\text{impact1}} = 0.8$ ft/s, $v_{\text{impact2}} =$

0.24 ft/s, g_y = -32.174 ft/s^2. There is no effective for due to pressure applied for this simulation, p = 0 lb/ft^2. The simulation had a total duration of 8 s with a time-step of Δt = 0.0004. The time lag on the impactor was t_{lag} = 0.1 s. STL files are output every 200 time-steps or at a time interval of 0.08 s. Contact checking on the flexible mesh was only done in the range -0.5 ft < y < 1.0 ft, for all x and z values (i.e. a horizontal strip). The distance check limit for this simulation was *distcheck* = 1.2 ft. The final parameter was the limit on the adjustable parameter, *blimit* = 75.

The simulation produced the time-lapse results shown in Figure 5.9. At t = 0 s, the initial configuration of the impactor and flexible structure is shown. Gravity was activated during the first time-step and the effects of this force are observed to damp to a steady-state value at approximately t = 0.5 s. Then, at t = 1.52 s, the impactor first contacts the flexible structure. In the images 3.12 s < t < 4.8 s contact is present. At some time after t = 4.8 s contact is lost and the impactor slides off the fabric. Finally, at t = 8 s, the structure has returned to the steady-state position under the influence of gravity only.

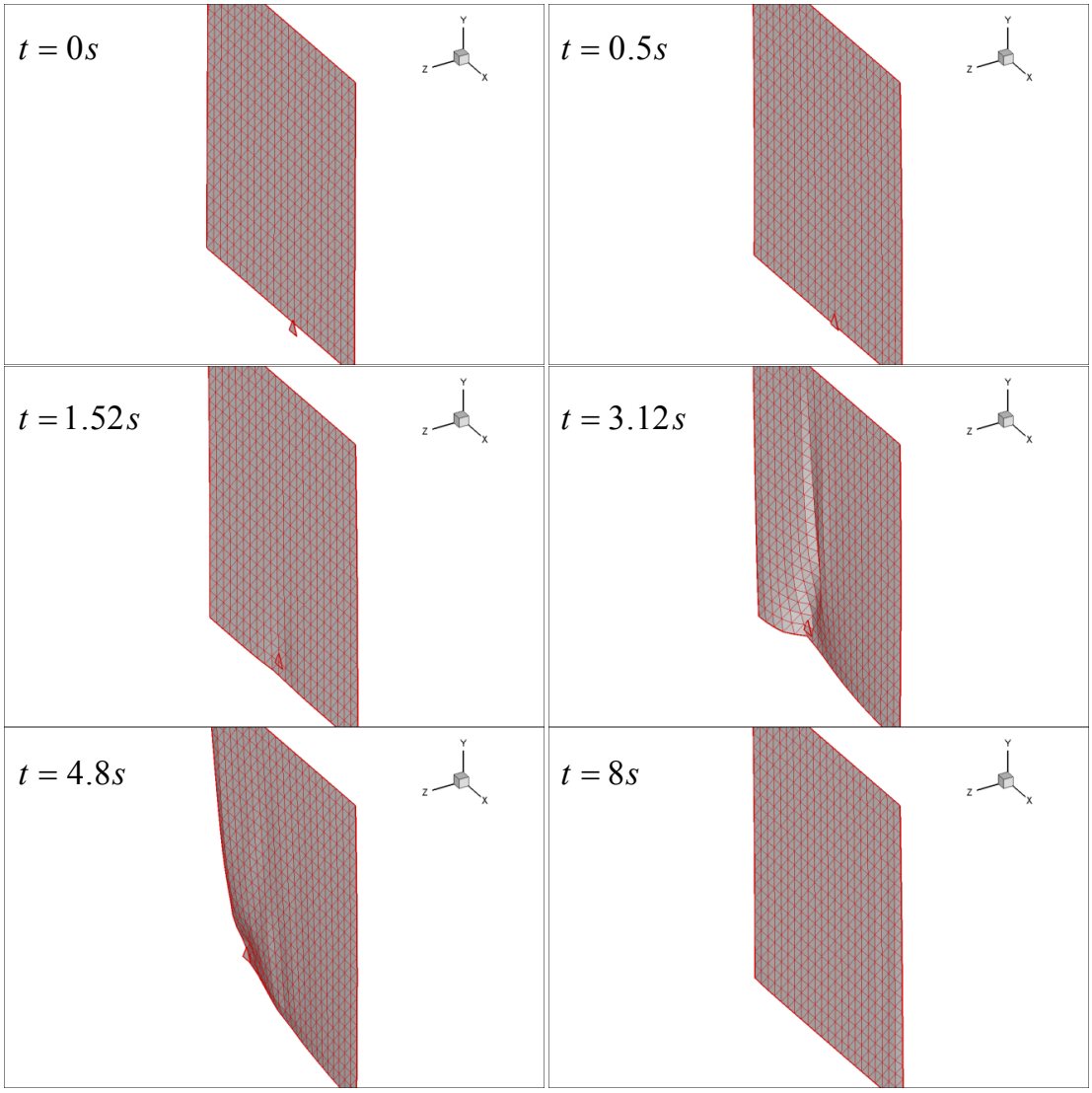

Figure 5.9. Single Impactor Triangle, Glancing Blow Animation Sequence

This case was used to demonstrate the utility of the MATLAB particle code's ability to handle contact events involving sliding contact.

5.4 Case 4: Sphere Passing through a Plate with a Slit

For this case, a quadrilateral plate with a slit in the middle was created. The coordinates and dimensions of the flexible structure in the initial undeformed configuration are shown in Figure 5.10. The area and average element size of the quadrilateral plate were equivalent to the flexible structure used in Cases 1 - 3. The plate was simply supported on all four edges, allowing a sphere to pass through the slit. The importance of this simulation was it forced the code to handle multiple impactors in the form of primitive shapes. Refer to Appendix I for the inputs to the MATLAB computer code for this case.

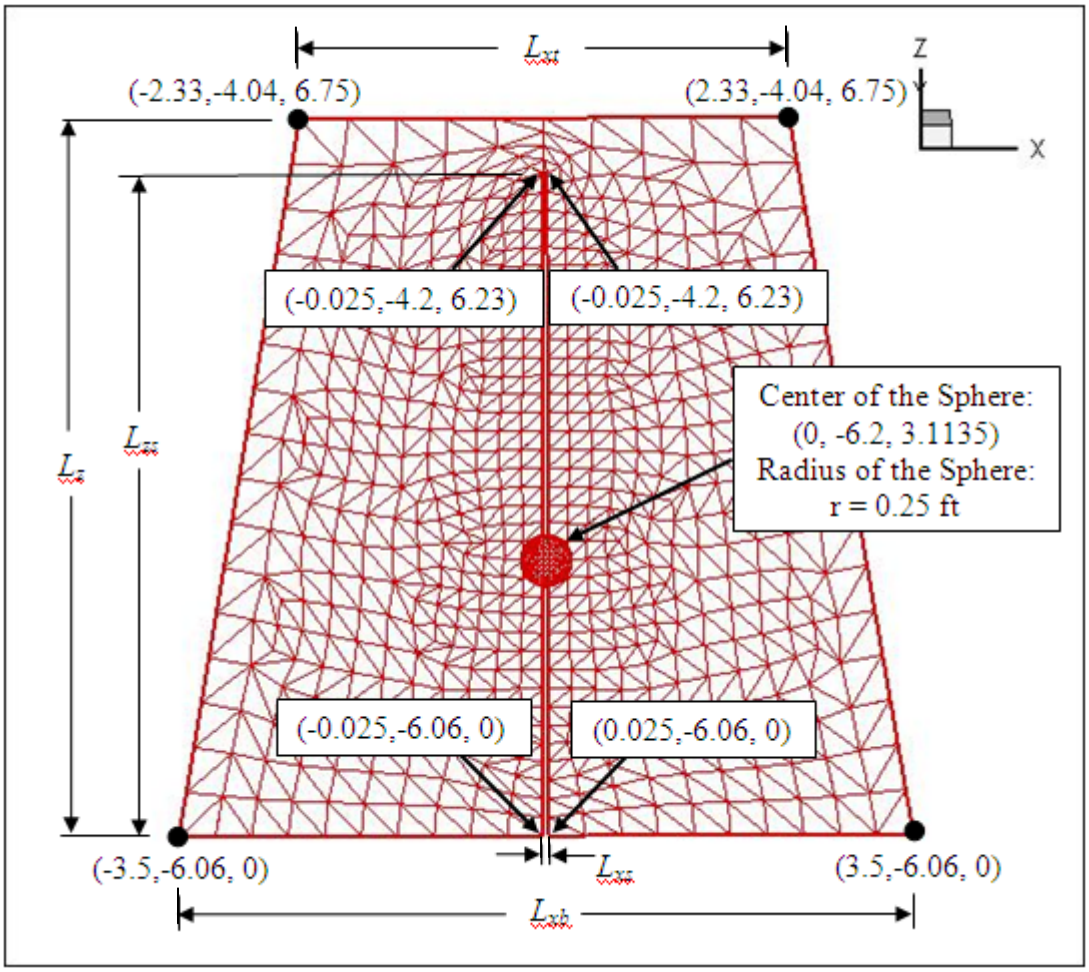

Figure 5.10. Case 4 Initial Flexible Structure and Sphere Configuration

The quadrilateral plate tapers in width from the bottom edge to the top edge (dimensions L_{xb} = 7 ft, L_{xt}= 4.66 ft, L_z = 6.75 ft). It is important to point out the orientation of the coordinate system has changed for this case from that of Cases 1, 2, and 3. In this case, the plate was slanted and was therefore located in all three planes, with the z-axis being the vertical axis. The slit was centered along the line, x = 0, with a slit width, L_{xs} = 0.05 ft and a slit height L_{zs} = 6.23 ft.

Since the orientation of the coordinate system has changed, Figure 5.2 has been replaced with Figure 5.11 to reflect this change. Figure 5.11 shows the gravitational force (f_{gz}), effective force due to pressure ($\underline{f}_i^p$), and velocity (v_{impact}) versus time for a given animation sequence.

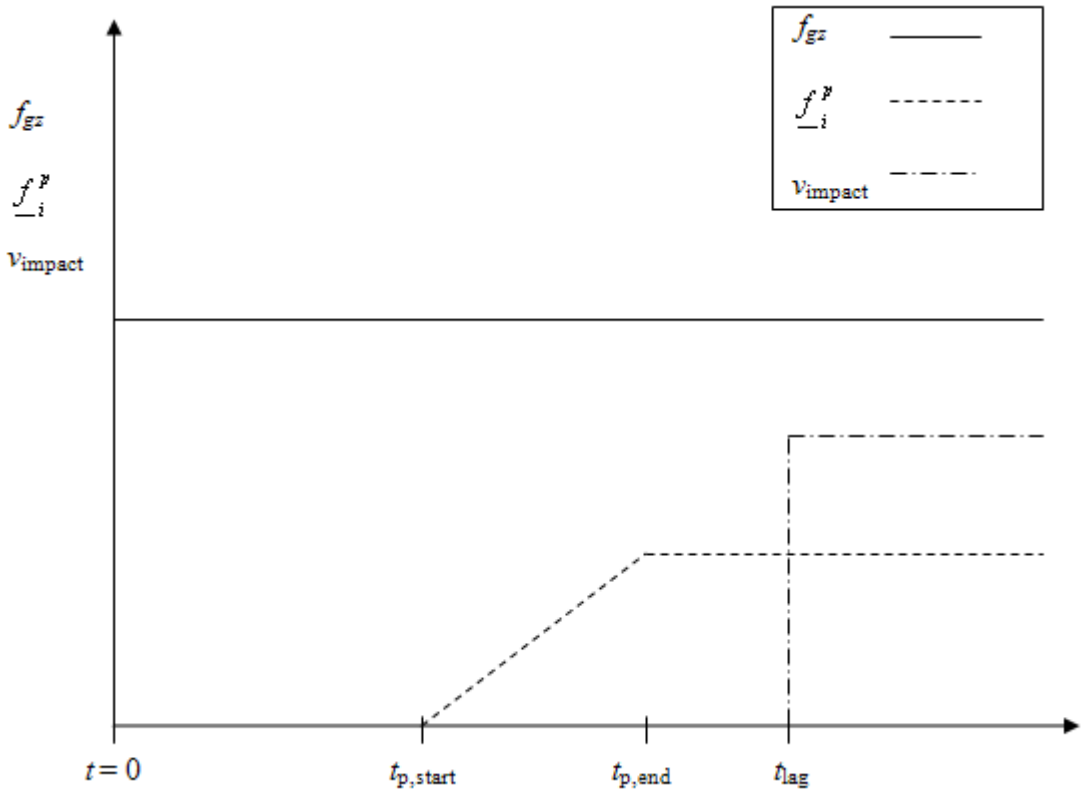

Figure 5.11. Forces and Velocity versus Time Plot

The sphere moved with a constant velocity v_{impact} in the positive y-direction. The values used for the parameters in the MATLAB particle code were: ρ^* = 0.0024 slug/ft^2, k_0 = 21.828 lb, k_b = 0.0000054 lb•ft^2, c = 0.0005 lb•s/ft, v_{impact} = 0.5 ft/s, g_z = 0 ft/s^2. There was no effective for due to pressure applied for this simulation, p = 0 lb/ft^2. The simulation had a total duration of 10 s with a time-step of Δt = 0.0002. The time lag on the sphere was t_{lag} = 0.1 s.

STL files were output every 500 time-steps or at a time interval of 0.1 s. Contact checking on the flexible mesh was only done in the range -0.4 ft < x < 0.4 ft, for all y and z values (i.e. a vertical strip matching the slope of the plate). The distance check limit for this simulation was *distcheck* = 0.7 ft. The final parameter was the limit on the adjustable parameter, *blimit* = 75.

The simulation produced the time-lapse results shown in Figure 5.12. At t = 0 s, the initial configuration of the sphere and flexible structure is shown. The gravitational force was not activated in this simulation therefore, there was no time lag needed for the effects of the gravity force to damp to a steady-state value. The sphere was only delayed until t = 0.1 s, when it begins to move. At t = 1.8 s, the sphere first contacts the flexible structure. In the images 2.6 s < t < 3.9 s contact is present. At some time after t = 3.9 s, contact is lost and the sphere passes through the slit. The image t = 4.2 s, shows the flexible structure returning to its initial configuration. Finally, at t = 8 s, the structure has returned to its initial configuration.

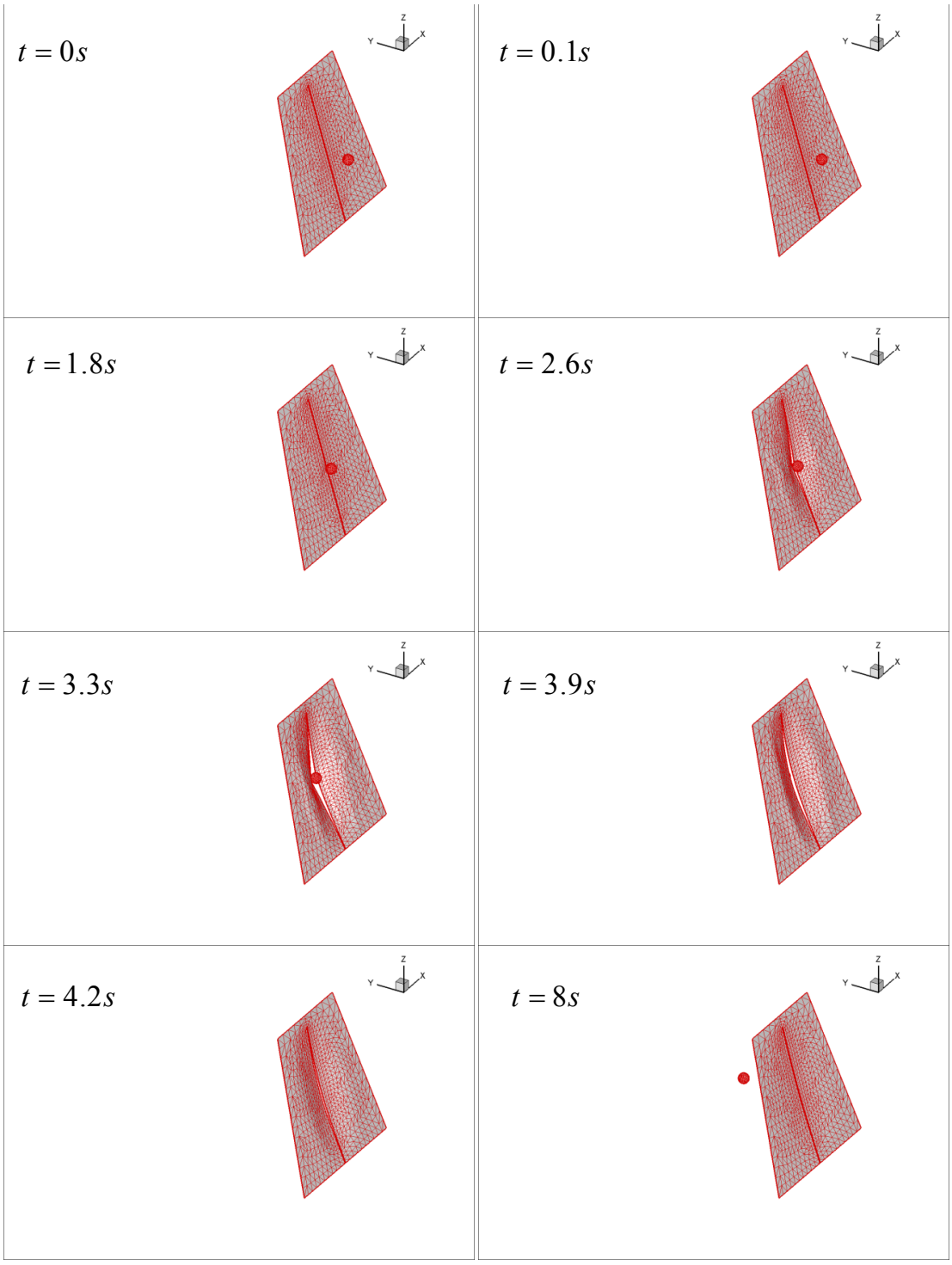

Figure 5.12. Sphere Through Plate Slit Animation Sequence

5.5 Case 5: Soldier Moving into Full Tent, No Pressure

The previous cases were used to demonstrate the utility of the contact algorithm, with the goal to ultimately produce the results presented here in Case 5. This case presents a single soldier impactor (referred to simply as "the soldier") moving into the flexible fabric hexagonal tent-like structure. The soldier model was represented as an STL surface mesh. In the subsequent simulations, the soldier model was non-articulating, rather, all vertices on the surface mesh moved with a constant velocity v_{impact} in the positive y-direction. The overall soldier and tent dimensions are shown in Figure 5.13. These dimensions are merely representative – they do not represent any particular human or conceived tent design. They were chosen for illustrative purposes only. The coordinates of the corner base nodes, the corner nodes at the top of the side panels, and at the peak of the tent are shown in Figure 5.14. In order to allow entry into the tent, one of the side panels was the slit quadrilateral plate described in Case 4 (Figure 5.10). Refer to Appendix J for the inputs to the MATLAB computer code for this case.

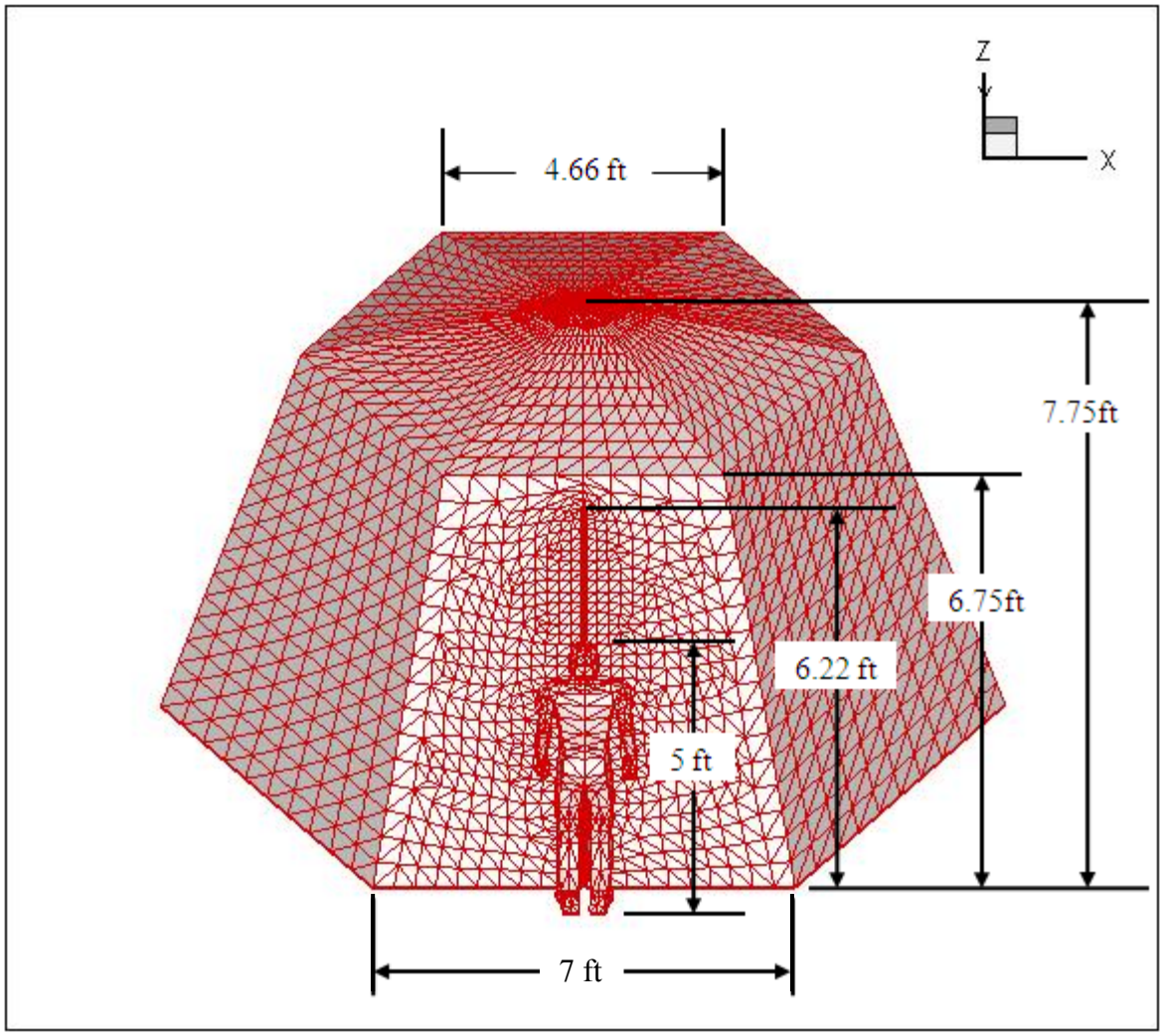

Figure 5.13. Initial Configuration of Soldier and Full Hexagonal-shaped Tent

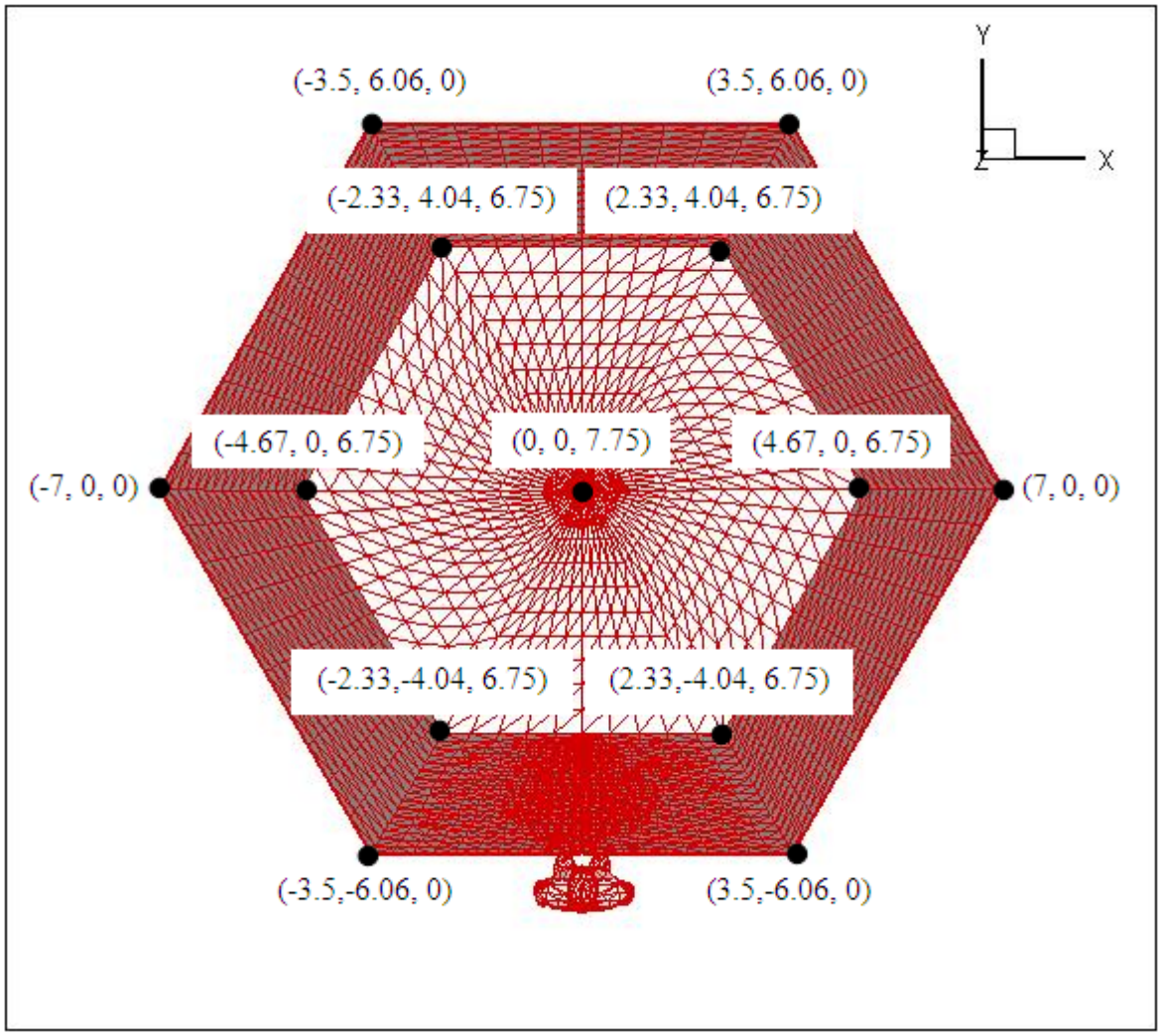

Figure 5.14. Pan View of Initial Soldier and Tent Configuration

Referring to Figure 5.11 provides a better understanding of when the given forces and velocities were applied with respect to time.

The numerical values for the parameters used in the MATLAB particle code were: $\rho^* = 0.0024$ slug/ft^2, $k_0 = 21.828$ lb, $k_b = 0.0000054$ lb•ft^2, $c = 0.0005$ lb•s/ft, $v_{impact} = 0.8$ ft/s, $g_z = -32.174$ ft/s^2. There was no effective force due to pressure applied for this simulation, $p = 0$ lb/ft^2. The simulation had a total duration of 10 s with a time-step of $\Delta t = 0.0002$. The time

lag on the soldier was t_{lag} = 2.6 s. STL files were output every 500 time-steps or at a time interval of 0.1 s. Contact checking on the flexible mesh was only done in the range -0.96 ft < x < 1.02 ft, for all y and z values (i.e. a vertical strip matching the slope of the door). The distance check limit for this simulation was *distcheck* = 0.7 ft. The final parameter was the limit on the adjustable parameter, *blimit* = 75.

The simulation produced the time-lapse results shown in Figure 5.15. At t = 0 s, the initial configuration of the soldier and the tent is shown. Gravity was activated during the first time-step and the effects of this force are observed to damp to a steady-state value at approximately t = 2.6 s, when the soldier begins moving toward the tent. Contact is first made between the soldier and the tent at t = 5.3 s. In the images 5.8 s < t < 6.8 s contact is present. At approximately t = 7 s, contact is lost and the soldier has completely traversed the door and is inside the tent. Then, the image t = 7.4 s shows the door returning to its initial position. Finally, at t = 10 s, the tent has returned to the steady-state position under the influence of gravity only.

The animation sequence provided in Figure 5.15 qualitatively shows the MATLAB particle code produced very realistic deformations during the contact sequence. Since the tent was not pre-tensed, a sagging effect was created when gravity was activated. Note the sharp indentations at the mid-sides of the tent's straight edges reflect the effects of gravity on the structural elements surrounding a simply supported edge vertex. Modeling the tent this way was chosen to provide some rigidity to the tent frame. The frame rigidity can be changed by varying the number of edge vertices which are simply supported.

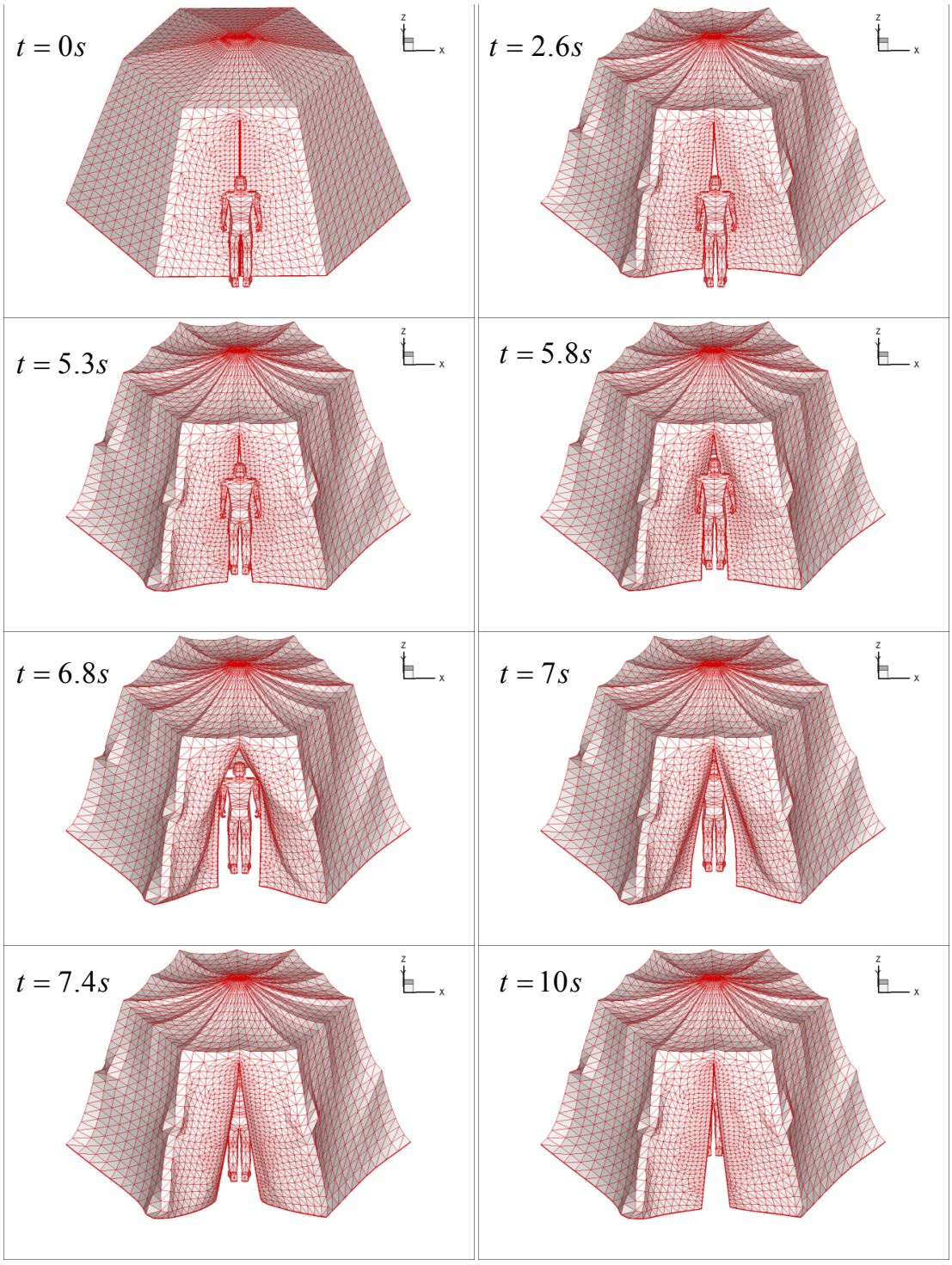

Figure 5.15. Single Soldier Entering Full Hexagonal-Shaped Tent Animation Sequence

5.5.1 Comparing Particle Model Results with LS-DYNA

After completing Case 5, it was desirable to compare the results obtained from the particle model with results obtained from the finite-element program, LS-DYNA. In order to do so, the same soldier and flexible structure geometry shown in Figures 5.13 and 5.14 were used. Since LS-DYNA reads and writes STL files, it was possible to directly import the soldier and flexible structure STL files into the program. Then, the necessary fabric properties used in Case 5 were directly input into LS-DYNA. The numerical values for the parameters used in LS-DYNA were: mass density $\rho = 0.757$ slug/ft^3, $E = 82{,}728$ lb/ft^2, $t = 0.00317$ ft. The time sequence for applying the gravity load and the human model motion were the same as Case 5. One property which was not directly analogous was the damping coefficient c. The global damping coefficient value input in LS-DYNA was $c = 0.9$. LS-DYNA was executed in explicit mode, whereby the time-step was controlled automatically. Figure 5.16 shows the location of vertex 1872.

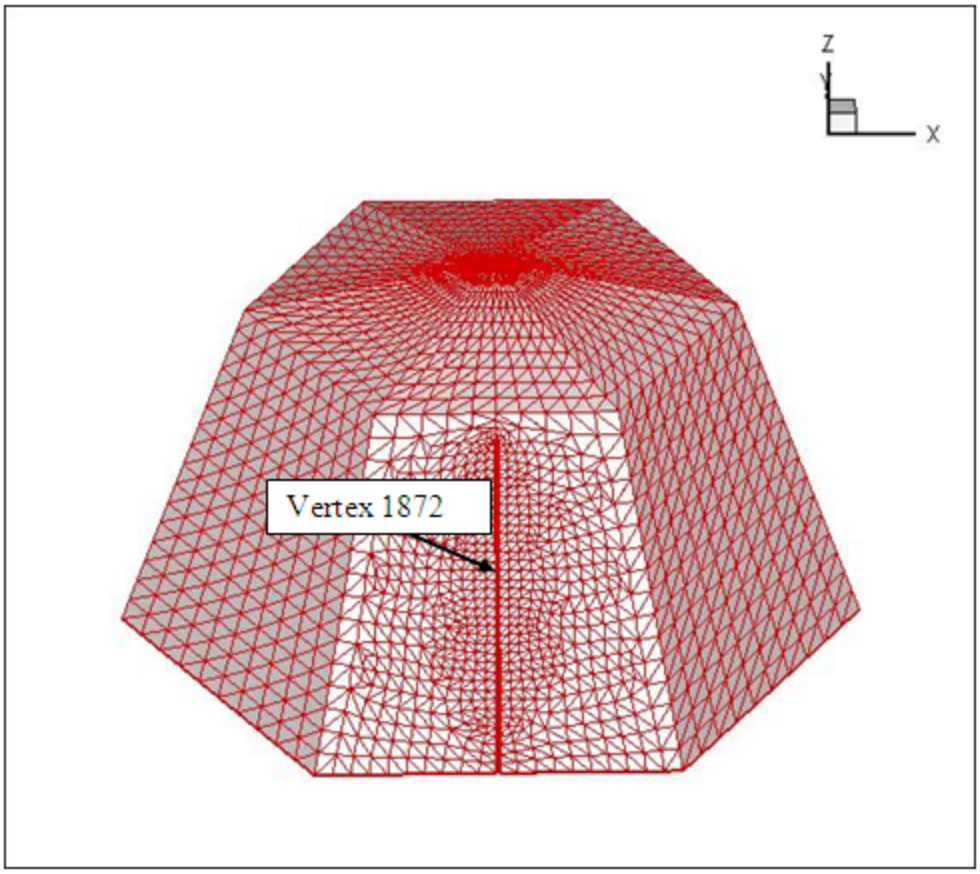

Figure 5.16. Location of Vertex 1872

Figure 5.17 provides a comparison of the position and velocity of vertex 1872 using a position and velocity versus time plot from the MATLAB code (top) above the *y*-position (middle) and *y*-velocity (bottom) versus time plots from LS-DYNA. For the MATLAB plot, it was only the *y*-position (red solid line) and the *y*-velocity (red dotted line) which was compared to the two LS-DYNA plots of the *y*-position and *y*-velocity. In Figure 5.17, the general overall shape of the *y*-position and *y*-velocity curves were very similar. The LS-DYNA curves were not as smooth as the particle model curves due to the difference in

damping coefficients. The peak of the curves and the steady-state positions were also very similar.

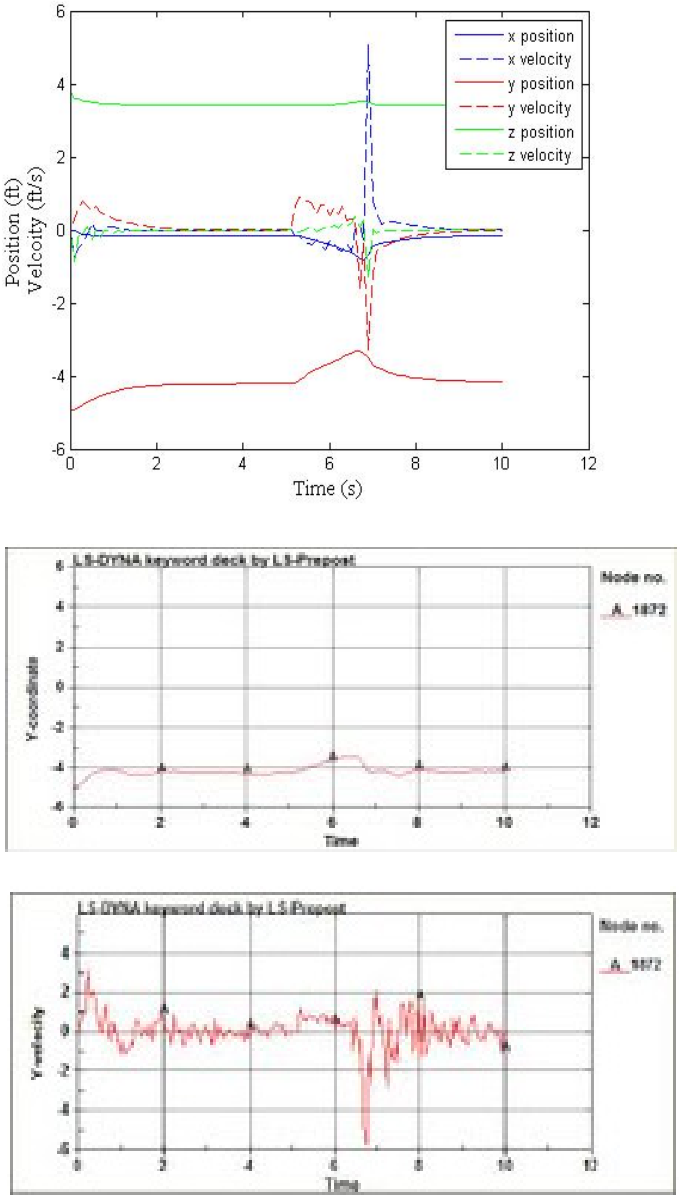

Figure 5.17. Particle Model Comparison with LS-DYNA Vertex 1872

Figure 5.18. Comparison Between Particle Model and LS-DYNA Animation Sequence

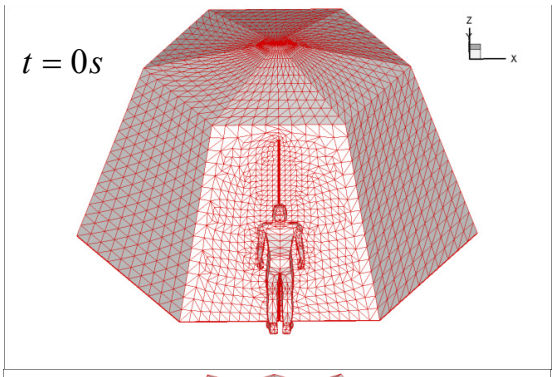
t = 0s

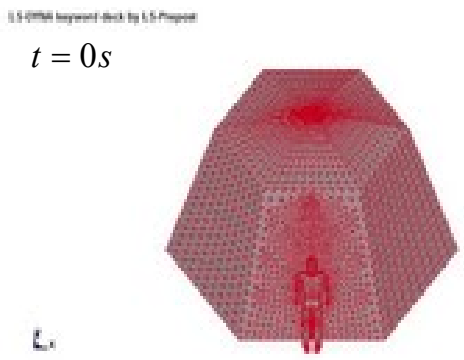
t = 0s

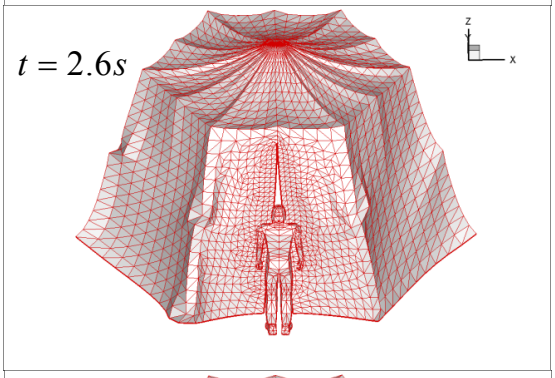
t = 2.6s

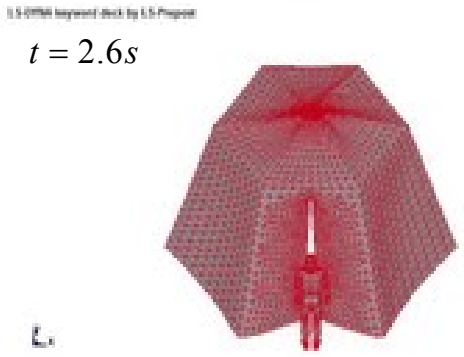
t = 2.6s

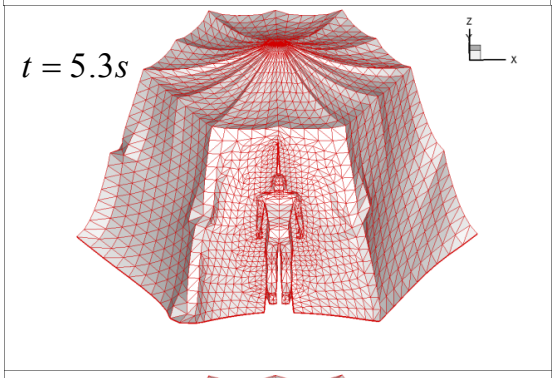
t = 5.3s

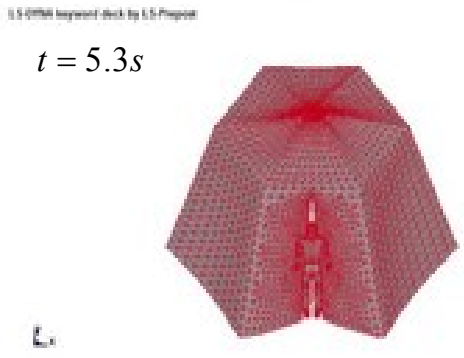
t = 5.3s

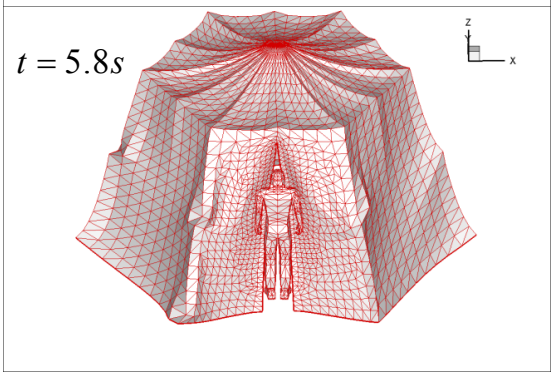
t = 5.8s

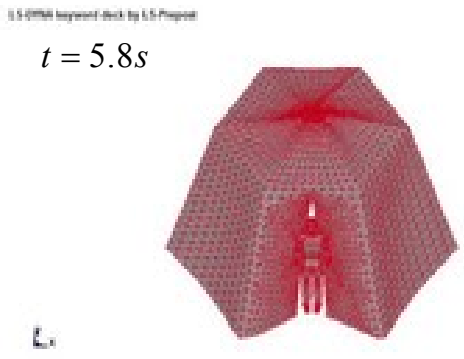
t = 5.8s

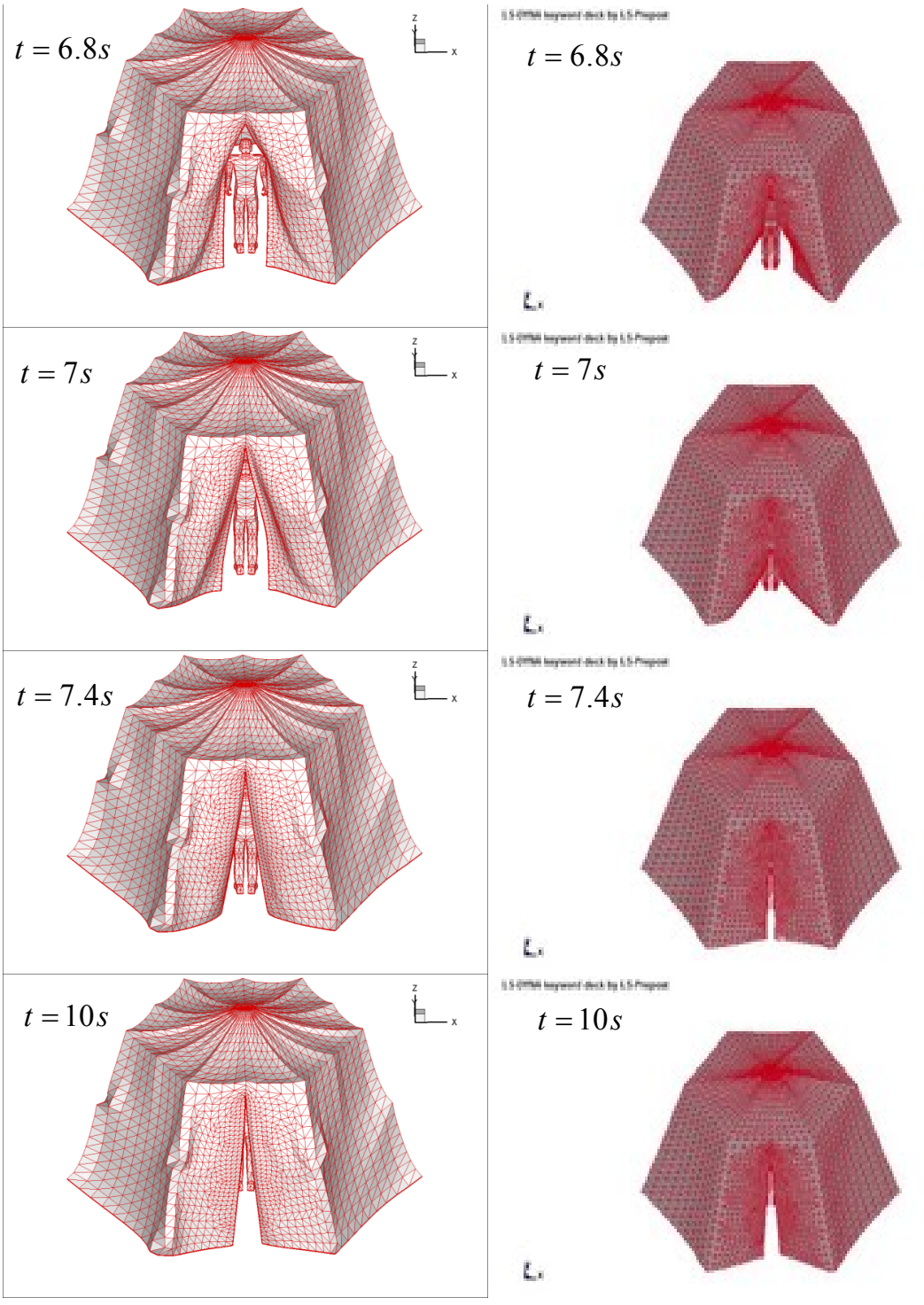
t = 6.8s
t = 7s
t = 7.4s
t = 10s
t = 6.8s
t = 7s
t = 7.4s
t = 10s

The animation sequence shown in Figure 5.18 shows snapshots of the particle model simulation (left) next to the LS-DYNA simulation (right). It is important to mention that although these simulations used the same soldier and tent geometry and material properties, there were some differences. First, the inability to match the damping coefficients caused some differences during the animation sequence. Also, the flexible structure was not constrained exactly the same in LS-DYNA as it was using the MATLAB computer code. In LS-DYNA, the mid-sides of the bottom section of the tent were not constrained. This eliminates what appears to be a sharp indentation in the mid-sides of the particle model simulation. Also, at t = 7 s and t = 7.4 s, the soldier in the LS-DYNA simulation has traversed the door earlier than in the particle model simulation. As a result, the deformation of the flexible structure using the particle model does not appear exactly the same as the LS-DYNA sequence. It is not exactly known why the models differ, but it may be that the LS-DYNA model was not constrained as much as the particle model, which makes it less stiff or it may be that LS-DYNA uses shell elements rather than the spring-mass system used by the particle model. However, the importance of this comparison was to show that the simulation using the MATLAB computer code produced very similar results to the LS-DYNA simulation.

5.6 Case 6: Soldier Moving into Full Tent, with Pressure

Case 6 uses the same soldier and flexible structure geometry and parameters as Case 5, but the results are presented with the addition of pressure. Referring to Figure 5.13 and Figure 5.14 provides the tent and soldier coordinates and dimensions. Applying pressure was an important feature that the MATLAB particle code had to contain. As a result, this simulation applied pressure while still handling a contact event. Referring to Figure 5.11 helps clarify when the given forces and velocities were applied with respect to time. Refer to Appendix K for the inputs to the MATLAB particle code for this case.

The numerical values for parameters used in the MATLAB particle code were: $\rho^* = 0.0024$ slug/ft^2, $k_0 = 21.828$ lb, $k_b = 0.0000054$ lb•ft^2, $c = 0.0005$ lb•s/ft, $v_{impact} = 0.8$ ft/s, $g_z = -32.174$ ft/s^2. There was an effective force due to pressure applied for this simulation, $p = 0.15$ lb/ft^2, $t_{p,start} = 2.6$ s and $t_{p,end} = 4.6$ s. The simulation had a total duration of 12 s with a time-step of $\Delta t = 0.00015$. The time lag on the soldier was $t_{lag} = 4.6$ s. STL files were output every 800 time-steps or at a time interval of 0.12 s. Contact checking on the flexible mesh was only done in the range -0.96 ft < x < 1.02 ft, for all y and z values (i.e. a vertical strip matching the slope of the door). The distance check limit for this simulation was *distcheck* = 0.7 ft. The limit on the adjustable parameter was, *blimit* = 75. An additional parameter was added for this case, *fixstretch* = 0.75 ft. This parameter adjusted the tent peak vertex and the first ring of vertices around the peak the value of *fixstretch*. This was done in the first time-step to pre-tension the tent with the goal of limiting the stretch caused by the effective force due to pressure.

The simulation produced the time-lapse results shown in Figure 5.19. At t = 0 s, the initial configuration of the soldier and the tent is shown. Gravity was activated during the first time-step and the effects of this force are observed to damp to a steady-state value at approximately t = 2.6 s, when the pressure force is first applied. The pressure force reaches its maximum value at t = 4.6 s, when the soldier begins moving toward the tent. Contact is first made between the soldier and the tent at t = 5.2 s. In the images 7.1 s < t < 8.3 s contact is present. At some point after t = 8.3 s, contact is lost and the soldier has completely traversed the door and is inside the tent. The image at t = 8.8 s shows the door returning to its position prior to contact. Finally, at t = 12 s, the tent is shown in the steady-state position under the influence of gravity and pressure only.

In the image t = 12 s, the bottom of the tent door is shown folded over. It is desirable to understand what is causing this result, but to this point, this cause has not been identified. Also, with simulations involving pressure, the MATLAB particle code has an inability to handle large pressure values. The deformation of the tent was very large even when very small pressure values were applied. Not many simulations were conducted involving pressure. As a result, additional simulations and analysis of how pressure is applied in the contact algorithm would be necessary to fully understand the effective force due to pressure.

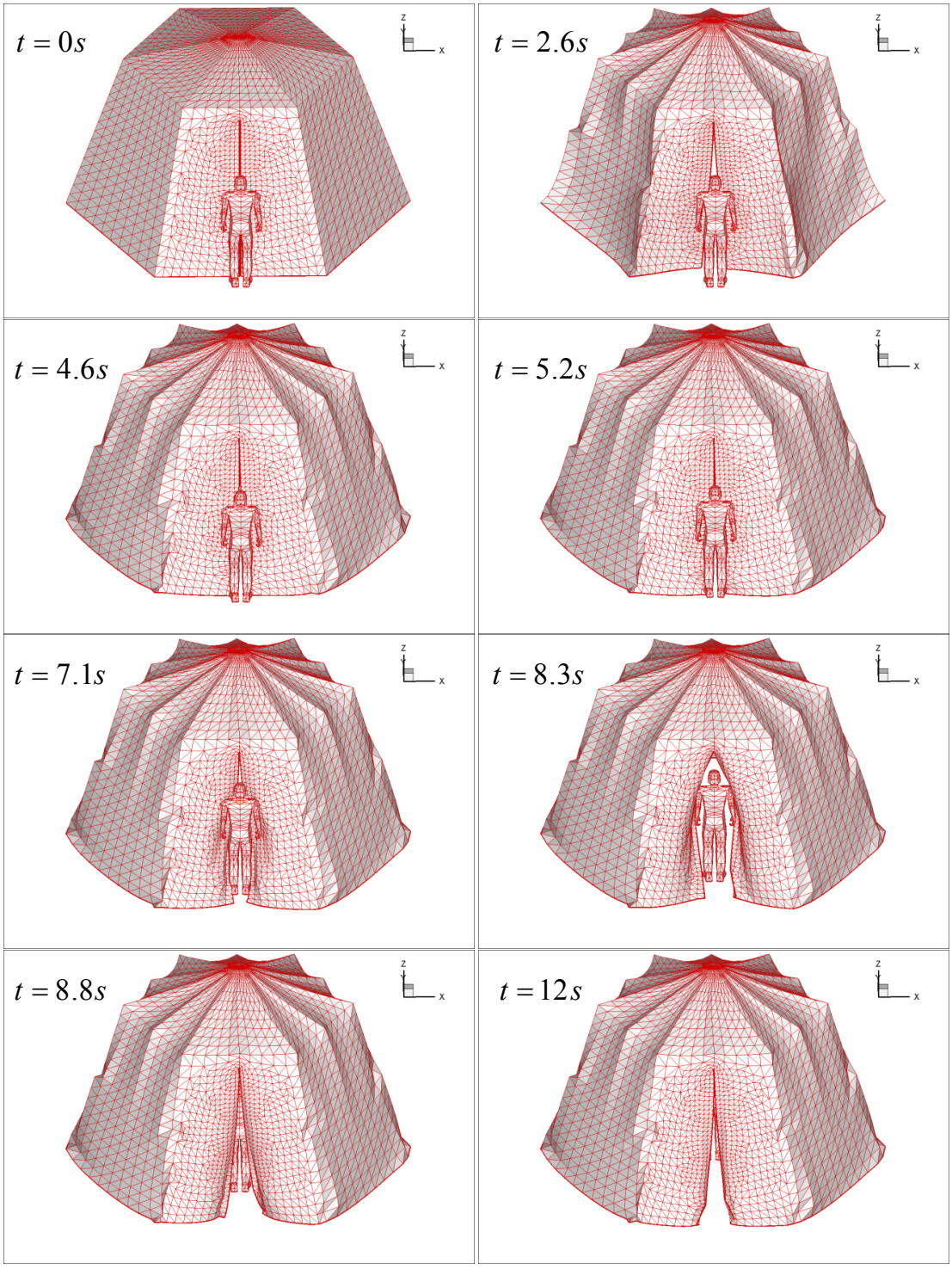

Figure 5.19. Single Soldier Entering Full Tent with Pressure Animation Sequence

5.7 Case 7: Soldier on a Gurney

The final case was the most complex contact interaction simulated by the MATLAB particle model. The particle model had to handle large structural deformations. This case modeled two soldiers carrying an injured soldier on a gurney; one soldier was placed at the head and feet, respectively, of another soldier who was positioned face-up as if lying on a gurney. Although the gurney was not modeled, this geometry replicates an entry event where two soldiers would enter a tent carrying a third soldier on a gurney. The tent geometry and properties used in this case were exactly the same as those used in Case 5 (Refer to Figures 5.13 and 5.14). The soldiers moved with a constant velocity v_{impact} in the positive y-direction. The difference between this case and Case 5 was the use of three soldier impactors in this case as opposed to one soldier in Case 5. Refer to Appendix L for the inputs to the MATLAB computer code for this case.

Referring to Figure 5.11 provides a better understanding of when the given forces and velocities were applied with respect to time.

The numerical values for parameters used in the MATLAB particle code were: $\rho^* = 0.0024$ slug/ft^2, $k_0 = 21.828$ lb, $k_b = 0.0000054$ lb•ft^2, $c = 0.0005$ lb•s/ft, $v_{\text{impact}} = 0.8$ ft/s, $g_z = -32.174$ ft/s^2. There was no effective force due to pressure applied for this simulation, $p = 0$ lb/ft^2. The simulation had a total duration of 16 s with a time-step of $\Delta t = 0.000125$. The time lag on the soldiers was $t_{\text{lag}} = 2.0$ s. STL files were output every 1280 time-steps or at a time interval of 0.16 s. Contact checking on the flexible mesh was only done in the range -0.96 ft $< x <$ 1.02 ft, for all y and z values (i.e. a vertical strip matching the slope of the door). The

distance check limit for this simulation was *distcheck* = 0.7 ft. The final parameter was the limit on the adjustable parameter, *blimit* = 75.

The simulation produced the time-lapse results shown in Figure 5.20. At t = 0 s, the initial configuration of the soldiers and the tent is shown. Gravity was activated during the first time-step and the effects of this force are observed to damp to a steady-state value at approximately t = 2.0 s, when the soldiers begin moving toward the tent. Contact is made between the first soldier and the tent at t = 4.5 s. Contact continues with the first soldier until some time after t = 6.25 s when the first soldier has completely traversed the door and is inside the tent. As this occurs, contact is made between the second soldier, lying on his back, and the tent. In the images 7.2 s < t < 8.8 s contact continues until some time after t = 8.8 s, when contact with the second soldier is lost and this soldier has completely traversed the door and is inside the tent as well. At some time after contact is lost with the second soldier, contact is made between the third soldier and the tent. Contact continues with the third soldier shown in the image at t = 12.8 s. At some time after t = 12.8 s, contact is lost and the third and final soldier has completely traversed the door and is inside the tent. Finally, at t = 16 s, the tent is shown in the steady-state position under the influence of gravity only.

Qualitatively, Figure 5.20 shows the MATLAB particle code produces very realistic deformations for the given entry event. For this event, the particle code handles a very complex contact interaction between the tent and three soldiers which produces large structural deformations.

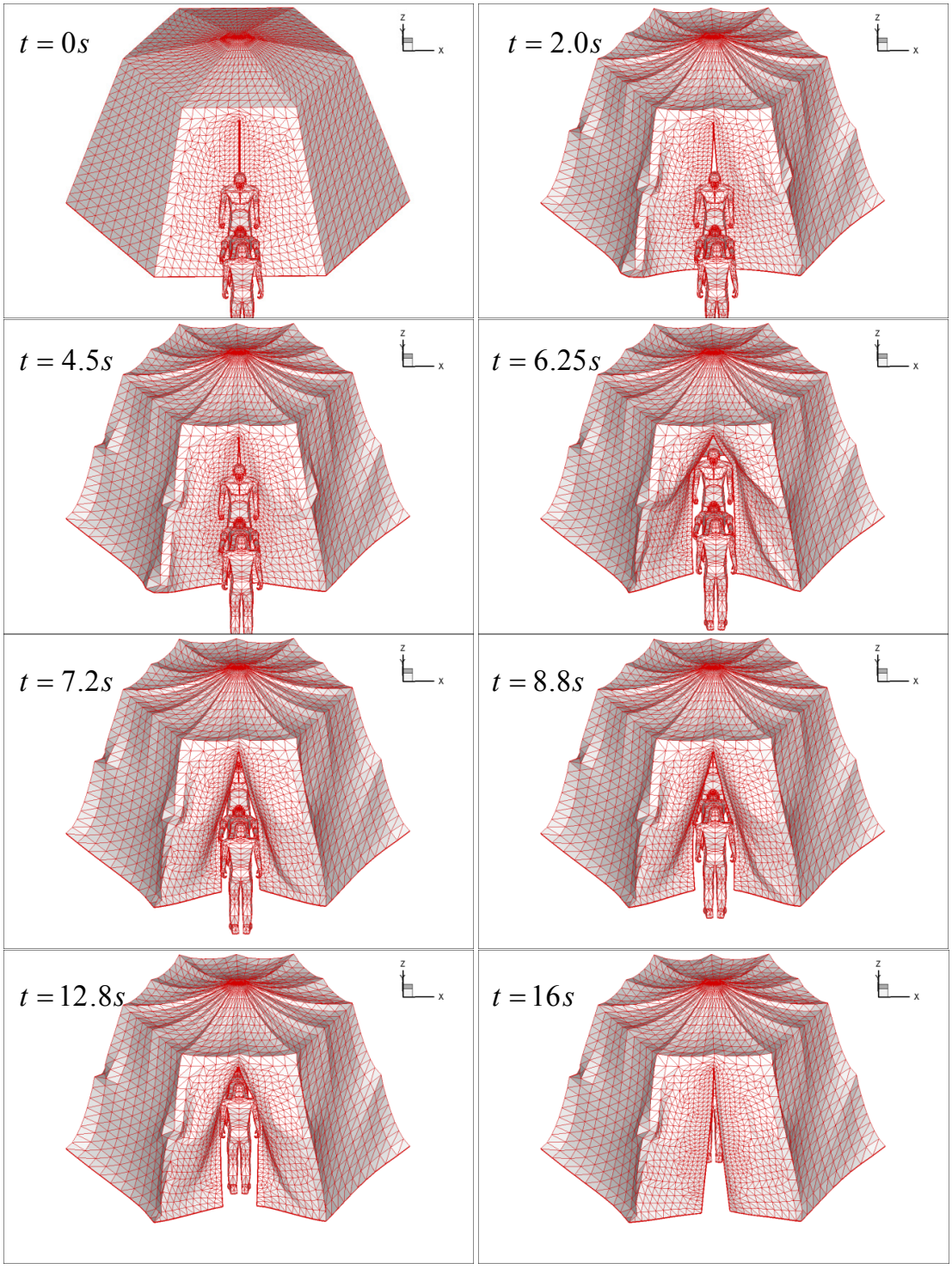

Figure 5.20. Soldier on Gurney Entering Full Tent Animation Sequence

To quantitatively view the results, Figure 5.21 shows the time-history results for a mid-side vertex located along the slit in the door (vertex 1872 with coordinates x = -0.025, y = -4.92, z = 3.8).

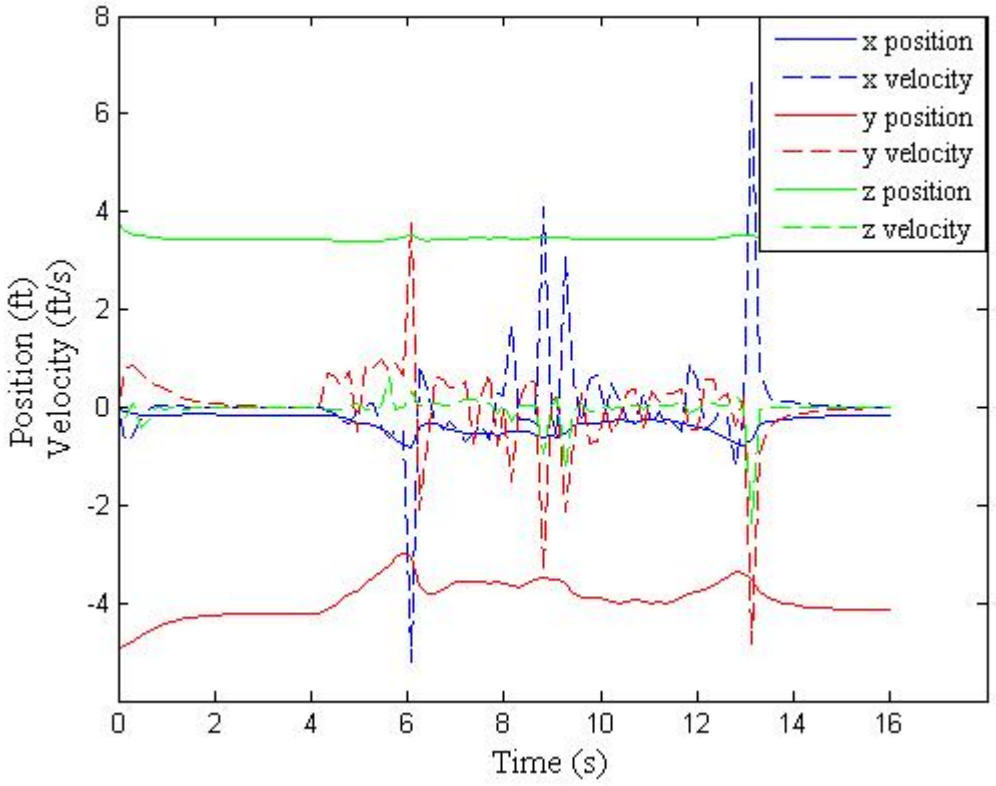

Figure 5.21. Time-History Plot for Structural Element Vertex 1872

Figure 5.21 coincides with the results described in Figure 5.20. The maximum penetration value over the total duration of the simulation is shown in Figure 5.22.

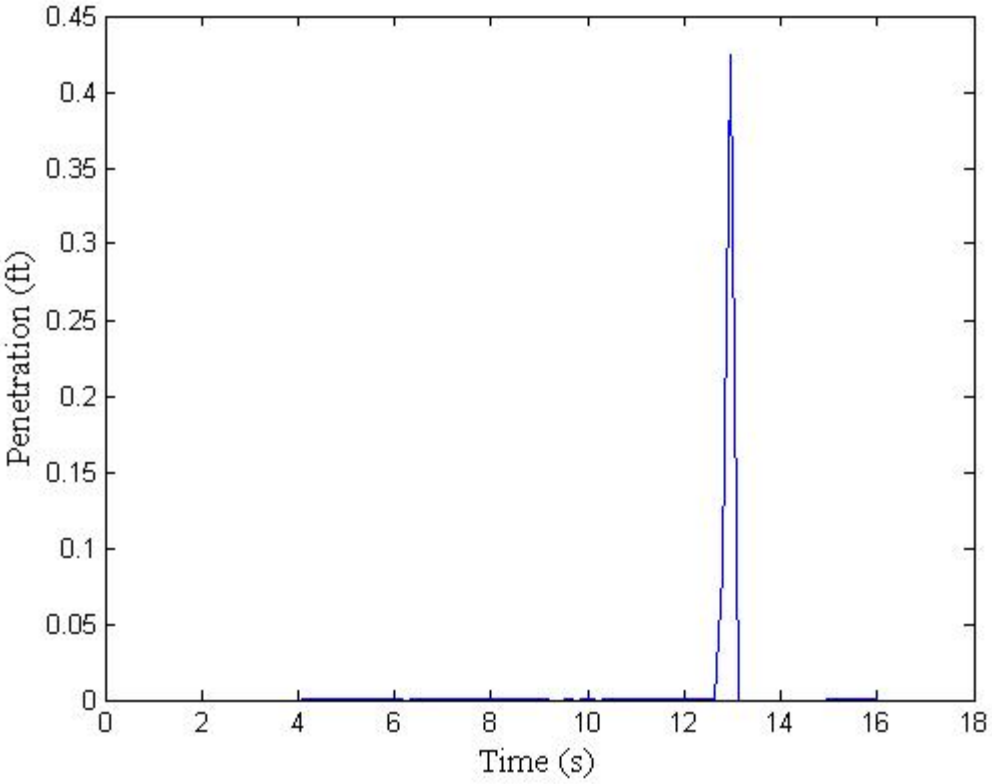

Figure 5.22. Time-History Plot of the Maximum Penetration

Figure 5.22 shows a long span of time when the penetration values were very small (i.e. violations of the contact algorithm were minor). But, it is noted that the spike shown in Figure 5.22 corresponds to a penetration value slightly larger than the element size. With the contact algorithm used, penetration was the definition of contact. The goal was to limit this penetration although violations do occur. This penetration value should not diminish the rest of the result which produced very small contact violations.

6 Conclusions and Recommendations

6.1 Conclusions

- A MATLAB computer code that implemented the particle-based formulation capable of handling stretching and bending stiffness, external forces, and contact was created and thoroughly tested. The computer code was validated where possible using classical beam and plate theories.
- A frictionless, inelastic collision/contact formulation was devised and implemented in the MATLAB computer code. The contact algorithm has been tested on a wide range of events simulating impact between rigid impactors and flexible structures and appears to work dependably.
- The computer code has been used to provide simulated ingress/egress events into a tent-like structure.
- The experimental procedure to measure actual fabric mechanical properties has been documented.
- The procedure to convert experimentally determined fabric mechanical properties to effective stiffness values useful for the particle code simulations has been documented.
- The MATLAB code reads and writes STL files making it compatible with an immersed boundary computational fluid dynamic code that can treat fluid-structure interactions.

- The results have been compared to simulations using the finite-element program, LS-DYNA.

6.2 Recommendations for Future Research

- Opportunities exist for making the code more efficient in order to seek reduced computation time.
- The stretching stiffness coefficient was successfully made independent of mesh size. It would be very useful to determine a way to do the same with the bending stiffness coefficient so it is not mesh-size dependent. This would eliminate the need for the tuning approach.
- It would be very interesting to take the output produced from the MATLAB computer code and use it as input to the CFD code to obtain one-way coupled results. This was the initial plan for this research and although the capability has now been developed, this has not yet been completed.
- Additional testing using different tent geometries, different fabric materials, and different soldier configurations could be very valuable to the understanding of the structural response over a range of parameters.
- It is recommended that further comparisons between the particle model and LS-DYNA be explored.

REFERENCES

Abramowitz, M., & Stegun, I. A. (Eds.). (1972). Handbook of Mathematical Functions with Formulas, Graphs, and Mathematical Tables. *55 , Applied Mathematics Series*, 896. U.S. Department of Commerce: National Bureau of Standards.

Baraff, D., & Witkin, A. (1998). Large Steps in Cloth Simulation. *Computer Graphics Proceedings (SIGGRAPH 98)*, (pp. 43-54). Orlando.

Baraff, D., Witkin, A., & Kass, M. (2003). Untangling Cloth. *Annual Conference Proceedings (ACM SIGGRAPH 2003)*, (pp. 862-870).

Bigliani, R., & Eischen, J. W. (2000). Collision Detection in Cloth Modeling. In D. H. House, & D. E. Breen, *Cloth Modeling and Animation* (pp. 197-217). Natick, Massachusetts: A K Peters.

Breen, D. E., House, D. H., & Wozny, M. J. (1994). Predicting the Drape of Woven Cloth Using Interacting Particles. *Computer Graphics Proceedings (SIGGRAPH '94)* , 365-372.

Choi, K.-J., & Ko, H.-S. (2002). Stable but Responsive Cloth. *Computer Graphics Proceedings (SIGGRAPH)*, (pp. 604-611).

(2006). Contact-Impact Algorithm. In *LS-DYNA Theory Manual* (pp. 26.1-26.46). Livermore, California: Livermore Software Technology Corporation.

Eischen, J. W., Deng, S., & Clapp, T. G. (1996). Finite-Element Modeling and Control of Flexible Fabric Parts. *Computer Graphics in Textiles and Apparel (IEEE Computer Graphics and Applications)* , 71-80.

Fontana, M., Rizzi, C., & Cugini, U. (2004). Physics-Based Modeling and Simulation of Functional cloth for Virtual Prototyping Applications. *ACM Symposium on Solid Modeling and Applications* (pp. 267-272). The Eurographics Association.

Gere, J. M., & Timoshenko, S. P. (1997). *Mechanics of Materials.* Boston: PWS Publishing Co.

Gu, X., Gortler, S. J., & Hoppe, H. (2002). Geometry Images. *ACM Transactions on Graphics 2002*, (pp. 355-361).

Huh, S., Metaxas, D. N., & Badler, N. I. (2001). Collision Resolutioins in Cloth Simulation. *IEEE Computer Animation Conference 2001.*

O'Brien, J. F., Hodgins, J. K., & Zordan, V. B. (1997). Combining Active and Passive Simulations for Secondary Motion. *Visual Proceedings (SIGGRAPH '97)* (pp. 1-2). Los Angeles: ACM.

Rohde, F. (1953). Large Deflections of a Cantilever Beam with Uniformly Distributed Load. *Quart. Appl. Math. 11* , 337-338.

(2008). Standard Test Method for Stiffness of Fabrics. D-1388. In *ASTM International.* West Conshohocken, PA: ASTM.

Sul, I. H., & Kang, T. J. (2004). Improvement of Drape Simulation Speed using Constrained Fabric Collision. *International Journal of Clothing Science and Technology* , 43-50.

Terzopoulos, D., & Fleischer, K. (1988). Modeling Inelastic Deformation: Viscoelasticity, Plasticity, Fracture. *Computer Graphics (SIGGRAPH '88) vol. 22(4)* (pp. 269-278). Atlanta: ACM.

Terzopoulos, D., Platt, J. B., & Fleischer, K. (1987). Elastically Deformable Models. *Computer Graphics (SIGGRAPH '87) vol. 21(4)* (pp. 205-214). Anaheim: ACM.

Timoshenko, S., & Woinowsky-Krieger, S. (1959). Simply Supported Rectangular Plates. In *Theory of Plates and Shells* (pp. 111-112). New York: McGraw-Hill.

Volino, P., & Magnenat Thalmann, N. (2000). Implementing Fast Cloth Simulation with Collision Response. *Proceedings of the Conference on Computer Graphics International (CGI-00)*, (pp. 257-268).

Volino, P., & Magnenat-Thalmann, N. (1994). Efficient Self-Collision Detection on Smoothly Discretised Surface Animation Using Geometrical Shape Regularity. *Computer Graphics Forum (Eurographics '94)* (pp. 155-166). Blackwell Publishers.

Zhang, D., & Yuen, M. M. (2000). Collision Detection for Clothed Human Animation. *Proceedings of the 8th Pacific Graphics Conference on Computer Graphics and Application (PACIFIC GRAPHICS-00)*, (pp. 328-337).

Zink, N., & Hardy, A. (2007). Cloth Simulation and Collision Detection using Geometry Images. *Proceedings of the 5th International Conference on Computer Graphics, Virtual Reality, Visualisation and Interaction in Africa (SIGGRAPH 2007)* (pp. 187-195). Grahamstown: ACM.

APPENDIX

A Equations of Motion Matlab Function Code

```
%Declaring variables used in both functions as global
global d0 nnodes m c k0 kb fxext fyext fzext fixed coords NNM bend
nconnect kap0 nelem vertex pmax tpstart tpend gx gy gz a

dvdt=[];

%This must be uncommented for simulations involving pressure
%for loop over the number of elements to get areas and normals used for
%pressure loading
% for ii=1:nelem
%       Ax=v(6*vertex(ii,1)-5);
%       Ay=v(6*vertex(ii,1)-3);
%       Az=v(6*vertex(ii,1)-1);
%
%       Bx=v(6*vertex(ii,2)-5);
%       By=v(6*vertex(ii,2)-3);
%       Bz=v(6*vertex(ii,2)-1);
%
%       Cx=v(6*vertex(ii,3)-5);
%       Cy=v(6*vertex(ii,3)-3);
%       Cz=v(6*vertex(ii,3)-1);
%
%       v1=sqrt((Bx-Ax)^2+(By-Ay)^2+(Bz-Az)^2);
%       v1x=(Bx-Ax);
%       v1y=(By-Ay);
%       v1z=(Bz-Az);
%
%       v2=sqrt((Cx-Ax)^2+(Cy-Ay)^2+(Cz-Az)^2);
%       v2x=(Cx-Ax);
%       v2y=(Cy-Ay);
%       v2z=(Cz-Az);
%
%       pnorm(ii)=sqrt((v1y*v2z-v1z*v2y)^2+(v1z*v2x-v1x*v2z)^2+(v1x*v2y-
                  v1y*v2x)^2);
%       pnormx(ii)=(v1y*v2z-v1z*v2y)/pnorm(ii);
%       pnormy(ii)=(v1z*v2x-v1x*v2z)/pnorm(ii);
%       pnormz(ii)=(v1x*v2y-v1y*v2x)/pnorm(ii);
%
%       elemarea(ii)=1/2*pnorm(ii);
% end

%Create a set of for loops to solve equations of motion for a number of
desired particles

%%%%%%%%%%%%%%%%%%%%%%%%%%%%%%%%%%%%%%%%%%%%%%%%%%%%%%%%%%%%%%%%%%%%
%Calculating the forces contributed due to stretching
for ii=1:nnodes
```

```
    ax=0;
    ay=0;
    az=0;
    if fixed(ii)==1
            axx(ii) = 0;
            ayy(ii) = 0;
            azz(ii) = 0;
            continue
    end
    for jj=3:NNM(ii,2)+2

           d0=sqrt((coords(NNM(ii,jj),1)-coords(NNM(ii,1),1))^2 +
               (coords(NNM(ii,jj),2)-coords(NNM(ii,1),2))^2 +
               (coords(NNM(ii,jj),3)-coords(NNM(ii,1),3))^2);
           d=sqrt((v(6*NNM(ii,jj)-5)-v(6*NNM(ii,1)-5))^2 +
              (v(6*NNM(ii,jj)-3)-v(6*NNM(ii,1)-3))^2 + (v(6*NNM(ii,jj)-1)-
              v(6*NNM(ii,1)-1))^2);

           nx=(v(6*NNM(ii,jj)-5)-v(6*NNM(ii,1)-5))/d;
           ny=(v(6*NNM(ii,jj)-3)-v(6*NNM(ii,1)-3))/d;
           nz=(v(6*NNM(ii,jj)-1)-v(6*NNM(ii,1)-1))/d;

           fx=fxext(ii)+(m(ii)*gx) +(k0/d0)*(d-d0)*nx - c*v(6*NNM(ii,1)-
               4);
           fy=fyext(ii)+(m(ii)*gy) +(k0/d0)*(d-d0)*ny - c*v(6*NNM(ii,1)-
               2);
           fz=fzext(ii)+(m(ii)*gz) +(k0/d0)*(d-d0)*nz - c*v(6*NNM(ii,1));

           ax=ax+(fx/m(ii));
           ay=ay+(fy/m(ii));
           az=az+(fz/m(ii));

    end

    axx(ii) = ax;
    ayy(ii) = ay;
    azz(ii) = az;

end

%%%%%%%%%%%%%%%%%%%%%%%%%%%%%%%%%%%%%%%%%%%%%%%%%%%%%%%%%%%%%%%%%%%%%%%%%%
%Calculating the forces contributed due to bending

 for ii=1:nconnect

            ax1=0;
            ay1=0;
            az1=0;
            ax2=0;
            ay2=0;
            az2=0;
```

```
ax3=0;
ay3=0;
az3=0;
ax4=0;
ay4=0;
az4=0;

i1= bend(ii,1);
i2= bend(ii,2);
i3= bend(ii,3);
i4= bend(ii,4);


L=(1/2)*sqrt((coords(i1,1)-coords(i3,1))^2 + (coords(i1,2)-
  coords(i3,2))^2 + (coords(i1,3)-coords(i3,3))^2);

if fixed(i1) && fixed(i2) && fixed(i3) || fixed(i1) &&
   fixed(i3) && fixed(i4) ==1
    continue
end

     x1=v(6*i1-5);
     y1=v(6*i1-3);
     z1=v(6*i1-1);
     x2=v(6*i2-5);
     y2=v(6*i2-3);
     z2=v(6*i2-1);
     x3=v(6*i3-5);
     y3=v(6*i3-3);
     z3=v(6*i3-1);
     x4=v(6*i4-5);
     y4=v(6*i4-3);
     z4=v(6*i4-1);

t12=sqrt((x2-x1)^2 + (y2-y1)^2 + (z2-z1)^2);
t12x=(x2-x1)/t12;
t12y=(y2-y1)/t12;
t12z=(z2-z1)/t12;

t14=sqrt((x4-x1)^2 + (y4-y1)^2 + (z4-z1)^2);
t14x=(x4-x1)/t14;
t14y=(y4-y1)/t14;
t14z=(z4-z1)/t14;

t12xt14=sqrt((t12y*t14z-t12z*t14y)^2 + (t12z*t14x-t12x*t14z)^2
        + (t12x*t14y-t12y*t14x)^2);

n124x=(t12y*t14z-t12z*t14y)/t12xt14;
n124y=(t12z*t14x-t12x*t14z)/t12xt14;
n124z=(t12x*t14y-t12y*t14x)/t12xt14;
```

```
t23=sqrt((x3-x2)^2 + (y3-y2)^2 + (z3-z2)^2);
t23x=(x3-x2)/t23;
t23y=(y3-y2)/t23;
t23z=(z3-z2)/t23;

t24=sqrt((x4-x2)^2 + (y4-y2)^2 + (z4-z2)^2);
t24x=(x4-x2)/t24;
t24y=(y4-y2)/t24;
t24z=(z4-z2)/t24;

t23xt24=sqrt((t23y*t24z-t23z*t24y)^2 + (t23z*t24x-t23x*t24z)^2
        + (t23x*t24y-t23y*t24x)^2);

n234x=(t23y*t24z-t23z*t24y)/t23xt24;
n234y=(t23z*t24x-t23x*t24z)/t23xt24;
n234z=(t23x*t24y-t23y*t24x)/t23xt24;

navg=sqrt(((n124x+n234x)/2)^2 +((n124y+n234y)/2)^2 +
     ((n124z+n234z)/2)^2);

n24x=((n124x+n234x)/2)/navg;
n24y=((n124y+n234y)/2)/navg;
n24z=((n124z+n234z)/2)/navg;

dot=(n124x*n234x + n124y*n234y + n124z*n234z);

if dot > 1
    dot=1;
end

dphi=acos(dot);

t12dotn234=(t12x*n234x + t12y*n234y + t12z*n234z);

dphi=-sign(t12dotn234)*dphi;

kap=dphi/L;

kap=kap - kap0(ii);

  f1x=-2*kb*kap/L*n24x;
  f1y=-2*kb*kap/L*n24y;
  f1z=-2*kb*kap/L*n24z;
  f2x=2*kb*kap/L*n24x;
  f2y=2*kb*kap/L*n24y;
  f2z=2*kb*kap/L*n24z;
  f3x=-2*kb*kap/L*n24x;
  f3y=-2*kb*kap/L*n24y;
  f3z=-2*kb*kap/L*n24z;
  f4x=2*kb*kap/L*n24x;
```

```
  f4y=2*kb*kap/L*n24y;
  f4z=2*kb*kap/L*n24z;


if fixed(i1)==1
    ax1=0;
    ay1=0;
    az1=0;
else
    ax1=(f1x/m(i1));
    ay1=(f1y/m(i1));
    az1=(f1z/m(i1));
end

if fixed(i2)==1
    ax2=0;
    ay2=0;
    az2=0;
else
    ax2=(f2x/m(i2));
    ay2=(f2y/m(i2));
    az2=(f2z/m(i2));
end

if fixed(i3)==1
    ax3=0;
    ay3=0;
    az3=0;
else
    ax3=(f3x/m(i3));
    ay3=(f3y/m(i3));
    az3=(f3z/m(i3));
end

 if fixed(i4)==1
     ax4=0;
     ay4=0;
     az4=0;
 else
     ax4=(f4x/m(i4));
     ay4=(f4y/m(i4));
     az4=(f4z/m(i4));
end

axx(i1) = axx(i1) + ax1;
ayy(i1) = ayy(i1) + ay1;
azz(i1) = azz(i1) + az1;
axx(i2) = axx(i2) + ax2;
ayy(i2) = ayy(i2) + ay2;
azz(i2) = azz(i2) + az2;
axx(i3) = axx(i3) + ax3;
ayy(i3) = ayy(i3) + ay3;
```

```
            azz(i3) = azz(i3) + az3;
            axx(i4) = axx(i4) + ax4;
            ayy(i4) = ayy(i4) + ay4;
            azz(i4) = azz(i4) + az4;

 end

%Uncomment the following section for simulations involving pressure

%%%%%%%%%%%%%%%%%%%%%%%%%%%%%%%%%%%%%%%%%%%%%%%%%%%%%%%%%%%%%%%%%%%%%%%%%%%%%
%%%%%%%%%%%%%%%%%
 %Calculating the forces contributed due to Pressure
%  for ii=1:nelem
%      ax1=0;
%      ay1=0;
%      az1=0;
%      ax2=0;
%      ay2=0;
%      az2=0;
%      ax3=0;
%      ay3=0;
%      az3=0;
%
%       i1= vertex(ii,1);
%       i2= vertex(ii,2);
%       i3= vertex(ii,3);
%
%       if t < tpstart
%           p=0;
%       elseif t > tpend
%           p=pmax;
%       else
%           p=pmax/(tpend - tpstart)*(t-tpstart);
%       end
%
%       fp1x=-(1/3)*p*elemarea(ii)*pnormx(ii);
%       fp1y=-(1/3)*p*elemarea(ii)*pnormy(ii);
%       fp1z=-(1/3)*p*elemarea(ii)*pnormz(ii);
%       fp2x=-(1/3)*p*elemarea(ii)*pnormx(ii);
%       fp2y=-(1/3)*p*elemarea(ii)*pnormy(ii);
%       fp2z=-(1/3)*p*elemarea(ii)*pnormz(ii);
%       fp3x=-(1/3)*p*elemarea(ii)*pnormx(ii);
%       fp3y=-(1/3)*p*elemarea(ii)*pnormy(ii);
%       fp3z=-(1/3)*p*elemarea(ii)*pnormz(ii);
%
%             if fixed(i1)==1
%                 ax1=0;
%                 ay1=0;
%                 az1=0;
%             else
%                 ax1=(fp1x/m(i1));
%                 ay1=(fp1y/m(i1));
```

```
%                 az1=(fp1z/m(i1));
%             end
%
%             if fixed(i2)==1
%                 ax2=0;
%                 ay2=0;
%                 az2=0;
%             else
%                 ax2=(fp2x/m(i2));
%                 ay2=(fp2y/m(i2));
%                 az2=(fp2z/m(i2));
%             end
%
%             if fixed(i3)==1
%                 ax3=0;
%                 ay3=0;
%                 az3=0;
%             else
%                 ax3=(fp3x/m(i3));
%                 ay3=(fp3y/m(i3));
%                 az3=(fp3z/m(i3));
%             end
%
%          axx(i1) = axx(i1) + ax1;
%          ayy(i1) = ayy(i1) + ay1;
%          azz(i1) = azz(i1) + az1;
%          axx(i2) = axx(i2) + ax2;
%          ayy(i2) = ayy(i2) + ay2;
%          azz(i2) = azz(i2) + az2;
%          axx(i3) = axx(i3) + ax3;
%          ayy(i3) = ayy(i3) + ay3;
%          azz(i3) = azz(i3) + az3;
%
%  end

%Accumulating forces on all structural vertices
     for ii=1:nnodes
          a(3*ii-2)=axx(ii);
          a(3*ii-1)=ayy(ii);
          a(3*ii) = azz(ii);

            aux1 = [v(6*ii-4); a(3*ii-2); v(6*ii-2); a(3*ii-1); v(6*ii);
a(3*ii)];
            dvdt = [dvdt; aux1];
     end

 return
```

B Runge-Kutta Matlab Function Code

```
%Runge-Kutta Function to solve the Equations of Motion
function [t,v]=RungeKutta_v2(t,v,h)

   dvdt = GridfunctBendTriangularRandom_v2(t, v);
   k1 = h*dvdt;
   dvdt = GridfunctBendTriangularRandom_v2(t+h/2, v+(k1')/2);
   k2 = h*dvdt;
   dvdt = GridfunctBendTriangularRandom_v2(t+h/2, v+(k2')/2);
   k3 = h*dvdt;
   dvdt = GridfunctBendTriangularRandom_v2(t+h, v+(k3'));
   k4 = h*dvdt;
   vaux = v' + (k1 + 2*k2 + 2*k3 + k4)/6;
   v=vaux';

return
```

C 11 x 11 Mesh Input File

121 — Total number of particles

1	0.1000000E+01	0.0000000E+00	0.0000000E+00
2	0.1000000E+01	0.1000000E+00	0.0000000E+00
3	0.9000000E+00	0.0000000E+00	0.0000000E+00
4	0.9000000E+00	0.1000000E+00	0.0000000E+00
5	0.1000000E+01	0.2000000E+00	0.0000000E+00
6	0.9000000E+00	0.2000000E+00	0.0000000E+00
7	0.1000000E+01	0.3000000E+00	0.0000000E+00
8	0.9000000E+00	0.3000000E+00	0.0000000E+00
9	0.1000000E+01	0.4000000E+00	0.0000000E+00
10	0.9000000E+00	0.4000000E+00	0.0000000E+00
11	0.1000000E+01	0.5000000E+00	0.0000000E+00
12	0.9000000E+00	0.5000000E+00	0.0000000E+00
13	0.1000000E+01	0.6000000E+00	0.0000000E+00
14	0.9000000E+00	0.6000000E+00	0.0000000E+00
15	0.1000000E+01	0.7000000E+00	0.0000000E+00
16	0.9000000E+00	0.7000000E+00	0.0000000E+00
17	0.1000000E+01	0.8000001E+00	0.0000000E+00
18	0.9000000E+00	0.8000001E+00	0.0000000E+00
19	0.1000000E+01	0.9000001E+00	0.0000000E+00
20	0.9000000E+00	0.9000001E+00	0.0000000E+00
21	0.1000000E+01	0.1000000E+01	0.0000000E+00
22	0.9000000E+00	0.1000000E+01	0.0000000E+00
23	0.8000000E+00	0.0000000E+00	0.0000000E+00
24	0.8000000E+00	0.9999999E-01	0.0000000E+00
25	0.8000000E+00	0.2000000E+00	0.0000000E+00
26	0.8000000E+00	0.3000000E+00	0.0000000E+00
27	0.8000000E+00	0.4000000E+00	0.0000000E+00
28	0.8000000E+00	0.5000000E+00	0.0000000E+00
29	0.8000000E+00	0.6000000E+00	0.0000000E+00
30	0.8000000E+00	0.7000000E+00	0.0000000E+00
31	0.8000000E+00	0.8000000E+00	0.0000000E+00
32	0.8000000E+00	0.9000001E+00	0.0000000E+00
33	0.8000000E+00	0.1000000E+01	0.0000000E+00
34	0.7000000E+00	0.0000000E+00	0.0000000E+00
35	0.7000000E+00	0.1000000E+00	0.0000000E+00
36	0.7000000E+00	0.2000000E+00	0.0000000E+00
37	0.7000000E+00	0.3000000E+00	0.0000000E+00
38	0.7000000E+00	0.4000000E+00	0.0000000E+00
39	0.7000000E+00	0.5000000E+00	0.0000000E+00
40	0.7000000E+00	0.6000000E+00	0.0000000E+00
41	0.7000000E+00	0.7000000E+00	0.0000000E+00
42	0.7000000E+00	0.8000001E+00	0.0000000E+00
43	0.7000000E+00	0.9000001E+00	0.0000000E+00

x, *y*, *z* coordinate information

```
44    0.7000000E+00  0.1000000E+01  0.0000000E+00
45    0.6000000E+00  0.0000000E+00  0.0000000E+00
46    0.6000000E+00  0.1000000E+00  0.0000000E+00
47    0.6000000E+00  0.2000000E+00  0.0000000E+00
48    0.6000000E+00  0.3000000E+00  0.0000000E+00
49    0.6000000E+00  0.4000000E+00  0.0000000E+00
50    0.6000000E+00  0.5000000E+00  0.0000000E+00
51    0.6000000E+00  0.6000000E+00  0.0000000E+00
52    0.6000000E+00  0.7000000E+00  0.0000000E+00
53    0.6000000E+00  0.8000001E+00  0.0000000E+00
54    0.6000000E+00  0.9000001E+00  0.0000000E+00
55    0.6000000E+00  0.1000000E+01  0.0000000E+00
56    0.5000000E+00  0.0000000E+00  0.0000000E+00
57    0.5000000E+00  0.1000000E+00  0.0000000E+00
58    0.5000000E+00  0.2000000E+00  0.0000000E+00
59    0.5000000E+00  0.3000000E+00  0.0000000E+00
60    0.5000000E+00  0.4000000E+00  0.0000000E+00
61    0.5000000E+00  0.5000000E+00  0.0000000E+00
62    0.5000000E+00  0.6000000E+00  0.0000000E+00
63    0.5000000E+00  0.7000000E+00  0.0000000E+00
64    0.5000000E+00  0.8000001E+00  0.0000000E+00
65    0.5000000E+00  0.9000001E+00  0.0000000E+00
66    0.5000000E+00  0.1000000E+01  0.0000000E+00
67    0.4000000E+00  0.0000000E+00  0.0000000E+00
68    0.4000000E+00  0.1000000E+00  0.0000000E+00
69    0.4000000E+00  0.2000000E+00  0.0000000E+00
70    0.4000000E+00  0.3000000E+00  0.0000000E+00
71    0.4000000E+00  0.4000000E+00  0.0000000E+00
72    0.4000000E+00  0.5000000E+00  0.0000000E+00
73    0.4000000E+00  0.6000000E+00  0.0000000E+00
74    0.4000000E+00  0.7000000E+00  0.0000000E+00
75    0.4000000E+00  0.8000001E+00  0.0000000E+00
76    0.4000000E+00  0.9000001E+00  0.0000000E+00
77    0.4000000E+00  0.1000000E+01  0.0000000E+00
78    0.3000000E+00  0.0000000E+00  0.0000000E+00
79    0.3000000E+00  0.1000000E+00  0.0000000E+00
80    0.3000000E+00  0.2000000E+00  0.0000000E+00
81    0.3000000E+00  0.3000000E+00  0.0000000E+00
82    0.3000000E+00  0.4000000E+00  0.0000000E+00
83    0.3000000E+00  0.5000000E+00  0.0000000E+00
84    0.3000000E+00  0.6000000E+00  0.0000000E+00
85    0.3000000E+00  0.7000000E+00  0.0000000E+00
86    0.3000000E+00  0.8000001E+00  0.0000000E+00
87    0.3000000E+00  0.9000001E+00  0.0000000E+00
88    0.3000000E+00  0.1000000E+01  0.0000000E+00
89    0.1999999E+00  0.0000000E+00  0.0000000E+00
90    0.1999999E+00  0.9999999E-01  0.0000000E+00
91    0.1999999E+00  0.2000000E+00  0.0000000E+00
92    0.1999999E+00  0.3000000E+00  0.0000000E+00
93    0.1999999E+00  0.4000000E+00  0.0000000E+00
94    0.1999999E+00  0.5000000E+00  0.0000000E+00
95    0.1999999E+00  0.6000000E+00  0.0000000E+00
96    0.1999999E+00  0.7000000E+00  0.0000000E+00
```

x, *y*, *z* coordinate information continued

```
 97    0.1999999E+00  0.8000001E+00  0.0000000E+00
 98    0.1999999E+00  0.9000001E+00  0.0000000E+00
 99    0.1999999E+00  0.1000000E+01  0.0000000E+00
100    0.9999990E-01  0.0000000E+00  0.0000000E+00
101    0.9999990E-01  0.1000000E+00  0.0000000E+00
102    0.9999990E-01  0.2000000E+00  0.0000000E+00
103    0.9999990E-01  0.3000000E+00  0.0000000E+00
104    0.9999990E-01  0.4000000E+00  0.0000000E+00
105    0.9999990E-01  0.5000000E+00  0.0000000E+00
106    0.9999990E-01  0.6000000E+00  0.0000000E+00
107    0.9999990E-01  0.7000000E+00  0.0000000E+00
108    0.9999990E-01  0.8000001E+00  0.0000000E+00
109    0.9999990E-01  0.9000001E+00  0.0000000E+00
110    0.9999990E-01  0.1000000E+01  0.0000000E+00
111    0.0000000E+00  0.0000000E+00  0.0000000E+00
112    0.0000000E+00  0.1000000E+00  0.0000000E+00
113    0.0000000E+00  0.2000000E+00  0.0000000E+00
114    0.0000000E+00  0.3000000E+00  0.0000000E+00
115    0.0000000E+00  0.4000000E+00  0.0000000E+00
116    0.0000000E+00  0.5000000E+00  0.0000000E+00
117    0.0000000E+00  0.6000000E+00  0.0000000E+00
118    0.0000000E+00  0.7000000E+00  0.0000000E+00
119    0.0000000E+00  0.8000001E+00  0.0000000E+00
120    0.0000000E+00  0.9000001E+00  0.0000000E+00
121    0.0000000E+00  0.1000000E+01  0.0000000E+00
```

x, *y*, *z* coordinate information continued

```
 1     2     2     3
 2     4     1     3     4     5
 3     4     1     2     4    23
 4     6     2     3     5     6    23    24
 5     4     2     4     6     7
 6     6     4     5     7     8    24    25
 7     4     5     6     8     9
 8     6     6     7     9    10    25    26
 9     4     7     8    10    11
10     6     8     9    11    12    26    27
11     4     9    10    12    13
12     6    10    11    13    14    27    28
13     4    11    12    14    15
14     6    12    13    15    16    28    29
15     4    13    14    16    17
16     6    14    15    17    18    29    30
17     4    15    16    18    19
18     6    16    17    19    20    30    31
19     4    17    18    20    21
20     6    18    19    21    22    31    32
21     3    19    20    22
22     4    20    21    32    33
23     4     3     4    24    34
24     6     4     6    23    25    34    35
25     6     6     8    24    26    35    36
26     6     8    10    25    27    36    37
```

nearest neighbor information for forces due to stretching

```
27      6      10      12      26      28      37      38
28      6      12      14      27      29      38      39
29      6      14      16      28      30      39      40
30      6      16      18      29      31      40      41
31      6      18      20      30      32      41      42
32      6      20      22      31      33      42      43
33      4      22      32      43      44
34      4      23      24      35      45
35      6      24      25      34      36      45      46
36      6      25      26      35      37      46      47
37      6      26      27      36      38      47      48
38      6      27      28      37      39      48      49
39      6      28      29      38      40      49      50
40      6      29      30      39      41      50      51
41      6      30      31      40      42      51      52
42      6      31      32      41      43      52      53
43      6      32      33      42      44      53      54
44      4      33      43      54      55
45      4      34      35      46      56
46      6      35      36      45      47      56      57
47      6      36      37      46      48      57      58
48      6      37      38      47      49      58      59
49      6      38      39      48      50      59      60
50      6      39      40      49      51      60      61
51      6      40      41      50      52      61      62
52      6      41      42      51      53      62      63
53      6      42      43      52      54      63      64
54      6      43      44      53      55      64      65
55      4      44      54      65      66
56      4      45      46      57      67
57      6      46      47      56      58      67      68
58      6      47      48      57      59      68      69
59      6      48      49      58      60      69      70
60      6      49      50      59      61      70      71
61      6      50      51      60      62      71      72
62      6      51      52      61      63      72      73
63      6      52      53      62      64      73      74
64      6      53      54      63      65      74      75
65      6      54      55      64      66      75      76
66      4      55      65      76      77
67      4      56      57      68      78
68      6      57      58      67      69      78      79
69      6      58      59      68      70      79      80
70      6      59      60      69      71      80      81
71      6      60      61      70      72      81      82
72      6      61      62      71      73      82      83
73      6      62      63      72      74      83      84
74      6      63      64      73      75      84      85
75      6      64      65      74      76      85      86
76      6      65      66      75      77      86      87
77      4      66      76      87      88
78      4      67      68      79      89
79      6      68      69      78      80      89      90
```

nearest neighbor information for forces due to stretching continued

```
 80      6     69     70     79     81     90     91
 81      6     70     71     80     82     91     92
 82      6     71     72     81     83     92     93
 83      6     72     73     82     84     93     94
 84      6     73     74     83     85     94     95
 85      6     74     75     84     86     95     96
 86      6     75     76     85     87     96     97
 87      6     76     77     86     88     97     98
 88      4     77     87     98     99
 89      4     78     79     90    100
 90      6     79     80     89     91    100    101
 91      6     80     81     90     92    101    102
 92      6     81     82     91     93    102    103
 93      6     82     83     92     94    103    104
 94      6     83     84     93     95    104    105
 95      6     84     85     94     96    105    106
 96      6     85     86     95     97    106    107
 97      6     86     87     96     98    107    108
 98      6     87     88     97     99    108    109
 99      4     88     98    109    110
100      4     89     90    101    111
101      6     90     91    100    102    111    112
102      6     91     92    101    103    112    113
103      6     92     93    102    104    113    114
104      6     93     94    103    105    114    115
105      6     94     95    104    106    115    116
106      6     95     96    105    107    116    117
107      6     96     97    106    108    117    118
108      6     97     98    107    109    118    119
109      6     98     99    108    110    119    120
110      4     99    109    120    121
111      3    100    101    112
112      4    101    102    111    113
113      4    102    103    112    114
114      4    103    104    113    115
115      4    104    105    114    116
116      4    105    106    115    117
117      4    106    107    116    118
118      4    107    108    117    119
119      4    108    109    118    120
120      4    109    110    119    121
121      2    110    120
```

nearest neighbor information for forces due to stretching continued

```
280
```

Total number of common edges for bending

```
  1      2      4      3
  3      2      5      4
  2      4     23      3
  2      5      6      4
  4      5      7      6
  5      6     24      4
  5      7      8      6
```

connectivity information for forces resisting bending deformation

```
 7      8     25      6
 6      7      9      8
 7      9     10      8
 8      9     11     10
 9     10     26      8
 9     11     12     10
10     11     13     12
11     12     27     10
11     13     14     12
13     14     28     12
12     13     15     14
13     15     16     14
14     15     17     16
15     16     29     14
15     17     18     16
16     17     19     18
17     18     30     16
17     19     20     18
19     20     31     18
18     19     21     20
19     21     22     20
21     22     32     20
 3      4     24     23
 4     24     34     23
23      4      6     24
 4      6     25     24
24      6      8     25
 6     25     35     24
 6      8     26     25
25      8     10     26
 8     26     36     25
 8     10     27     26
10     27     37     26
26     10     12     27
10     12     28     27
27     12     14     28
12     28     38     27
12     14     29     28
28     14     16     29
14     29     39     28
14     16     30     29
16     30     40     29
29     16     18     30
16     18     31     30
30     18     20     31
18     31     41     30
18     20     32     31
31     20     22     32
20     32     42     31
20     22     33     32
22     33     43     32
23     24     35     34
34     24     25     35
```

connectivity information for forces resisting bending deformation continued

```
24      35      45      34
24      25      36      35
25      36      46      35
35      25      26      36
25      26      37      36
36      26      27      37
26      37      47      36
26      27      38      37
37      27      28      38
27      38      48      37
27      28      39      38
28      39      49      38
38      28      29      39
28      29      40      39
39      29      30      40
29      40      50      39
29      30      41      40
40      30      31      41
30      41      51      40
30      31      42      41
31      42      52      41
41      31      32      42
31      32      43      42
42      32      33      43
32      43      53      42
32      33      44      43
33      44      54      43
34      35      46      45
45      35      36      46
35      46      56      45
35      36      47      46
46      36      37      47
36      47      57      46
36      37      48      47
37      48      58      47
47      37      38      48
37      38      49      48
48      38      39      49
38      49      59      48
38      39      50      49
49      39      40      50
39      50      60      49
39      40      51      50
40      51      61      50
50      40      41      51
40      41      52      51
51      41      42      52
41      52      62      51
41      42      53      52
52      42      43      53
42      53      63      52
42      43      54      53
43      54      64      53
```

connectivity information for forces resisting bending deformation continued

53	43	44	54
43	44	55	54
44	55	65	54
45	46	57	56
46	57	67	56
56	46	47	57
46	47	58	57
57	47	48	58
47	58	68	57
47	48	59	58
58	48	49	59
48	59	69	58
48	49	60	59
49	60	70	59
59	49	50	60
49	50	61	60
60	50	51	61
50	61	71	60
50	51	62	61
61	51	52	62
51	62	72	61
51	52	63	62
52	63	73	62
62	52	53	63
52	53	64	63
63	53	54	64
53	64	74	63
53	54	65	64
64	54	55	65
54	65	75	64
54	55	66	65
55	66	76	65
56	57	68	67
67	57	58	68
57	68	78	67
57	58	69	68
58	69	79	68
68	58	59	69
58	59	70	69
69	59	60	70
59	70	80	69
59	60	71	70
70	60	61	71
60	71	81	70
60	61	72	71
61	72	82	71
71	61	62	72
61	62	73	72
72	62	63	73
62	73	83	72
62	63	74	73
73	63	64	74
63	74	84	73

connectivity information for forces resisting bending deformation continued

```
63      64      75      74
64      75      85      74
74      64      65      75
64      65      76      75
75      65      66      76
65      76      86      75
65      66      77      76
66      77      87      76
67      68      79      78
78      68      69      79
68      79      89      78
68      69      80      79
79      69      70      80
69      80      90      79
69      70      81      80
70      81      91      80
80      70      71      81
70      71      82      81
81      71      72      82
71      82      92      81
71      72      83      82
82      72      73      83
72      83      93      82
72      73      84      83
73      84      94      83
83      73      74      84
73      74      85      84
84      74      75      85
74      85      95      84
74      75      86      85
85      75      76      86
75      86      96      85
75      76      87      86
76      87      97      86
86      76      77      87
76      77      88      87
77      88      98      87
78      79      90      89
79      90     100      89
89      79      80      90
79      80      91      90
90      80      81      91
80      91     101      90
80      81      92      91
91      81      82      92
81      92     102      91
81      82      93      92
82      93     103      92
92      82      83      93
82      83      94      93
93      83      84      94
83      94     104      93
83      84      95      94
```

connectivity information for forces resisting bending deformation continued

```
 94     84     85     95
 84     95    105     94
 84     85     96     95
 85     96    106     95
 95     85     86     96
 85     86     97     96
 96     86     87     97
 86     97    107     96
 86     87     98     97
 97     87     88     98
 87     98    108     97
 87     88     99     98
 88     99    109     98
 89     90    101    100
100     90     91    101
 90    101    111    100
 90     91    102    101
 91    102    112    101
101     91     92    102
 91     92    103    102
102     92     93    103
 92    103    113    102
 92     93    104    103
103     93     94    104
 93    104    114    103
 93     94    105    104
 94    105    115    104
104     94     95    105
 94     95    106    105
105     95     96    106
 95    106    116    105
 95     96    107    106
106     96     97    107
 96    107    117    106
 96     97    108    107
 97    108    118    107
107     97     98    108
 97     98    109    108
108     98     99    109
 98    109    119    108
 98     99    110    109
 99    110    120    109
100    101    112    111
111    101    102    112
101    102    113    112
112    102    103    113
102    103    114    113
113    103    104    114
103    104    115    114
114    104    105    115
104    105    116    115
115    105    106    116
105    106    117    116
```

connectivity information for forces resisting bending deformation continued

```
116    106    107    117
106    107    118    117
117    107    108    118
107    108    119    118
118    108    109    119
108    109    120    119
119    109    110    120
109    110    121    120
```

connectivity information for forces resisting bending deformation continued

```
40
```

Total number of boundary nodes

```
  1    0.1000000E+01  0.0000000E+00  0.0000000E+00
  2    0.1000000E+01  0.1000000E+00  0.0000000E+00
  3    0.9000000E+00  0.0000000E+00  0.0000000E+00
  5    0.1000000E+01  0.2000000E+00  0.0000000E+00
  7    0.1000000E+01  0.3000000E+00  0.0000000E+00
  9    0.1000000E+01  0.4000000E+00  0.0000000E+00
 11    0.1000000E+01  0.5000000E+00  0.0000000E+00
 13    0.1000000E+01  0.6000000E+00  0.0000000E+00
 15    0.1000000E+01  0.7000000E+00  0.0000000E+00
 17    0.1000000E+01  0.8000001E+00  0.0000000E+00
 19    0.1000000E+01  0.9000001E+00  0.0000000E+00
 21    0.1000000E+01  0.1000000E+01  0.0000000E+00
 22    0.9000000E+00  0.1000000E+01  0.0000000E+00
 23    0.8000000E+00  0.0000000E+00  0.0000000E+00
 33    0.8000000E+00  0.1000000E+01  0.0000000E+00
 34    0.7000000E+00  0.0000000E+00  0.0000000E+00
 44    0.7000000E+00  0.1000000E+01  0.0000000E+00
 45    0.6000000E+00  0.0000000E+00  0.0000000E+00
 55    0.6000000E+00  0.1000000E+01  0.0000000E+00
 56    0.5000000E+00  0.0000000E+00  0.0000000E+00
 66    0.5000000E+00  0.1000000E+01  0.0000000E+00
 67    0.4000000E+00  0.0000000E+00  0.0000000E+00
 77    0.4000000E+00  0.1000000E+01  0.0000000E+00
 78    0.3000000E+00  0.0000000E+00  0.0000000E+00
 88    0.3000000E+00  0.1000000E+01  0.0000000E+00
 89    0.1999999E+00  0.0000000E+00  0.0000000E+00
 99    0.1999999E+00  0.1000000E+01  0.0000000E+00
100    0.9999990E-01  0.0000000E+00  0.0000000E+00
110    0.9999990E-01  0.1000000E+01  0.0000000E+00
111    0.0000000E+00  0.0000000E+00  0.0000000E+00
112    0.0000000E+00  0.1000000E+00  0.0000000E+00
113    0.0000000E+00  0.2000000E+00  0.0000000E+00
114    0.0000000E+00  0.3000000E+00  0.0000000E+00
115    0.0000000E+00  0.4000000E+00  0.0000000E+00
116    0.0000000E+00  0.5000000E+00  0.0000000E+00
117    0.0000000E+00  0.6000000E+00  0.0000000E+00
118    0.0000000E+00  0.7000000E+00  0.0000000E+00
119    0.0000000E+00  0.8000001E+00  0.0000000E+00
120    0.0000000E+00  0.9000001E+00  0.0000000E+00
121    0.0000000E+00  0.1000000E+01  0.0000000E+00
```

boundary node coordinates

```
 1       0       0       0
 2       0       0       0
 3       0       0       0
 4       0       0       0
 5       0       0       0
 6       0       0       0
 7       0       0       0
 8       0       0       0
 9       0       0       0
10       0       0       0
11       0       0       0
12       0       0       0
13       0       0       0
14       0       0       0
15       0       0       0
16       0       0       0
17       0       0       0
18       0       0       0
19       0       0       0
20       0       0       0
21       0       0       0
22       0       0       0
23       0       0       0
24       0       0       0
25       0       0       0
26       0       0       0
27       0       0       0
28       0       0       0
29       0       0       0
30       0       0       0
31       0       0       0
32       0       0       0
33       0       0       0
34       0       0       0
35       0       0       0
36       0       0       0
37       0       0       0
38       0       0       0
39       0       0       0
40       0       0       0
41       0       0       0
42       0       0       0
43       0       0       0
44       0       0       0
45       0       0       0
46       0       0       0
47       0       0       0
48       0       0       0
49       0       0       0
50       0       0       0
51       0       0       0
52       0       0       0
```

x, *y*, and *z* external forces for each particle

```
 53       0       0       0
 54       0       0       0
 55       0       0       0
 56       0       0       0
 57       0       0       0
 58       0       0       0
 59       0       0       0
 60       0       0       0
 61       0       0       1
 62       0       0       0
 63       0       0       0
 64       0       0       0
 65       0       0       0
 66       0       0       0
 67       0       0       0
 68       0       0       0
 69       0       0       0
 70       0       0       0
 71       0       0       0
 72       0       0       0
 73       0       0       0
 74       0       0       0
 75       0       0       0
 76       0       0       0
 77       0       0       0
 78       0       0       0
 79       0       0       0
 80       0       0       0
 81       0       0       0
 82       0       0       0
 83       0       0       0
 84       0       0       0
 85       0       0       0
 86       0       0       0
 87       0       0       0
 88       0       0       0
 89       0       0       0
 90       0       0       0
 91       0       0       0
 92       0       0       0
 93       0       0       0
 94       0       0       0
 95       0       0       0
 96       0       0       0
 97       0       0       0
 98       0       0       0
 99       0       0       0
100       0       0       0
101       0       0       0
102       0       0       0
103       0       0       0
104       0       0       0
105       0       0       0
```

x, *y*, and *z* external forces for each particle continued

```
106     0     0     0
107     0     0     0
108     0     0     0
109     0     0     0
110     0     0     0
111     0     0     0
112     0     0     0
113     0     0     0
114     0     0     0
115     0     0     0
116     0     0     0
117     0     0     0
118     0     0     0
119     0     0     0
120     0     0     0
121     0     0     0
```

x, *y*, and *z* external forces for each particle continued

```
  1     1
  2     1
  3     1
  4     0
  5     1
  6     0
  7     1
  8     0
  9     1
 10     0
 11     1
 12     0
 13     1
 14     0
 15     1
 16     0
 17     1
 18     0
 19     1
 20     0
 21     1
 22     1
 23     1
 24     0
 25     0
 26     0
 27     0
 28     0
 29     0
 30     0
 31     0
 32     0
 33     1
 34     1
 35     0
```

free (0) or simply supported (1) boundary conditions for each particle

```
36      0
37      0
38      0
39      0
40      0
41      0
42      0
43      0
44      1
45      1
46      0
47      0
48      0
49      0
50      0
51      0
52      0
53      0
54      0
55      1
56      1
57      0
58      0
59      0
60      0
61      0
62      0
63      0
64      0
65      0
66      1
67      1
68      0
69      0
70      0
71      0
72      0
73      0
74      0
75      0
76      0
77      1
78      1
79      0
80      0
81      0
82      0
83      0
84      0
85      0
86      0
87      0
88      1
```

free (0) or simply supported (1) boundary conditions for each particle continued

```
 89       1
 90       0
 91       0
 92       0
 93       0
 94       0
 95       0
 96       0
 97       0
 98       0
 99       1
100       1
101       0
102       0
103       0
104       0
105       0
106       0
107       0
108       0
109       0
110       1
111       1
112       1
113       1
114       1
115       1
116       1
117       1
118       1
119       1
120       1
121       1
```

free (0) or simply supported (1) boundary conditions for each particle continued

```
200
```

Total number of elements

```
  1       1       2       3
  2       3       2       4
  3       4       2       5
  4       5       6       4
  5       7       6       5
  6       8       6       7
  7       7       9       8
  8       8       9      10
  9      10       9      11
 10      11      12      10
 11      13      12      11
 12      14      12      13
 13      13      15      14
 14      14      15      16
 15      16      15      17
```

element connectivity information for all of the elements

```
16      17      18      16
17      19      18      17
18      20      18      19
19      19      21      20
20      20      21      22
21       4      23       3
22      24      23       4
23       4       6      24
24      24       6      25
25      25       6       8
26       8      26      25
27      10      26       8
28      27      26      10
29      10      12      27
30      27      12      28
31      28      12      14
32      14      29      28
33      16      29      14
34      30      29      16
35      16      18      30
36      30      18      31
37      31      18      20
38      20      32      31
39      22      32      20
40      33      32      22
41      34      23      24
42      24      35      34
43      25      35      24
44      36      35      25
45      25      26      36
46      36      26      37
47      37      26      27
48      27      38      37
49      28      38      27
50      39      38      28
51      28      29      39
52      39      29      40
53      40      29      30
54      30      41      40
55      31      41      30
56      42      41      31
57      31      32      42
58      42      32      43
59      43      32      33
60      33      44      43
61      34      35      45
62      45      35      46
63      46      35      36
64      36      47      46
65      37      47      36
66      48      47      37
67      37      38      48
68      48      38      49
```

element connectivity information for all of the elements continued

```
 69      49      38      39
 70      39      50      49
 71      40      50      39
 72      51      50      40
 73      40      41      51
 74      51      41      52
 75      52      41      42
 76      42      53      52
 77      43      53      42
 78      54      53      43
 79      43      44      54
 80      54      44      55
 81      46      56      45
 82      57      56      46
 83      46      47      57
 84      57      47      58
 85      58      47      48
 86      48      59      58
 87      49      59      48
 88      60      59      49
 89      49      50      60
 90      60      50      61
 91      61      50      51
 92      51      62      61
 93      52      62      51
 94      63      62      52
 95      52      53      63
 96      63      53      64
 97      64      53      54
 98      54      65      64
 99      55      65      54
100      66      65      55
101      67      56      57
102      57      68      67
103      58      68      57
104      69      68      58
105      58      59      69
106      69      59      70
107      70      59      60
108      60      71      70
109      61      71      60
110      72      71      61
111      61      62      72
112      72      62      73
113      73      62      63
114      63      74      73
115      64      74      63
116      75      74      64
117      64      65      75
118      75      65      76
119      76      65      66
120      66      77      76
121      67      68      78
```

element connectivity information for all of the elements continued

122	78	68	79
123	79	68	69
124	69	80	79
125	70	80	69
126	81	80	70
127	70	71	81
128	81	71	82
129	82	71	72
130	72	83	82
131	73	83	72
132	84	83	73
133	73	74	84
134	84	74	85
135	85	74	75
136	75	86	85
137	76	86	75
138	87	86	76
139	76	77	87
140	87	77	88
141	79	89	78
142	90	89	79
143	79	80	90
144	90	80	91
145	91	80	81
146	81	92	91
147	82	92	81
148	93	92	82
149	82	83	93
150	93	83	94
151	94	83	84
152	84	95	94
153	85	95	84
154	96	95	85
155	85	86	96
156	96	86	97
157	97	86	87
158	87	98	97
159	88	98	87
160	99	98	88
161	100	89	90
162	90	101	100
163	91	101	90
164	102	101	91
165	91	92	102
166	102	92	103
167	103	92	93
168	93	104	103
169	94	104	93
170	105	104	94
171	94	95	105
172	105	95	106
173	106	95	96
174	96	107	106

element connectivity information for all of the elements continued

```
175     97    107     96
176    108    107     97
177     97     98    108
178    108     98    109
179    109     98     99
180     99    110    109
181    100    101    111
182    111    101    112
183    112    101    102
184    102    113    112
185    103    113    102
186    114    113    103
187    103    104    114
188    114    104    115
189    115    104    105
190    105    116    115
191    106    116    105
192    117    116    106
193    106    107    117
194    117    107    118
195    118    107    108
196    108    119    118
197    109    119    108
198    120    119    109
199    109    110    120
200    120    110    121
```

element connectivity information for all of the elements continued

D Cantilever Bending Test Spreadsheet Results

Report for: College of Textiles North Carolina State University, Physical Testing Lab
Date of Report: 12/9/2009
ASTM D1388-Stiffness of Fabrics **Worksheet for Raw Data**
Sample Identification: Canvas Material

Specimen Number	Overhang Lengths (o) units=cm (Report to nearest 0.1 cm)		Bending Length (C) c=0/2 units=cm		Flexural Rigidity (G) G=W x c^3 units=mg.cm	
	Warp (Machine)	**Filling (Cross)**	**Warp**	**Filling**	**W**	**F**
Specimen 1	8.1	8.5				
	8.7	9.3				
	8.3	8.4				
	8.6	9.3				
Specimen 1 Average	**8.4**	**8.9**	**4.2**	**4.4**	**2824.6**	**3301.8**
Specimen 2	9.1	9.1				
	9.1	9.7				
	8.5	8.5				
	8.6	9.1				
Specimen 2 Average	**8.8**	**9.1**	**4.4**	**4.6**	**3246.3**	**3559.3**
Specimen 3	8.8	9.2				
	8.7	10.0				
	8.5	8.6				
	8.9	10.1				
Specimen 3 Average	**8.7**	**9.5**	**4.4**	**4.7**	**3137.2**	**4017.7**
Specimen 4	8.9	9.5				
	8.5	10.2				
	8.0	8.7				
	8.6	9.5				
Specimen 4 Average	**8.5**	**9.5**	**4.3**	**4.7**	**2900.7**	**4017.7**
TOTAL AVERAGE	**8.6**	**9.2**	**4.3**	**4.6**	**3027.2**	**3724.1**

ASTM D3776-Mass per Unit Area (Weight) of Woven Fabric (Needed to calculate flexural rigidity.)
(Weigh all 8 1" x 8" specimens before measuring stiffness.)

Total Wt. in Grams:	15.60
Total Area in sq. inches:	64.00
Fabric mass/area (mg/cm^2):	37.79
Fabric mass/area (oz/yd^2):	11.14

0.0026 **0.0032**

*Flexural Rigidity in units lb-in

E Case 1 Main Matlab Code

```
clc
clear all

%Declaring variables used in both functions as global
global d0 nnodes m c k0 kb fxext fyext fzext fixed coords NNM bend
nconnect kap0 nelem vertex pmax tpstart tpend gx gy gz a

%Defining the input parameters
t=0;                %initial time
tfinal = 10;        %final time
h = 0.0004;         %time-step
N=tfinal/h;         %total number of steps
hstl=250;           %number of steps between STL files
mperarea=0.0024;    %mass per unit area
k0=21.828;          %stretching stiffness coefficient input in the code
kb=.0000054;        %bending stiffness coefficient
c= 0.0005;          %damping coefficient
pmax=0.0;           %maximum pressure
tpstart=0;          %time at which pressure force begins
tpend=0;            %time at which pressure force = pmax
gx=0.0;             %acceleration due to gravity in the x-direction
gy=-32.174;         %acceleration due to gravity in the y-direction
gz=0;               %acceleration due to gravity in the z-direction

neglimit = -0.5;        %negative limit for box method
poslimit = 3.0;         %positive limit for box method
contactcheckelem = [];
distcheck = 1.5;        %radius for the distance check method
soldiertlag = 0.1;      %time the impactor begins moving
boostlimit = 40;        %limit on the adjustable parameter b
boostmax=0;
boostcounter=0;

vimpact1=0.4;           %velocity of the impactor

plotcounter=0;
stlcount=1;

%Open, read, and close the text file for the tent geometry
fid = fopen('hextentbendstifftune_refined.txt', 'r');
nnodes = fscanf(fid, '%d',1);
for i=1:nnodes
    nnum=fscanf(fid, '%d',1);
    for j=1:3
        coords(nnum,j)=fscanf(fid, '%f', 1);
    end
```

```
end

for i=1:nnodes
    nnum=fscanf(fid, '%d',1);
    nneighbors=fscanf(fid,'%d',1);
    NNM(i,1)=nnum;
    NNM(i,2)=nneighbors;
    for j=1:nneighbors
        NNM(nnum,j+2)=fscanf(fid,'%d',1);
    end
end

nconnect=fscanf(fid,'%d',1);
for i=1:nconnect
    for j=1:4
        bend(i,j)=fscanf(fid, '%d', 1);
    end
end

npossiblebc=fscanf(fid, '%d', 1);
fixed(1:nnodes) = 0;
for i=1:npossiblebc
    nnum=fscanf(fid, '%d', 1);
    for j=1:3
    fixdummy=fscanf(fid, '%f', 1);
    end
end

force = zeros(nnodes,3);
for i=1:nnodes
    nnum=fscanf(fid, '%d', 1);
    for j=1:3
        force(nnum,j)=fscanf(fid, '%f', 1);
    end
end

%Only use this if going to leave the fixed part in the input file
for i=1:nnodes
    nnum=fscanf(fid, '%d', 1);
    fixed(nnum)=fscanf(fid, '%d', 1);
end

nelem=fscanf(fid, '%d', 1);
for i=1:nelem
    nnum=fscanf(fid, '%d', 1);
    for j=1:3
        vertex(nnum,j)=fscanf(fid, '%d', 1);
    end
end
fclose(fid);
```

```
%Open, read, close text file for the impactor
fid = fopen('single impactor point.txt', 'r');
nnodes1 = fscanf(fid, '%d',1);
coords1=zeros(nnodes1,3);
for i=1:nnodes1
    nnum=fscanf(fid, '%d',1);
    for j=1:3
        coords1(nnum,j)=fscanf(fid, '%f', 1);
    end
end

nelem1=fscanf(fid, '%d', 1);
vertex1=zeros(nnodes1,3);
for i=1:nelem1
    nnum=fscanf(fid, '%d', 1);
    for j=1:3
        vertex1(nnum,j)=fscanf(fid, '%d', 1);
    end
end
fclose(fid);

m = zeros(1,nnodes);

%Loop to assign the mass to each particle based on element area
%Also define the range of elements which are checked for contact
for ii=1:nelem
      m1=0;
      m2=0;
      m3=0;

      i1= vertex(ii,1);
      i2= vertex(ii,2);
      i3= vertex(ii,3);

      Ax=coords(i1,1);
      Ay=coords(i1,2);
      Az=coords(i1,3);

      Bx=coords(i2,1);
      By=coords(i2,2);
      Bz=coords(i2,3);

      Cx=coords(i3,1);
      Cy=coords(i3,2);
      Cz=coords(i3,3);

      %Assigning possible contact elements based on the box method limits
      if (neglimit < Ay && Ay < poslimit) && (neglimit < By && By <
          poslimit) && (neglimit < Cy && Cy < poslimit)
          contactcheckelem = [contactcheckelem; ii];
      end
```

```
      v1=sqrt((Bx-Ax)^2+(By-Ay)^2+(Bz-Az)^2);
      v1x=(Bx-Ax);
      v1y=(By-Ay);
      v1z=(Bz-Az);

      v2=sqrt((Cx-Ax)^2+(Cy-Ay)^2+(Cz-Az)^2);
      v2x=(Cx-Ax);
      v2y=(Cy-Ay);
      v2z=(Cz-Az);

      pnorm=sqrt((v1y*v2z-v1z*v2y)^2+(v1z*v2x-v1x*v2z)^2+(v1x*v2y-
            v1y*v2x)^2);

      elemarea=1/2*pnorm;

      m1=(1/3)*mperarea*elemarea;
      m2=(1/3)*mperarea*elemarea;
      m3=(1/3)*mperarea*elemarea;

      m(i1)= m(i1) + m1;
      m(i2)= m(i2) + m2;
      m(i3)= m(i3) + m3;

end


%If the initial surface is curved, need to define an initial kappa
%Need to loop over the number of connections, just like in gridfunct,
%Calculate kap0, may have to do some checks incase kap>90 or so

 for hh=1:nconnect
          i1= bend(hh,1);
          i2= bend(hh,2);
          i3= bend(hh,3);
          i4= bend(hh,4);

          L=(1/2)*sqrt((coords(i1,1)-coords(i3,1))^2 + (coords(i1,2)-
             coords(i3,2))^2 + (coords(i1,3)-coords(i3,3))^2);

            x1=coords(i1,1);
            y1=coords(i1,2);
            z1=coords(i1,3);
            x2=coords(i2,1);
            y2=coords(i2,2);
            z2=coords(i2,3);
            x3=coords(i3,1);
            y3=coords(i3,2);
            z3=coords(i3,3);
            x4=coords(i4,1);
```

```
y4=coords(i4,2);
z4=coords(i4,3);

t12=sqrt((x2-x1)^2 + (y2-y1)^2 + (z2-z1)^2);
t12x=(x2-x1)/t12;
t12y=(y2-y1)/t12;
t12z=(z2-z1)/t12;

t14=sqrt((x4-x1)^2 + (y4-y1)^2 + (z4-z1)^2);
t14x=(x4-x1)/t14;
t14y=(y4-y1)/t14;
t14z=(z4-z1)/t14;

t12xt14=sqrt((t12y*t14z-t12z*t14y)^2 + (t12z*t14x-t12x*t14z)^2
        + (t12x*t14y-t12y*t14x)^2);

n124x=(t12y*t14z-t12z*t14y)/t12xt14;
n124y=(t12z*t14x-t12x*t14z)/t12xt14;
n124z=(t12x*t14y-t12y*t14x)/t12xt14;

t23=sqrt((x3-x2)^2 + (y3-y2)^2 + (z3-z2)^2);
t23x=(x3-x2)/t23;
t23y=(y3-y2)/t23;
t23z=(z3-z2)/t23;

t24=sqrt((x4-x2)^2 + (y4-y2)^2 + (z4-z2)^2);
t24x=(x4-x2)/t24;
t24y=(y4-y2)/t24;
t24z=(z4-z2)/t24;

t23xt24=sqrt((t23y*t24z-t23z*t24y)^2 + (t23z*t24x-t23x*t24z)^2
        + (t23x*t24y-t23y*t24x)^2);

n234x=(t23y*t24z-t23z*t24y)/t23xt24;
n234y=(t23z*t24x-t23x*t24z)/t23xt24;
n234z=(t23x*t24y-t23y*t24x)/t23xt24;

navg=sqrt(((n124x+n234x)/2)^2 +((n124y+n234y)/2)^2 +
     ((n124z+n234z)/2)^2);

n24x=((n124x+n234x)/2)/navg;
n24y=((n124y+n234y)/2)/navg;
n24z=((n124z+n234z)/2)/navg;

dot=(n124x*n234x + n124y*n234y + n124z*n234z);

if dot > 1
    dot=1;
end
```

```
            dphi=acos(dot);

            t12dotn234=(t12x*n234x + t12y*n234y + t12z*n234z);

            dphi=-sign(t12dotn234)*dphi;

            kap0(hh)=dphi/L;
 end

%%%%Preallocation of variables
    ximpactinit=zeros(1,nnodes1);
    yimpactinit=zeros(1,nnodes1);
    zimpactinit=zeros(1,nnodes1);
    contact=zeros(1,nnodes1);
    preimpactdotsign=zeros(1,nnodes1);
    ximpact=zeros(1,nnodes1);
    yimpact=zeros(1,nnodes1);
    zimpact=zeros(1,nnodes1);
    vximpact=zeros(1,nnodes1);
    vyimpact=zeros(1,nnodes1);
    vzimpact=zeros(1,nnodes1);
    Px=zeros(1,nnodes1);
    Py=zeros(1,nnodes1);
    Pz=zeros(1,nnodes1);
    centroidx=zeros(1,nnodes1);
    centroidy=zeros(1,nnodes1);
    centroidz=zeros(1,nnodes1);
    Pcent=zeros(1,nnodes1);
    v1=zeros(1,nnodes1);
    v1x=zeros(1,nnodes1);
    v1y=zeros(1,nnodes1);
    v1z=zeros(1,nnodes1);
    v2=zeros(1,nnodes1);
    v2x=zeros(1,nnodes1);
    v2y=zeros(1,nnodes1);
    v2z=zeros(1,nnodes1);
    v3=zeros(1,nnodes1);
    v3x=zeros(1,nnodes1);
    v3y=zeros(1,nnodes1);
    v3z=zeros(1,nnodes1);
    pnorm=zeros(1,nnodes1);
    pnormx=zeros(1,nnodes1);
    pnormy=zeros(1,nnodes1);
    pnormz=zeros(1,nnodes1);
    vAP=zeros(1,nnodes1);
    vAPx=zeros(1,nnodes1);
    vAPy=zeros(1,nnodes1);
    vAPz=zeros(1,nnodes1);
    ndotvAP=zeros(1,nnodes1);
    Qx=zeros(1,nnodes1);
    Qy=zeros(1,nnodes1);
    Qz=zeros(1,nnodes1);
```

```
    AQ=zeros(1,nnodes1);
    AQx=zeros(1,nnodes1);
    AQy=zeros(1,nnodes1);
    AQz=zeros(1,nnodes1);
    BQ=zeros(1,nnodes1);
    BQx=zeros(1,nnodes1);
    BQy=zeros(1,nnodes1);
    BQz=zeros(1,nnodes1);
    CQ=zeros(1,nnodes1);
    CQx=zeros(1,nnodes1);
    CQy=zeros(1,nnodes1);
    CQz=zeros(1,nnodes1);
    elemarea=zeros(1,nnodes1);
    area1=zeros(1,nnodes1);
    area2=zeros(1,nnodes1);
    area3=zeros(1,nnodes1);
    areatotal=zeros(1,nnodes1);
    contactelem=zeros(1,nnodes1);
    x=zeros(1,nnodes1);
    y=zeros(1,nnodes1);
    z=zeros(1,nnodes1);
    QPx=zeros(1,nnodes1);
    QPy=zeros(1,nnodes1);
    QPz=zeros(1,nnodes1);
    maxdistnode=zeros(1,length(contactcheckelem));
    maxdist=zeros(1,length(contactcheckelem));

%Assigning external force values from input text file
for s=1:nnodes
    fxext(s)=force(s,1);
    fyext(s)=force(s,2);
    fzext(s)=force(s,3);
end

vel = zeros(1,3*nnodes);
v0 = zeros(1,6*nnodes);

%for loop to store initial conditions of the mesh
for r=1:nnodes
    aux = [coords(r,1) vel(3*r-2) coords(r,2) vel(3*r-1) coords(r,3)
vel(3*r)];
    v0(1,6*r-5:6*r) = aux;
end

%Command when using the Runge-Kutta ODE Solver
v=v0;
vvector=v0;
tvector=t;
penetrate=0;

%For loop to store initial conditions of the impactor
for i=1:nnodes1
```

```
    ximpactinit(i)=coords1(i,1);
    yimpactinit(i)=coords1(i,2);
    zimpactinit(i)=coords1(i,3);
end

count=0;
numimpact=nnodes1;


%Creating STL file for Initial Conditions
   fOut = sprintf('SingleImpactor.%d.stl',1);
   fid = fopen(fOut, 'wt');
   fprintf(fid,'solid object \n');

   for i=1:nelem
    n1 = vertex(i,1);
    n2 = vertex(i,2);
    n3 = vertex(i,3);
    fprintf(fid,'  facet normal  %f %f %f\n',1.0,0.0,0.0);
    fprintf(fid,'    outer loop \n');
    vertx1 = vvector(1,6*n1-5);
    verty1 = vvector(1,6*n1-3);
    vertz1 = vvector(1,6*n1-1);
    vertx2 = vvector(1,6*n2-5);
    verty2 = vvector(1,6*n2-3);
    vertz2 = vvector(1,6*n2-1);
    vertx3 = vvector(1,6*n3-5);
    verty3 = vvector(1,6*n3-3);
    vertz3 = vvector(1,6*n3-1);
    fprintf(fid, '      vertex %f %f %f\n',vertx1,verty1,vertz1);
    fprintf(fid, '      vertex %f %f %f\n',vertx2,verty2,vertz2);
    fprintf(fid, '      vertex %f %f %f\n',vertx3,verty3,vertz3);
    fprintf(fid,'    endloop \n');
    fprintf(fid,'  endfacet \n');
   end

    for i=1:nelem1
    fprintf(fid,'  facet normal  %f %f %f\n',1.0,0.0,0.0);
    fprintf(fid,'    outer loop \n');
    fprintf(fid, '      vertex %f  %f %f \n'
       ,ximpactinit(vertex1(i,1)),yimpactinit(vertex1(i,1)),zimpactinit(ve
       rtex1(i,1)));
    fprintf(fid, '      vertex %f %f %f\n'
       ,ximpactinit(vertex1(i,2)),yimpactinit(vertex1(i,2)),zimpactinit(ve
       rtex1(i,2)));
    fprintf(fid, '      vertex %f %f %f\n'
       ,ximpactinit(vertex1(i,3)),yimpactinit(vertex1(i,3)),zimpactinit(ve
       rtex1(i,3)));
    fprintf(fid,'    endloop \n');
    fprintf(fid,'  endfacet \n');
    end
```

```
     fprintf(fid,'endsolid object');
     fclose(fid);


%Where the code actually begins, call Runge-Kutta function
for i=1:N
[t,v]=RungeKutta_v2(t,v,h);

    for k=1:numimpact

        if t < soldiertlag
            ximpact(k)=ximpactinit(k);
            yimpact(k)=yimpactinit(k);
            zimpact(k)=zimpactinit(k);
            vximpact(k)=0;
            vyimpact(k)=0;
            vzimpact(k)=0;
        else
            ximpact(k)=ximpactinit(k);
            yimpact(k)=yimpactinit(k);
            zimpact(k)=zimpactinit(k)-vimpact1*(t-soldiertlag);
            vximpact(k)=0;
            vyimpact(k)=0;
            vzimpact(k)=-vimpact1;
        end
    end

  maxpen=0;
  maxdistnode=zeros(1,length(contactcheckelem));
  maxdist=zeros(1,length(contactcheckelem));

 if t == soldiertlag || t > soldiertlag

 %Embedded for loops, k over the impactors, j over the possible contact
 %elements
 for k=1:numimpact

   for j=1:length(contactcheckelem)
      Ax(k)=v(6*vertex(contactcheckelem(j),1)-5);
      Ay(k)=v(6*vertex(contactcheckelem(j),1)-3);
      Az(k)=v(6*vertex(contactcheckelem(j),1)-1);

      Bx(k)=v(6*vertex(contactcheckelem(j),2)-5);
      By(k)=v(6*vertex(contactcheckelem(j),2)-3);
      Bz(k)=v(6*vertex(contactcheckelem(j),2)-1);

      Cx(k)=v(6*vertex(contactcheckelem(j),3)-5);
      Cy(k)=v(6*vertex(contactcheckelem(j),3)-3);
      Cz(k)=v(6*vertex(contactcheckelem(j),3)-1);

      Px(k)=ximpact(k);
```

```
        Py(k)=yimpact(k);
        Pz(k)=zimpact(k);

        centroidx(k)= (Ax(k)+Bx(k)+Cx(k))/3;
        centroidy(k)= (Ay(k)+By(k)+Cy(k))/3;
        centroidz(k)= (Az(k)+Bz(k)+Cz(k))/3;

        Pcent(k)= sqrt((Px(k)-centroidx(k))^2+(Py(k)-centroidy(k))^2+(Pz(k)-
                  centroidz(k))^2);

      %Use of the distance check method to limit contact checks
        if Pcent(k) > distcheck

            if j==length(contactcheckelem)
                preimpactdotsign(k)=0;
            end

            continue
        else

        v1(k)=sqrt((Bx(k)-Ax(k))^2+(By(k)-Ay(k))^2+(Bz(k)-Az(k))^2);
        v1x(k)=(Bx(k)-Ax(k));
        v1y(k)=(By(k)-Ay(k));
        v1z(k)=(Bz(k)-Az(k));

        v2(k)=sqrt((Cx(k)-Ax(k))^2+(Cy(k)-Ay(k))^2+(Cz(k)-Az(k))^2);
        v2x(k)=(Cx(k)-Ax(k));
        v2y(k)=(Cy(k)-Ay(k));
        v2z(k)=(Cz(k)-Az(k));

        v3(k)=sqrt((Cx(k)-Bx(k))^2+(Cy(k)-By(k))^2+(Cz(k)-Bz(k))^2);
        v3x(k)=(Cx(k)-Bx(k));
        v3y(k)=(Cy(k)-By(k));
        v3z(k)=(Cz(k)-Bz(k));

        pnorm(k)=sqrt((v1y(k)*v2z(k)-v1z(k)*v2y(k))^2+(v1z(k)*v2x(k)-
                  v1x(k)*v2z(k))^2+(v1x(k)*v2y(k)-v1y(k)*v2x(k))^2);
        pnormx(k)=(v1y(k)*v2z(k)-v1z(k)*v2y(k))/pnorm(k);
        pnormy(k)=(v1z(k)*v2x(k)-v1x(k)*v2z(k))/pnorm(k);
        pnormz(k)=(v1x(k)*v2y(k)-v1y(k)*v2x(k))/pnorm(k);

        vAP(k)=sqrt((Px(k)-Ax(k))^2+(Py(k)-Ay(k))^2+(Pz(k)-Az(k))^2);
        vAPx(k)=(Px(k)-Ax(k));
        vAPy(k)=(Py(k)-Ay(k));
        vAPz(k)=(Pz(k)-Az(k));


ndotvAP(k)=(pnormx(k)*vAPx(k))+(pnormy(k)*vAPy(k))+(pnormz(k)*vAPz(k));

        Qx(k)=Ax(k)+vAPx(k)-(ndotvAP(k)*pnormx(k));
```

```
        Qy(k)=Ay(k)+vAPy(k)-(ndotvAP(k)*pnormy(k));
        Qz(k)=Az(k)+vAPz(k)-(ndotvAP(k)*pnormz(k));

        AQ(k)=sqrt((Qx(k)-Ax(k))^2+(Qy(k)-Ay(k))^2+(Qz(k)-Az(k))^2);
        AQx(k)=(Qx(k)-Ax(k));
        AQy(k)=(Qy(k)-Ay(k));
        AQz(k)=(Qz(k)-Az(k));

        BQ(k)=sqrt((Qx(k)-Bx(k))^2+(Qy(k)-By(k))^2+(Qz(k)-Bz(k))^2);
        BQx(k)=(Qx(k)-Bx(k));
        BQy(k)=(Qy(k)-By(k));
        BQz(k)=(Qz(k)-Bz(k));

        CQ(k)=sqrt((Qx(k)-Cx(k))^2+(Qy(k)-Cy(k))^2+(Qz(k)-Cz(k))^2);
        CQx(k)=(Qx(k)-Cx(k));
        CQy(k)=(Qy(k)-Cy(k));
        CQz(k)=(Qz(k)-Cz(k));

        elemarea(k)=1/2*pnorm(k);
        area1(k)=1/2*sqrt((v1y(k)*AQz(k)-v1z(k)*AQy(k))^2+(v1z(k)*AQx(k)-
                 v1x(k)*AQz(k))^2+(v1x(k)*AQy(k)-v1y(k)*AQx(k))^2);
        area2(k)=1/2*sqrt((AQy(k)*v2z(k)-AQz(k)*v2y(k))^2+(AQz(k)*v2x(k)-
                 AQx(k)*v2z(k))^2+(AQx(k)*v2y(k)-AQy(k)*v2x(k))^2);
        area3(k)=1/2*sqrt((v3y(k)*BQz(k)-v3z(k)*BQy(k))^2+(v3z(k)*BQx(k)-
                 v3x(k)*BQz(k))^2+(v3x(k)*BQy(k)-v3y(k)*BQx(k))^2);
        areatotal(k)=area1(k)+area2(k)+area3(k);

          if areatotal(k) > elemarea(k) + 0.0001 &&
                   j==length(contactcheckelem)
              preimpactdotsign(k) = 0;
              break
          elseif areatotal(k) > elemarea(k) + 0.0001
              continue
          else
             contactelem(k)=contactcheckelem(j); %put this back up here
             QP=sqrt((Px(k)-Qx(k))^2+(Py(k)-Qy(k))^2+(Pz(k)-Qz(k))^2);
             QPx(k)=(Px(k)-Qx(k));
             QPy(k)=(Py(k)-Qy(k));
             QPz(k)=(Pz(k)-Qz(k));

normdotQPtrial=(pnormx(k)*QPx(k))+(pnormy(k)*QPy(k))+(pnormz(k)*QPz(k));
             trialsign=sign(normdotQPtrial);
          end

          if i > 1
              if preimpactdotsign(k) == 0
                 preimpactdotsign(k) = trialsign;
                 break
              elseif trialsign == preimpactdotsign(k)
                 break
              else
                 if maxdistnode(j) == 0
```

```
                maxdistnode(j)=k;
                maxdist(j) = QP;
                break
              elseif QP < maxdist(j)
                break
              else
                maxdistnode(j)=k;
                maxdist(j) = QP;
                break
              end

          end
        end

      end

   end
 end

 %Loop over the possible contact elements
 for j = 1:length(contactcheckelem)

     if maxdistnode(j)==0
         continue
     end

     k = maxdistnode(j);


vdotnorm=(vximpact(k)*pnormx(k))+(vyimpact(k)*pnormy(k))+(vzimpact(k)*pnor
mz(k));
            vnormalx=vdotnorm*pnormx(k);
            vnormaly=vdotnorm*pnormy(k);
            vnormalz=vdotnorm*pnormz(k);

            if maxdist(j) > maxpen
               maxpen = maxdist(j);
            end

               contact(k)=contact(k)+1;


               boostaux = (maxdist(j)/(abs(vdotnorm)*h))+1;
               if boostaux < boostlimit
                   boost = boostaux;
               else
                   boost = boostlimit;
                   boostcounter=boostcounter+1;
               end
```

```
            if boost > boostmax
                    boostmax = boost;
            end

     %Updating the velocities of the contact element vertices
            v(6*vertex(contactelem(k),1)-4) = boost*vnormalx;
            v(6*vertex(contactelem(k),1)-2) = boost*vnormaly;
            v(6*vertex(contactelem(k),1)) = boost*vnormalz;

            v(6*vertex(contactelem(k),2)-4) = boost*vnormalx;
            v(6*vertex(contactelem(k),2)-2) = boost*vnormaly;
            v(6*vertex(contactelem(k),2)) = boost*vnormalz;

            v(6*vertex(contactelem(k),3)-4) = boost*vnormalx;
            v(6*vertex(contactelem(k),3)-2) = boost*vnormaly;
            v(6*vertex(contactelem(k),3)) = boost*vnormalz;

 end
 end

    plotcounter=plotcounter+1;
    t=t+h
    if plotcounter==hstl
       vvector=[vvector; v];
       tvector=[tvector; t];
       penetrate=[penetrate; maxpen];

       stlcount=stlcount+1;

%Creating STL files while the code is running instead of waiting until it
%completes
           for k=1:numimpact
             x(k)=ximpact(k);
             y(k)=yimpact(k);
             z(k)=zimpact(k);
           end

           fOut = sprintf('SingleImpactor.%d.stl',stlcount);
           fid = fopen(fOut, 'wt');
           fprintf(fid,'solid object \n');

             for ii=1:nelem
               n1 = vertex(ii,1);
               n2 = vertex(ii,2);
               n3 = vertex(ii,3);
               fprintf(fid,'  facet normal  %f %f %f\n',1.0,0.0,0.0);
               fprintf(fid,'    outer loop \n');
               vertx1 = vvector(stlcount,6*n1-5);
               verty1 = vvector(stlcount,6*n1-3);
               vertz1 = vvector(stlcount,6*n1-1);
               vertx2 = vvector(stlcount,6*n2-5);
```

```
                verty2 = vvector(stlcount,6*n2-3);
                vertz2 = vvector(stlcount,6*n2-1);
                vertx3 = vvector(stlcount,6*n3-5);
                verty3 = vvector(stlcount,6*n3-3);
                vertz3 = vvector(stlcount,6*n3-1);
                fprintf(fid, '      vertex %f %f %f\n'
                      ,vertx1,verty1,vertz1);
                fprintf(fid, '      vertex %f %f %f\n'
                      ,vertx2,verty2,vertz2);
                fprintf(fid, '      vertex %f %f %f\n'
                      ,vertx3,verty3,vertz3);
                fprintf(fid,'    endloop \n');
                fprintf(fid,'  endfacet \n');
              end

                for ii=1:nelem1
                  fprintf(fid,'  facet normal  %f %f %f\n',1.0,0.0,0.0);
                  fprintf(fid,'    outer loop \n');
                  fprintf(fid, '      vertex %f %f %f\n'
                      ,x(vertex1(ii,1)),y(vertex1(ii,1)),z(vertex1(ii,1)));
                  fprintf(fid, '      vertex %f %f %f\n'
                      ,x(vertex1(ii,2)),y(vertex1(ii,2)),z(vertex1(ii,2)));
                  fprintf(fid, '      vertex %f %f %f\n'
                      ,x(vertex1(ii,3)),y(vertex1(ii,3)),z(vertex1(ii,3)));
                  fprintf(fid,'    endloop \n');
                  fprintf(fid,'  endfacet \n');
                end

            fprintf(fid,'endsolid object');
            fclose(fid);

              plotcounter=0;
      end

end

%Plot statement to show maximum penetration vs. time
figure(1),plot(tvector,penetrate);

%Plot statement to show x,y,and z positions and velocities for the given
%particles
figure(265),plot(tvector,vvector(:,1585),'b-',tvector,vvector(:,1586),'b--
',tvector,vvector(:,1587),'r-',tvector,vvector(:,1588),'r--
',tvector,vvector(:,1589),'g-',tvector,vvector(:,1590),'g--');
figure(276),plot(tvector,vvector(:,1651),'b-',tvector,vvector(:,1652),'b--
',tvector,vvector(:,1653),'r-',tvector,vvector(:,1654),'r--
',tvector,vvector(:,1655),'g-',tvector,vvector(:,1656),'g--');
```

F Case 2 Main Matlab Code (Input Parameters Only)

```
%Defining the input parameters
t=0;                %initial time
tfinal = 12;        %final time
h = 0.0004;         %time-step
N=tfinal/h;         %total number of steps
hstl=300;           %number of steps between STL files
mperarea=0.0024;    %mass per unit area
k0=21.828;          %stretching stiffness coefficient input in the code
kb=.0000054;        %bending stiffness coefficient
c= 0.0005;          %damping coefficient
pmax=0.0;           %maximum pressure
tpstart=0;          %time at which pressure force begins
tpend=0;            %time at which pressure force = pmax
gx=0.0;             %acceleration due to gravity in the x-direction
gy=-32.174;         %acceleration due to gravity in the y-direction
gz=0.0;             %acceleration due to gravity in the z-direction

neglimit = -0.5;        %negative limit for box method
poslimit = 1.8;         %positive limit for box method
contactcheckelem = [];
distcheck = 1.5;        %radius for the distance check method
soldiertlag = 0.1;      %time the impactor begins moving
boostlimit = 40;        %limit on the adjustable parameter b
boostmax=0;
boostcounter=0;

vimpact1=0.55;          %velocity of impactor 1
vimpact2=0.5;           %velocity of impactor 2
vimpact3=0.4;           %velocity of impactor 3
vimpact4=0.3;           %velocity of impactor 4
vimpact5=0.1;           %velocity of impactor 5
```

G Case 2 Multiple Impactor Sample Input File

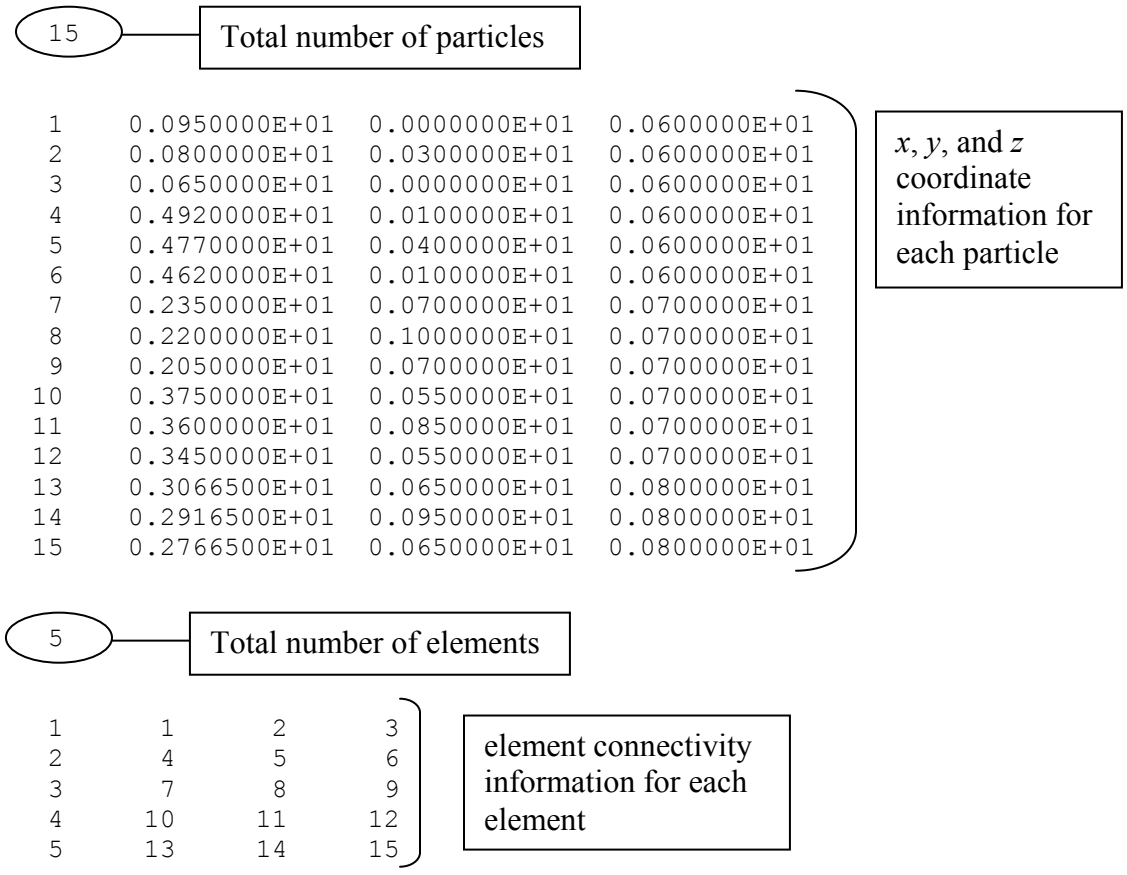

H Case 3 Main Matlab Code (Input Parameters Only)

```
%Defining the input parameters
t=0;                 %initial time
tfinal = 8;          %final time
h = 0.0004;          %time-step
N=tfinal/h;          %total number of steps
hstl=200;            %number of steps between STL files
mperarea=0.0024;     %mass per unit area
k0=21.828;           %stretching stiffness coefficient input in the code
kb=.0000054;         %bending stiffness coefficient
c= 0.0005;           %damping coefficient
pmax=0.0;            %maximum pressure
tpstart=0;           %time at which pressure force begins
tpend=0;             %time at which pressure force = pmax
gx=0.0;              %acceleration due to gravity in the x-direction
gy=-32.174;          %acceleration due to gravity in the y-direction
gz=0.0;              %acceleration due to gravity in the z-direction

neglimit = -0.5;         %negative limit for box method
poslimit = 1.0;          %positive limit for box method
contactcheckelem = [];
distcheck = 1.2;         %radius for the distance check method
soldiertlag = 0.1;       %time the impactor begins moving
boostlimit = 75;         %limit on the adjustable parameter b
boostmax=0;
boostcounter=0;

vimpact1=0.8;            %velocity of the impactor in the -x-direction
vimpact2=0.24;           %velocity of the impactor in the -z-direction
```

I Case 4 Main Matlab Code (Input Parameters Only)

```
%Defining the input parameters
t=0;                %initial time
tfinal = 10;        %final time
h = 0.0002;         %time-step
N=tfinal/h;         %total number of steps
hstl=500;           %number of steps between STL files
mperarea=0.0024;    %mass per unit area
k0=21.828;          %stretching stiffness coefficient input in code
kb=.0000054;        %bending stiffness coefficient
c= 0.0005;          %damping coefficient
pmax=0.0;           %max pressure
tpstart=0;          %time at which pressure begins
tpend=0;            %time at which pressure = pmax
gx=0.0;             %acceleration due to gravity in the x-direction
gy=0.0;             %acceleration due to gravity in the y-direction
gz=0.0;             %acceleration due to gravity in the z-direction

neglimit = -0.4;        %negative limit for the box method
poslimit = 0.4;         %positive limit for the box method
contactcheckelem = [];
distcheck = 0.7;        %radius for the distance check method
soldiertlag = 0.1;      %time the impactor begins moving
boostlimit = 75;        %limit on the adjustable parameter b
boostmax=0;
boostcounter=0;

vimpact1=0.5;           %velocity of the impactor
```

J Case 5 Main Matlab Code (Input Parameters Only)

```
%Defining the input parameters
t=0;                 %initial time
tfinal = 10;         %final time
h = 0.0002;          %time-step
N=tfinal/h;          %total number of steps
hstl=500;            %number of steps between STL files
mperarea=0.0024;     %mass per unit area
k0=21.828;           %stretching stiffness coefficient input in code
kb=.0000054;         %bending stiffness coefficient
c= 0.0005;           %damping coefficient
pmax=0.0;            %max pressure
tpstart=0;           %time at which pressure begins
tpend=0;             %time at which pressure = pmax
gx=0.0;              %acceleration due to gravity in the x-direction
gy=0.0;              %acceleration due to gravity in the y-direction
gz=-32.174;          %acceleration due to gravity in the z-direction

neglimit = -0.96;        %negative limit for box method
poslimit = 1.02;         %positive limit for box method
contactcheckelem = [];
distcheck = 0.7;         %radius for the distance check method
soldiertlag = 2.6;       %time the impactor begins moving
boostlimit = 75;         %limit on the adjustable parameter b
boostmax=0;
boostcounter=0;


vimpact1=0.8;            %velocity of the impactor
```

K Case 6 Main Matlab Code (Input Parameters Only)

```
%Defining the input parameters
t=0;                %initial time
tfinal = 12;        %final time
h = 0.00015;        %time-step
N=tfinal/h;         %total number of steps
hstl=800;           %number of steps between STL files
mperarea=0.0024;    %mass per unit area
k0=21.828;          %stretching stiffness coefficient input in code
kb=.0000054;        %bending stiffness coefficient
c= 0.0005;          %damping coefficient
pmax=0.15;          %max pressure
tpstart=2.6;        %time at which pressure begins
tpend=4.6;          %time at which pressure = pmax
gx=0.0;             %acceleration due to gravity in the x-direction
gy=0.0;             %acceleration due to gravity in the y-direction
gz=-32.174;         %acceleration due to gravity in the z-direction

neglimit = -0.96;       %negative limit for box method
poslimit = 1.02;        %positive limit for box method
contactcheckelem = [];
distcheck = 0.7;        %radius for the distance check method
soldiertlag = 4.6;      %time the impactor begins moving
boostlimit = 75;        %limit on the adjustable parameter b
boostmax=0;
boostcounter=0;

fixstretch=0.75;        %distance nodes are stretched during first time-
                         step

vimpact1=0.8;           %velocity of the impactor
```

L Case 7 Main Matlab Code (Input Parameters Only)

```
%Defining the input parameters
t=0;                 %initial time
tfinal = 16;         %final time
h = 0.000125;        %time-step
N=tfinal/h;          %total number of steps
hstl=1280;           %number of steps between STL files
mperarea=0.0024;     %mass per unit area
k0=21.828;           %stretching stiffness coefficient input in code
kb=.0000054;         %bending stiffness coefficient
c= 0.0005;           %damping coefficient
pmax=0.0;            %max pressure
tpstart=0;           %time at which pressure begins
tpend=0;             %time at which pressure = pmax
gx=0.0;              %acceleration due to gravity in the x-direction
gy=0.0;              %acceleration due to gravity in the y-direction
gz=-32.174;          %acceleration due to gravity in the z-direction

neglimit = -0.96;        %negative limit for the box method
poslimit = 1.02;         %positive limit for the box method
contactcheckelem = [];
distcheck = 0.7;         %radius for the distance check method
soldiertlag = 2.0;       %time the impactor begins moving
boostlimit = 75;         %limit on the adjustable parameter
boostmax=0;
boostcounter=0;


vimpact1=0.8;            %velocity of the impactor
```